CL degradation of Y_2SiO_5:Ce thin films coated with SnO_2

by

Elizabeth (Liza) Coetsee

(B.Sc Hons)

A dissertation submitted in fulfilment of the requirements for the degree

MAGISTER SCIENTIAE

in the

Faculty of Natural and Agricultural Sciences

Department of Physics

at the

University of the Free State

Republic of South Africa

Supervisor: Prof. H.C. Swart

Co-supervisor: Prof. J.J. Terblans

May 2006

This thesis is dedicated to my father, mother, twin brothers , 2 sisters, Stafford, Master Godfrey and Cindy

Acknowledgements:

Before I express my appreciation and gratitude to the following people I first of all want to thank our beloved *Father in Heaven* for the gift of living.

- Prof. H. C. Swart for his professional leadership as my supervisor and for his wisdom, patience and energy that encouraged me.
- Prof. J. J. Terblans for his *special* contribution, always understanding and professional attitude.
- Paul Ripley from Phosphor Technology Ltd for supplying the Y_2SiO_5:Ce phosphor.
- Martin Ntwaeaborwa for his phosphor discussions on phosphors.
- My friends and personnel at the University of the Free State. Dr. C. Theron for RBS analysis at Ithemba labs in Cape Town.
- Ulrich Buttner for his guidance and assistance in growing thin films with the PLD technique at Stellenbosch University.
- Dr. K. T. Hillie for his help.
- Werner Jordaan for his assistance in doing XPS, SEM and EDX at the CSIR-NML.
- Ina Claasens for doing AFM on the thin films at Mintek, Johannesburg.
- Prof. P.W.J. van Wyk of the electron microscopy unit at UFS.
- Prof. W. van der Westhuizen from Geology, UFS for XRD measurements.
- The CSIR and NRF for financial assistance.
- My wonderful father, Gert, for being the best role model as a father there could ever be and dearest mother, Marie, for her endless love and for being my guardian angel, twin brothers Andries and Gert, two sisters Marleen and Emmie, Ina van Wyk (father's sister) and David Collett.
- Grand Master Eddie Jacobsen for his respect, consideration, mentorship, energy and professional leadership while training to also achieve a Masters degree in martial arts.
- Masters Melanie, Jan, Godfrey and Cindy and the rest of my martial arts family for their endless discussions, encouragements and interest in physics.
- Last but not least, my friend, Stafford Mew.

Abstract

The degradation of the cathodoluminescence (CL) intensity of cerium-doped yttrium silicate (Y_2SiO_5:Ce) phosphor thin films and commercially available Y_2SiO_5:Ce phosphor powders from Phosphor technology, England, were investigated for possible application in low voltage field emission displays (FEDs). Thin films of Y_2SiO_5:Ce were pulsed laser ablated on Si (100) substrates by using a XeCl (308 nm) excimer laser, in an oxygen (O) ambient gas pressure of 7.5×10^{-4} Torr, with laser energy of 81.81 mJ, repetition rate of 10 Hz, substrate temperature of 400°C, target to substrate distance of 3.7 cm and by using 6600 pulses. Some of the phosphor thin films were coated with tin oxide (SnO_2), with the same deposition parameters as for the Y_2SiO_5:Ce phosphor layer except for the amount of pulses that was reduced to 1200 pulses. A SnO_2 layer was ablated onto some of the thin films in order to investigate the effect of the coated layer on the surface and on the degradation of the CL intensity.

Rutherford backscattering (RBS) was used to measure the film thicknesses. The results showed a non uniform Y_2SiO_5:Ce layer covered with a 58 nm thick SnO_2 layer. Scanning electron microscopy (SEM), atomic force microscopy (AFM) and energy dispersive spectroscopy (EDS) were use to study the surface morphology of the thin films. The results indicated that the Y_2SiO_5:Ce phosphor was ablated onto the Si (100) substrate surface as micron-sized spherical particles and that the SnO_2 layer was ablated as a uniform coated layer covering the surface of the substrate and the randomly distributed spherical Y_2SiO_5:Ce particles. SEM was also use to study the surface morphology of the Y_2SiO_5:Ce phosphor powders and the results showed that the particles were agglomerated. X-ray diffraction (XRD), that was used to measure the crystal planes of both the thin films and the powders, revealed the monoclinic crystal structure of Y_2SiO_5:Ce.

Auger electron spectroscopy (AES), X-ray photoelectron spectroscopy (XPS) and CL spectroscopy were used to monitor changes in the surface chemical composition and luminous efficiency of the Y_2SiO_5:Ce phosphor powders and thin films (coated and uncoated). AES and CL spectroscopy measurementswere done with 2 keV energy electrons and with beam current densities between 26.3 $mA.cm^{-2}$ and 52.63 $mA.cm^{-2}$, in high vacuum and in oxygen pressures of 1×10^{-8}, 1×10^{-7} and 1×10^{-6} Torr. AES indicated adventitious carbon (C) on the surface before CL measurements were made.

C was depleted from the surface during electron bombardment. Residual gas mass analysis (RGA) showed that C was removed from the surface as volatile gas species. RGA with the electron beam on resulted in a higher intensity of CO_2, CO and H_2O gas species, compared to when the electron beam was off. This is consistent with the electron stimulated surface chemical reaction (ESSCR) model, whereby the electron beam dissociates the oxygen gas species into reactive atomic species, which then reacts with the carbon on the surface to form the volatile CO_2 and CO gas species.

Auger peak to peak heights (APPH) for oxygen and silicon on both the uncoated thin film and the powder surface stayed almost constant. The CL intensity (measured at 440 nm) increased within the first 300 $C.cm^{-2}$, which is the result of the depletion of the carbon from the surface, and then it stayed constant for prolonged electron bombardment. The carbon results in an extra layer on the thin film surface that increases the energy loss of the incoming electrons. This results in the creation of fewer electron – hole pairs for photon emission during radiative recombination.

The CL emission spectrum resulted in the characteristic double shoulder peak of Y_2SiO_5:Ce with the two main peak positions at 440 and 500 nm (blue light) before and after 24 hrs of electron bombardment for the uncoated thin film, coated thin film and for the powders. Light emission in the rare earth, Ce^{3+}, is due to the 5d ? 4f transition due to the splitting effects of the 4f energy level. The 4f energy level splits due to the effect of the crystal field in Y_2SiO_5 as the host material, into the $^2F_{7/2}$ and the $^2F_{5/2}$ energy levels. The broad band emission of Y_2SiO_5:Ce is the result of the different splitting effects due to the crystal field.

The relatively high CL intensity of the thin films is attributed to the spherically shaped phosphor particles grown on the surface of the Si (100) substrate. The SnO_2 was also successfully ablated as a coating layer. The SnO_2 coating layer increases the energy loss of the incoming electrons which results in a lower CL intensity. The CL intensity for the uncoated thin film was therefore higher than for the coated thin film. The CL intensity stayed almost constant for the 24 hrs of electron bombardment of both the coated and uncoated thin films.

The CL intensity for the phosphor powders, however, behaved differently. The intensity showed an increase after about 300 $C.cm^{-2}$. The CL emission spectrum

showed an increase in a second broad band at a wavelength of 650 nm after 24 hr electron bombardment. It was proved with XPS that this second broad band is due to the formation of a luminescent silicon dioxide (SiO_2) layer on the surface of the Y_2SiO_5:Ce phosphor powders, as a result of the electron surface stimulated reactions (ESSCR). The increase in the CL intensity is thus due to the luminescent SiO_2 layer that was formed as a result of electron beam irradiation that causes the Si-O bonds to break and to form intrinsic defects at 1.9 eV (650 nm) and 2.7 eV (459 nm). XPS also indicated that the Ce concentration on the surface layer increased during the degradation process and the formation of CeO_2 and CeH_3 also resulted from the degradation process. The phosphor powders degraded from a blue light emitting phosphor before electron bombardment to a whitish light emitting phosphor after 24 hr, as a result of the luminescent SiO_2 layer formed during degradation.

Keywords

Y_2SiO_5:Ce: An inorganic phosphor, intentionally doped with the rare earth, Cerium, for blue light emission.

Cathodoluminescence: A phenomenon whereby the emission of light occurs due to electron beam irradiation.

Degradation: Reduction of the efficiency of a phosphor material through prolonged electron bombardment.

ESSCR: Electron Surface Stimulated Chemical Reaction (ESSCR).

SiO_2: A wide band gap semiconductor that only emits light due to defects or intentionally doped impurities.

Coated layer: An extra layer intentionally grown onto the phosphor surface to investigate the effect on the degradation of the CL intensity.

Table of Contents

Chapter 1

This chapter commences with a brief introduction on phosphor applications in the FED devices, which leads to the aim of this study on the degradation of Y_2SiO_5:Ce thin films. It also includes the layout of the thesis.

1. Introduction

Liquid Crystal Displays (LCDs), plasma displays (PDs) and field emission displays (FEDs) are the most popular examples of flat panel display (FPD) technology, which are competing on equal footing with cathode ray tubes (CRTs) in the display market. The latest research studies on FPD technology are aimed at improving luminescent efficiency of phosphor screens of PD and FEDs [1, 2, 3]. FEDs require higher efficiency at lower voltages (lower than 10 kV, in comparison with CRTs that require voltages between 20 and 30 kV).

The lower voltages mean FEDs operate with low energy electrons which have a shallower penetration depth for cathodoluminescence (CL). To maintain brightness and constant power, the FEDs thus require higher current densities. High current densities have been found to decrease the degradation of the CL intensity of traditional sulphide-based phosphors used in FEDs [10].

Today, much attention has been focused on luminescent properties of oxide-based phosphors which are possible candidates to replace sulphide-based phosphors whose degradation is detrimental to the emitter tips of FEDs [4, 6]. Compared to sulphide-based phosphors, oxide phosphors have been found to be more stable at high temperature, high pressure and high current densities needed for the FED environment [7, 8].

Thin film phosphor materials have some advantages over powders in the FED environment, such as the reduction of light scattering and the good thermal contact between the screen and the faceplate [9]. Pulsed laser deposition (PLD) is a technique used to grow thin films with an important feature of maintaining the stoichiometry of

the target material [9, 10]. Surface morphology and thickness can be controlled by varying some of the growth parameters, such as the ambient gas pressure and the number of pulses [10, 11].

Extensive research on the degradation of the sulphide-based phosphor, ZnS, resulted in a model called the electron-stimulated surface chemical reaction (ESSCR) [3, 10, 12, 13]. The data collected was on ZnS thin films and powders, both doped with activators such as Ag, Cl, Cu, Au, Al or Mn. According to the ESSCR model, the reactive gas molecules adsorb onto the surface of the ZnS phosphors. The molecules are dissociated by the electron beam from molecular species to form reactive atomic species, which result in the formation of a ZnO surface layer and volatile SO_2, with the consequent loss of the cathodoluminescence (CL) intensity [14].

The CL intensity decreases due to the formation of the non-luminescent ZnO surface layer. The decrease in the CL intensity could not be explained by the formation of the ZnO layer alone, thus a defect theory has been proposed to reconcile the difference [4]. The defect theory involves point defects (see Chapter 3) that are created during the surface chemical reactions. The oxygen atom substitutes a sulphur atom (or occupies a sulphur vacancy) in the lattice, creating a non-luminescent trap. These non-luminescent traps compete with the CL process and cause a loss in CL intensity.

Shin et. al. [15] reported results on coating ZnS:Mn phosphor with SnO_2, to investigate the effect on the degradation of the CL intensity. The degradation of the CL intensity is consistent with the well known ESSCR [12]. Coating the surface of the phosphors is one possibility of decreasing the degradation rate. The coating should be thin enough to be transparent at low energies and it should not influence the chromaticity and brightness of the phosphor [6].

Y_2SiO_5:Ce is a blue emitting rare earth phosphor. Light emission in rare earth phosphors is due to characteristic luminescence where electron hole pairs get created in the atom itself, emitting photons as they recombine. Ce^{3+} (trivalent cerium) has only one electron in the 4f shell. The 4f energy level splits into the $^2F_{5/2}$ and the $^2F_{7/2}$ levels due to the electron having the ability to exhibit a + 1/2 or – 1/2 spin. Light emission is due to the 5d ? 4f transition, resulting in the double emission with peaks

at 395 and 423 nm [16]. The CL efficiency of an Al-compound coated Y_2SiO_5:Ce phosphor was improved due to the presence of a small side peak at the long wavelength part of the spectrum where the eye sensitivity is higher [17]. This, however, resulted in a change in chromaticity. Klaassen et al. [18] analyzed the degradation of a few phosphors. It was found that the degradation of Y_2SiO_5:Ce was caused by a decreased energy flow to the Ce^{+3} ions, which may be due to a decrease in the effective luminescent Ce^{+3} concentration.

2. Aim of this study

The aim of this study was to investigate the following aspects concerning the Y_2SiO_5:Ce phosphor:

1. Ablating Y_2SiO_5:Ce phosphor thin films onto Si (100) substrates with the use of the XeCl excimer laser in pulsed laser deposition.
2. Ablating a SnO_2 layer onto some of the phosphor thin films in order to investigate the effect of a coating layer on the degradation and on the CL intensity.
3. Characterisation of the thin films (Rutherford Backscattering (RBS), Scanning Electron Microscopy (SEM), X-Ray Diffraction, (XRD), Energy Dispersive X-Ray analysis (EDX) and Atomic Force Microscopy (AFM)) and the phosphor powders.
4. Monitor changes in the surface composition, due to electron bombardment of the Y_2SiO_5:Ce phosphor powders and thin films in an O_2 gas ambient, with Auger Electron Spectroscopy (AES) and X-Ray Photo Electron Spectroscopy (XPS).
5. Comparison of the coated, non-coated and powders with each other.
6. The formulation of a degradation mechanism of Y_2SiO_5:Ce under electron bombardment.

3. Layout of the thesis

Chapter 1 includes the introduction and aim of this study, followed by some history and theory on phosphors, luminescence and application in FEDs and CRTs in *chapter*

2. *Chapter 3* deals with the theory and the ESSCR model on degradation, theory on defects and total internal reflection and it includes results from literature studies. The theory on the technique of thin film preparation (PLD) and characterization (RBS, SEM, AFM, EDS and XRD) can be found in *chapter 4* as well as background on AES and XPS that was used to monitor the sample surface. It also outlines the experimental procedures. *Chapter 5* contains the results obtained and the discussions for the characterization of the phosphor powders, the emission mechanism in Ce^{3+} and the formation of SiO_2 on the surface. *Chapter 6* contains the results and discussion for the characterization of the thin films. *Chapter 7* contains the results and discussions for the CL and AES done in different O_2 gas ambient and beam currents, as well as the light emission process from the thin film surface. The conclusion as well as the future work is outlined in *chapter 8*.

References

1. X. W. Sun and H. S. Kwok, Appl. Phys. A, Mat. Sci. Proc, **69** (1999) 39.
2. H. C. Swart, J. S. Sebastian, T. A. Trottier, S. L. Jones and P. H. Holloway, J. Vac. Sci. Technol. A, **14(3)** (1996) 1697.
3. P. H. Holloway, J. Sebastian, T. Trottier, S. Jones, H. C. Swart and R. O. Peterson, Mat. Res. Soc. Symp. Proc , **424** (1997) 425.
4. H. C. Swart and K. T. Hillie, Surf. Interface Anal, **30** (2000) 383.
5. P. J. Marsh, J. Silver, A. Vecht and A. Newport, J. Lumin, **97** (2002) 229.
6. J. M. Fitz-Gerald, T. A. Trottier, R. K. Singh and P. H. Holloway, Appl. Phys. Lett, **72** (1998) 1838.
7. Q. Y. Zhang, K. Pita, S. Buddhudu and C. H. Kam, J. Phys. D: Appl. Phys, **35** (2002) 3085.
8. O. M. Ntwaeaborwa, K. T. Hillie and H. C. Swart, Phys. Stat. Sol. C, **1** (2004) 2366.
9. K. T. Hillie, C. Curren and H. C. Swart, Appl. Surf. Sci, **177** (2001) 73.
10. K. T. Hillie and H. C. Swart, Appl. Surf. Sci, **183** (2001) 304.
11. Chen Li-Chyng, Particulates generated by pulsed laser ablation, in Pulsed Laser Deposition of Thin Films (eds. D. B. Chrisey, G. K. Hulber), John Wiley & Sons, Inc , New York, (1994) p. 167.
12. J. Sebastian, S. Jones, T. Trottier, H. C. Swart and P. Holloway, J. SID, **3/4** (1995) 147.
13. P. H. Holloway, T. A. Trottier, B. Abrams, C. Kondoleon, S. L. Jones, J. S. Sebastian and W. J. Thomas, J. Vac. Sci. Technol. B, **17(2)** (1999) 758.
14. L. Oosthuizen, H. C. Swart, P. E. Viljoen, P. H. Holloway and G. L. P. Berning, Appl. Surf. Sci, **120** (1997) 9.
15. S. H. Shin, J. H. Kang, D. Y. Jeon and D. S. Zang, J. Solid State Chem, **178** (2005) 2205.
16. E. J. Bosze, G. A. Hirata and J. McKittrick, Mat. Proc. Symp. Mat. Res. Soc. Proc, **558** (1999) 15.
17. R. Y. Lee and S. W. Kim, J. of Lumin, **93** (2001) 93.
18. D. B. M. Klaassen and D. M. de Leeuw, J. Lumin, **37** (1987) 21.

Chapter 2

Phosphors

This chapter begins with the history on phosphors, it gives a brief description on FEDs and CRTs and ends off with the theory about luminescence and the background about the Y_2SiO_5:Ce phosphor.

The word *phosphor* was invented in the early 17th century and it is said that Vincentinus Casciarolo of Bologna, Italy, found a heavy crystalline stone with a gloss at the foot of a volcano, and fired it in a charcoal oven intending to convert it to a noble metal. Casciarolo obtained no metals but found that his sintered stone emitted red light in the dark after exposure to sunlight. This stone was called the "Bolognian stone" [1]. From the knowledge now known, the stone found appears to have been barite ($BaSO_4$), with the fired product being BaS, which is now known to be a host for phosphor materials. Similar findings were reported from many places in Europe after the first discovery, and these light-emitting stones were named *phosphors*.

The word phosphor means "light bearer" in Greek, and appears in Greek myths as the personification of the morning star Venus. The word *phosphorescence*, which means persisting light emission from a substance after the exciting radiation has ceased, was derived from the word *phosphor*. The Japanese were reported to have prepared phosphorescent paint from seashells, before the discovery of the Bolognian stone. This fact is described in a 10th century Chinese document (Song dynasty).

The word *fluorescence* means the light emission from a substance during the time when it is exposed to exciting radiation. *Luminescence* is defined as the phenomenon in which the electronic state of a substance is excited by some kind of external energy and the excitation energy is given off as light. The word *light* includes not only electromagnetic waves in the visible region of 400 and 700 nm, but also those in the neighbouring region on both ends, i.e. the near-ultraviolet and the near-infrared regions [1]. Luminescence is divided into fluorescence and phosphorescence according to the duration time of the after-glow. As mentioned, the after-glow that

can be perceived by the human eye, namely that persists for longer than 0.1 s after cessation of excitation is usually called phos phorescence [1]. The excited electrons in phosphorescent materials can remain in a meta stable energy state for minutes to weeks before emitting light. Like fluorescent materials, these materials emit light continuously when they are excited by ultraviolet or visible light.

When the excitation source is extinguished, phosphorescent materials continue to emit light. It is this light (called afterglow) that we perceive as glow-in-the-dark. The afterglow decreases (or decays) over time after the excitation source has been extinguished. Some phosphor manufacturers state that the decrease is exponential, but this is usually incorrect. Most long-persistence phosphors exhibit what is called hyperbolic decay (see Figure 1). The equation describing this decay is [2]:

$$I(t) = I_0 \frac{ß^a}{(ß + t)^a} \tag{1}$$

where t is time in seconds, I_0 is the initial luminance (measured in candelas per square meter), I(t) is the luminance at time t, and α and β are constants that depend on the chemical composition and physical properties of the material.

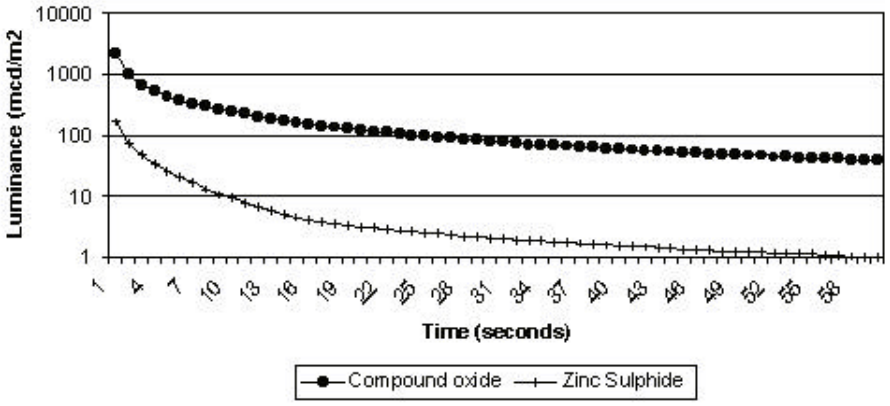

Figure 1: Typical hyperbolic afterglow decay [2].

The application of phosphors can be classified as: 1 – light sources; 2 – display devices represented by cathode-ray tubes; 3 – detector systems such as X-ray screens and 4 – other simple applications such as luminous paint with long persistent phosphorescence.

Phosphors are the central component of an increasing number of functional devices such as flat panel displays and electroluminescent display panels [1, 3]. Interest in FEDs is reported from many industries including notebook computers, medical, industrial and military visual-display manufacturers [4].

Phosphors are inorganic luminescent materials that emit photons when irradiated with high energy particles such as electrons or photons [5]. Figure 2 shows the wavelengths of the blue, green and red regions in our visible light spectrum

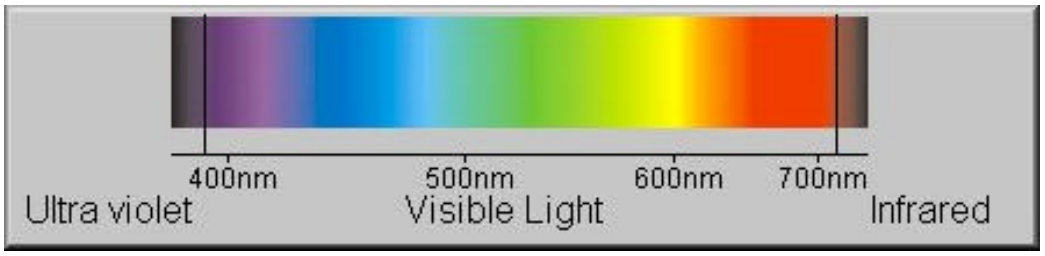

Figure 2: Wavelength of blue, green and red light [6].

Luminescent materials absorb energy from external energy sources such as high energy photons, electrons, electric fields, friction, chemical reactions and other non-thermal sources. The most important component of any display panel is the screen that is coated with these luminescent materials which are the phosphors. Cathode-ray tubes have been the dominant display technology for many years, but the need for lower power consumption and portability opened the door for new technology [7].

2.1 Cathode-ray tubes (CRTs)

The basic operation of a CRT consists of three electron guns, each emitting an electron beam that is scanned across the phosphor screen, see figure 3.

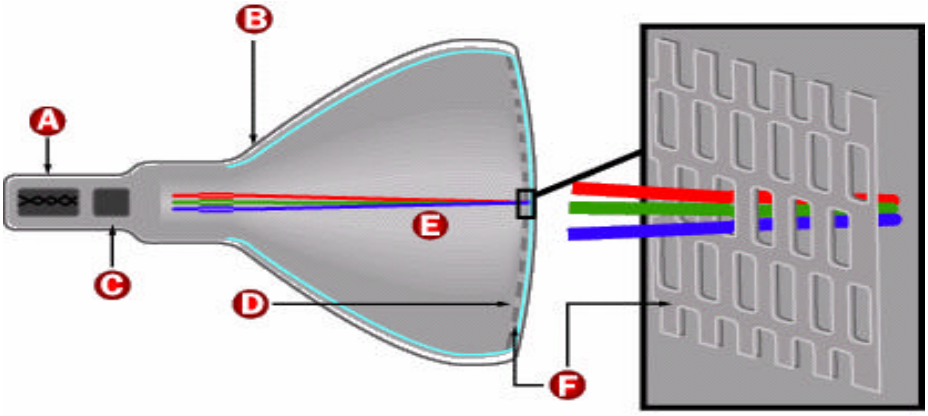

A – Cathode
B – Conductive coating
C – Anode
D – Phosphor coated screen
E – Electron beams
F – Shadow mask

Figure 3: CRTs used in televisions and computers [8].

In CRTs, the cathode is a heated filament positioned in a vacuum created in a glass tube. The ray is a stream of electrons that naturally pour off a heated cathode into the vacuum. The anode attracts the electrons; a focusing and accelerating anode focuses and accelerates the electrons towards the phosphor-coated screen. The tube is wrapped with copper windings that act as steering coils. The coils create magnetic fields inside the tube that steers the beam towards the screen. By controlling the voltages in the coil, the electron beam can be positioned at any point on the screen. However, CRTs are very bulky, and if a bigger screen is required, the length of the tube must increase. FEDs require a distance of a few millimetres towards the screen [8].

2.2 Field emission displays (FEDs)

FEDs are an alternative to CRTs, with the electron source an array of field emitter tips as the cathode. Images are formed on the phosphor coated screen (anode) by the impingement of electrons, emitted from the emitter tips, arranged in a grid. Each phosphor pixel has its own set of field emitters [8, 9] (see figure 4).

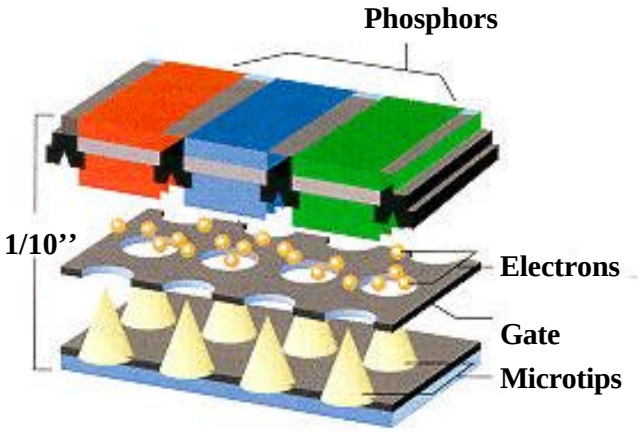

Figure 4: Schematic diagram of a FED [10].

The emitter tips are either made of metals like molybdenum, tungsten, platinum, or of semiconductors like silicon or diamonds. The substrate supporting the tips is covered by a dielectric film that provides isolation. A metal thin film deposited over this dielectric layer serves as a gate electrode or a focusing electrode to improve the resolution of the FED pixels.

The electrons tunnel from the array of tips and get accelerated towards phosphors placed between a few micrometers to a few millimetres away from the tip. The phosphors may be patterned to define the pixel, in which case three different phosphors are deposited to achieve the primary colours of red, green and blue [11].

As mentioned before, FEDs need improvement in conditions for ideal operation such as low voltages, high pressures and high current densities. Research on finding the 'best' phosphor for ideal operation in FEDs, led to the investigation of critical properties such as luminescence, brightness, chromaticity, efficiency, conductivity, particle size and maintenance. [11].

2.3 Emission of light

Light is a form of energy. To create light, another form of energy must be supplied. There are two common ways for this to occur, incandescence and luminescence.

2.3.1 Incandescence

Incandescence is light from heat energy. If something is heated to a high enough temperature it will begin to glow. When the tungsten filament of an ordinary incandescent light bulb is heated it glows brightly. The sun and stars glow by incandescence. Incandescent light is produced by lattice vibrations, called phonons, which emit part of their energy in the form of electromagnetic radiation [12].

2.3.2 Luminescence

Luminescence takes place at normal and low temperatures. Light emission is produced by the relaxation of electrons from excited to ground states which produces photons with energies equal to the energy difference between the two transition states. The most common techniques of excitation are i) photoluminescence, ii) cathodoluminescence, iii) thermoluminescence and iv) electroluminescence.

i) Photoluminescence:

This is luminescence by which electromagnetic radiation, i.e. photons, are used to excite the material, usually done by ultraviolet light.

ii) Cathodoluminescence:

This is the process by which a beam of electrons excites the material to luminesce. Figure 5 shows a schematic diagram of luminescence process where photons are emitted from excitation electron beam bombardment.

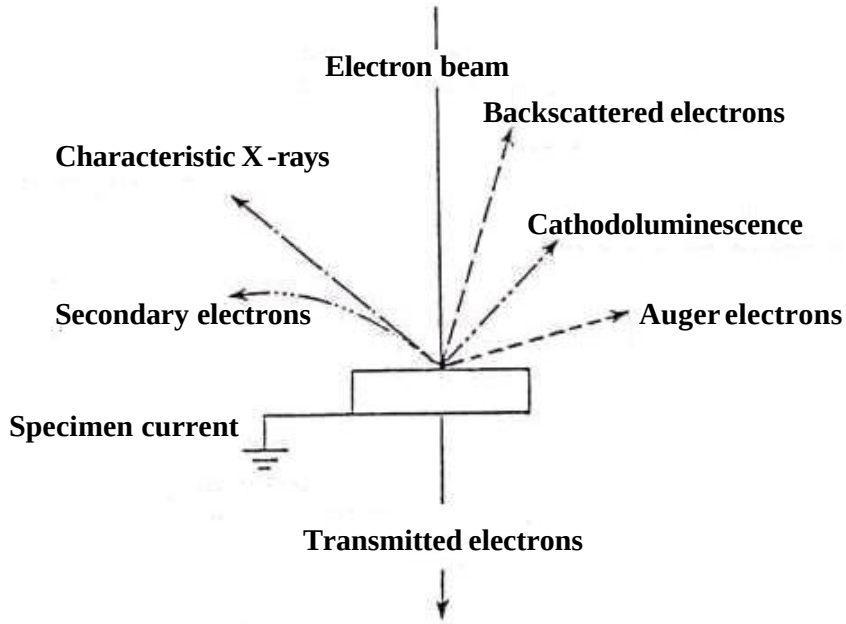

Figure 5: Schematic diagram of photons emitted by excitation occurring due to an electron beam bombardment [13].

iii) Thermoluminescence

Thermoluminescence is phosphorescence triggered by temperatures above a certain point. This should not be confused with incandescence, which occurs at higher temperatures; in thermoluminescence, heat is not the primary source of the energy, only the trigger for the release of energy that originally came from another source. It may be that all phosphorescent materials have a minimum temperature; but many have a minimum triggering temperature below normal temperatures and are not normally thought of as thermoluminescent materials [12].

iv) Electroluminescence

This process occurs if a high electric field is applied across the luminescent material. Electron-hole pairs get excited due to the applied field and as they recombine, they emit photons [1, 12].

Luminescent materials are either electrically semiconducting (band gaps < 3 eV) or insulating (band gaps > 3 eV). The difference in band gaps give rise to two mechanisms of luminescence; band gap and characteristic luminescence.

2.4 Band gap luminescence

Band gap luminescence is light emission from semiconductors due to different crystal structures. A crystal consists of a periodic arrangement of atoms, which is called a crystal lattice. There are many different kinds of crystal lattices and are classified according to their symmetries. In an isolated state, each atom has electrons that exist in discrete electronic energy levels and the states of these bound electrons are characterized by atomic wave functions. Their discrete energy levels, however, will have finite spectral width in the condensed state because of the overlaps between electronic wave functions belonging to different atoms. This is because electrons can become itinerant between atoms, until finally they fall into delocalized electronic states called electronic energy bands. The lower energy state, the valence band, gets occupied by electrons originating from bound electrons of atoms.

The energy bands having higher energies are not occupied by electrons at 0 K and are called conduction bands. Usually, in materials having crystal symmetries such as zinc-blende structures, there is no electronic state between the top of the valence band (the highest state of occupied bands) and the bottom of the conduction band (the lowest state of unoccupied bands); this region is called the band gap. Unoccupied states are called conduction bands, due to the fact that an electron in a conduction band is almost freely mobile if it is excited from a valence band.

Electrons in valence bands cannot be mobile because of a fundamental property of electrons, i.e. only two electrons (spin up and down) can occupy an electronic state. It is therefore necessary for electrons in the valence band to have empty states in order for them to move freely when an electric field is applied. After an electron is excited to the conduction band, a hole that remains in the valence band behaves as if it were a mobile particle with a positive charge. This particle is called a hole [1]. Figure 6 shows a schematic diagram of excitation to the conduction band and relaxation to the valence band.

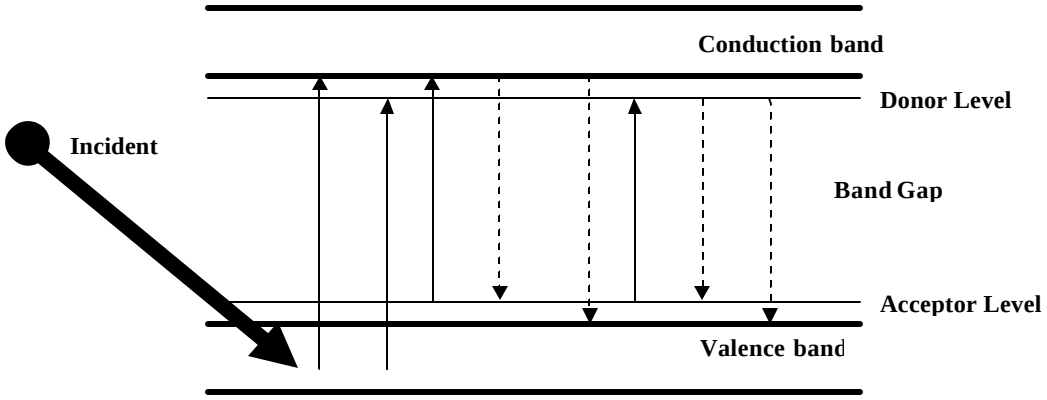

Figure 6: Schematic diagram of excitation to the conduction band and donor level and relaxation to the valence band and acceptor level.

Excitation occurs due to energy transfer from the incident, high energy, particles to electrons in the valence band. If the energy transferred is high enough the electrons get excited to the higher energy levels. Relaxation (dotted lines) is the release of the extra energy as a photon while it is de-excited back to the lower energy levels, thus luminescence occurs

A material having the above mentioned energy bands is called a semiconductor and is most commonly used for conduction purposes, other than for luminescence in phosphors. Semiconductors fall on the conduction spectrum between an insulator and a full scale conductor. Empty bands, which contain no electrons, are not expected to contribute to the electrical conductivity of a material. Partially filled bands contain electrons as well as available energy levels at slightly higher energies. These unoccupied energy levels enable carriers to gain energy when moving in an applied electric field. Electrons in a partially filled band therefore contribute to the electrical conductivity of the material.

One of the main reasons that semiconductors are useful in electronics is that their electronic properties can be greatly altered in a controllable way by adding small amounts of impurities. These impurities are called dopants. Heavy doping of a semiconductor can increase its conductivity by a factor greater than a billion.

When semiconductors (the host material) are doped with impurities, the lattice of the semiconductors is distorted and the energy level structures of the semiconductors are also affected. For example, when in Si an As atom (Group V) is substituted for a Si atom (Group IV), one electron in the outermost electronic orbit in the N shell of the As atom is easily released and moves almost freely in the Si lattice, because the number of electrons in the N shell of As (5) is one more than that in the M shell of Si (4). Thus, impurities that supply electrons to be freed easily are called donors.

On the contrary, when a Ga atom (Group III) is substituted for a Si atom, one electron is attracted from a Si atom, forming a hole that moves freely in the Si lattice. Thus, impurities that supply free holes easily are called acceptors. In a donor, one excess electron orbits around the positively charged nucleus, as in a hydrogen atom. This electron moves around in a semiconductor crystal so that the Coulomb interaction between the nucleus and the electron is weakened. The radius of the electron orbit becomes large under these conditions and the electron is greatly affected by the periodic potential of the crystal.

Therefore, the excess electron of the donor can be released from its nucleus by an excitation of small energy. This means that the donor level is located very close to the bottom of the conduction band, as shown in figure 6. Similarly the acceptor level is located very close to the top of the valence band. Impurity levels with small ionization energies are called shallow impurity levels; others can be located very deep in the forbidden band. Luminescence takes place through these impurity levels with wavelengths longer than the band gap wavelength [1].

If a semiconductor has equal numbers of electrons and holes, which means no impurities or that the semiconductor is pure enough that the impurities in it, do not appreciably affect its electrical behaviour, it is called an intrinsic semiconductor. The carriers in this case are created by thermally or optically excited electrons from the full valence band to the empty conduction band. The concentration of carriers in an intrinsic semiconductor is strongly dependent on the temperature. At low temperatures, the valence band is completely full, making the material an insulator. Increasing the temperature leads to an increase in the number of carriers and a corresponding increase in conductivity. A semiconductor that has been doped with

impurities to modify the number and type of free charge carriers present is called an extrinsic semiconductor [14, 15].

2.5 Characteristic luminescence

Characteristic luminescence occurs by doping the host lattice with either transition (3d) or rare-earth (4f) metal ions (impurities) that substitute for host lattice cations. An electron gets excited to a higher energy level in the atom itself, see figure 7.

Rare earth ions from Ce^{3+} (atomic number of 58) to Yb^{3+} (70) have partially filled 4f orbitals with energy levels characteristic to each ion and show a variety of luminescent properties around the visible region. Many of these ions can be used as luminescent ions in phosphors. There are 15 rare earth materials and the lanthanides are those rare earths with the atomic numbers between 57 (La) and 71 (Lu). The 4f electronic energy levels of lanthanide ions are characteristic of each ion.

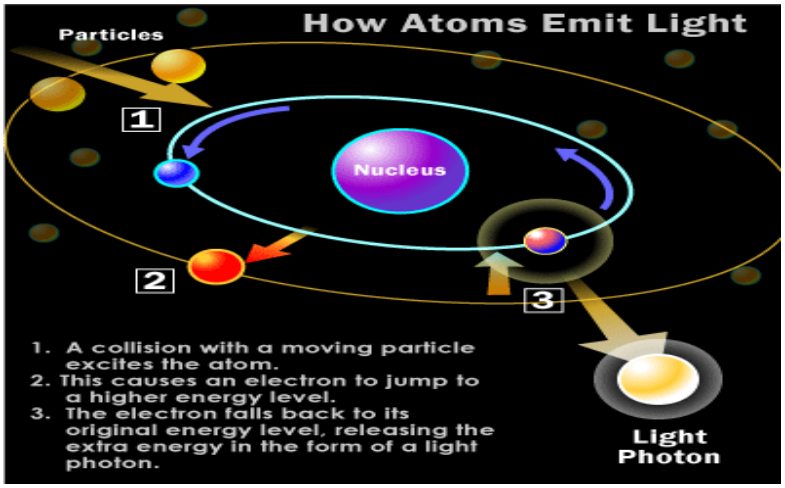

Figure 7: Schematic diagram of how atoms emit light [16].

The levels are not affected much by the environment because 4f electrons are shielded from external electric fields by the outer $5s^2$ and $5p^6$ electrons. This is in strong contrast with transition metal ions, whose 3d electrons, located in an outer orbit, are heavily affected by the environmental or crystal electric field [1]. Typical phosphors

used in CRTs and FEDs consist of a host matrix doped with activators such as the rare earths (4f) and the transition metals (3d) [3].

2.6 Y_2SiO_5:Ce

Y_2SiO_5:Ce is a blue emitting, rare earth doped phosphor that is currently being investigated for use in FEDs. Light emission is due to characteristic luminescence where electron hole pairs are created in the atom itself, emitting photons as they recombine. Ce^{3+} (Trivalent Cerium) has only one electron in the 4f shell, with an electron configuration of $[Xe].4f^1.5d^1.6s^2$. The 4f energy level splits into the $^2F_{5/2}$ and the $^2Ff_{7/2}$ levels due to the electron having the ability to exhibit a + 1/2 or – 1/2 spin. Light emission is due to the 5d ? 4f transition, resulting in the double shoulder peak see figure 8[5, 17].

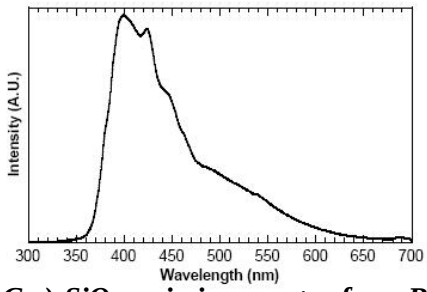

Figure 8: $(Y_{1-x}Ce_x)_2SiO_5$ emission spectra from Bosze et al [18].

The primary electrons get scattered throughout the host crystal, eventually transferring energy to the Ce^{3+} ion (situated in the band gap of the host material) resulting in excitation of the $4f^1$ electron. The luminescence photon energy depends strongly on the structure of the host crystal through the crystal-field splitting of the 4f state [1].

If an atom in a crystal is surrounded by ions, there exists a “crystal field” due to the interactions of the ions on the atom. Due to the symmetric effects, this crystal field causes the energy levels of the atom to split. A splitting of energy levels (“crystal field splitting”) occurs because the orientation of the “d” orbital wave function will increase the electron energy when the orbital is located in a region of high electron

density. In crystals the d_{xy}, d_{xz}, d_{yz}, d_{z^2} and $d_{x^2-y^2}$ energy orbitals, see figure 9, split up, depending on their cation's coordination [19].

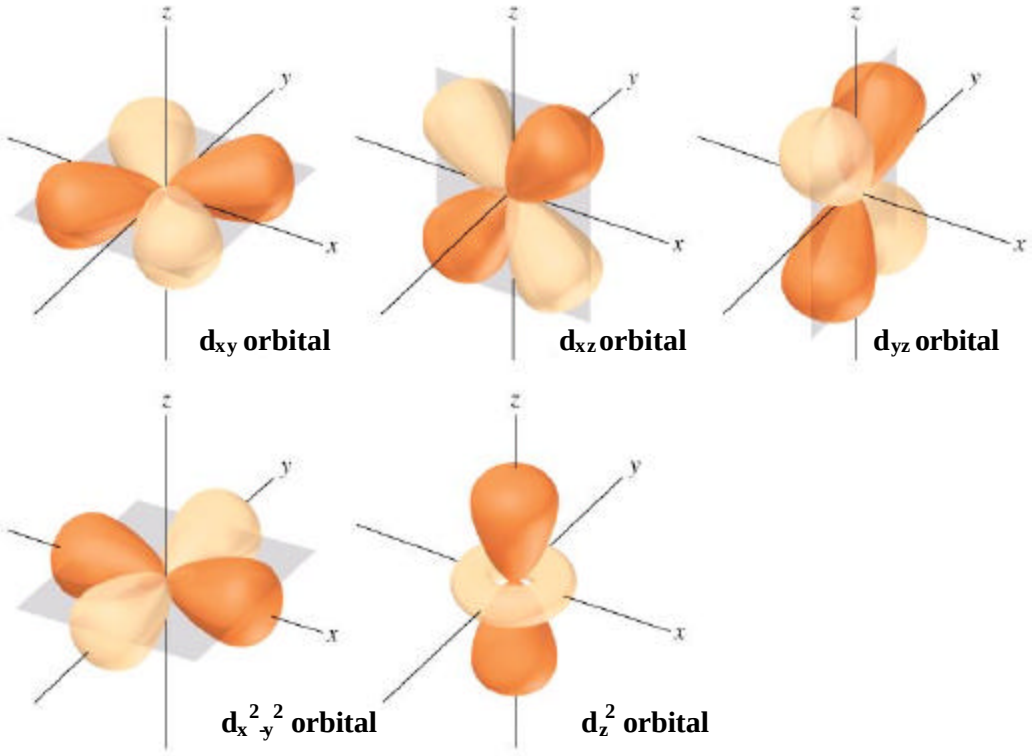

Figure 9: Schematic diagram of the 5 d energy orbitals in an atom [20].

In atoms, all "d" orbitals have the same energy because their only difference is the orientation of the orbitals. However, in a molecule, the outermost electrons may interact with other electrons if they are orientated correctly.

The 5d orbitals of an atom have the same energy associated with them. However, if an outside force is brought near the atom, the orientations of the different "d" orbitals cause them to act differently from one another. The electrons from the other atoms surrounding the specific atom, cause the "d" orbitals to split in regards to their energy. The splitting of the orbitals is called crystal field splitting, as mentioned above. Figure 10 shows the energy levels of an atom.

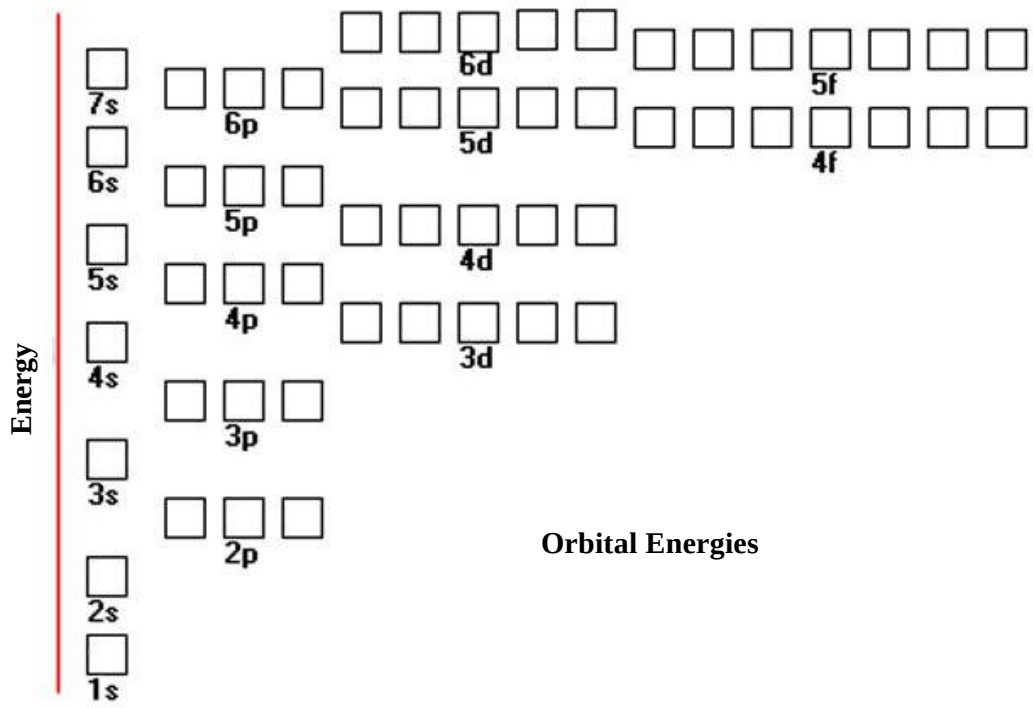

Figure 10: Schematic diagram of the Orbital Energies of an atom [21].

The colours of many solids are due to the crystal field splitting of the "d" orbitals. When a transition metal is surrounded by anions (as in a crystal), the "d" orbitals are no longer all the same energy. The anions increase the energy of the orbitals closest to it. The other orbitals must decrease in energy.

Figure 11 shows the yttrium orthosilicate (Y_2SiO_5) structure where four of the oxygen atoms are bound in a silicon tetrahedron with each corner joining two yttrium octahedrons and the fifth oxygen atoms, which are not involved with the silicon tetrahedron, are shared between four yttrium octahedrons in a rod-like chain [22].

There are many types of silicates, whose properties depend on the number of oxygen atoms that are charged instead of bonded and the cations that pair with the negative charge [23].

Y_2SiO_5:Ce is highly stable physically and chemically with respect to time and temperature as compared with other well-studied phosphor materials like ZnS and CdS. It is studied for its polymorphous nature and interesting properties related to its luminescence when doped with various rare earth ions [24].

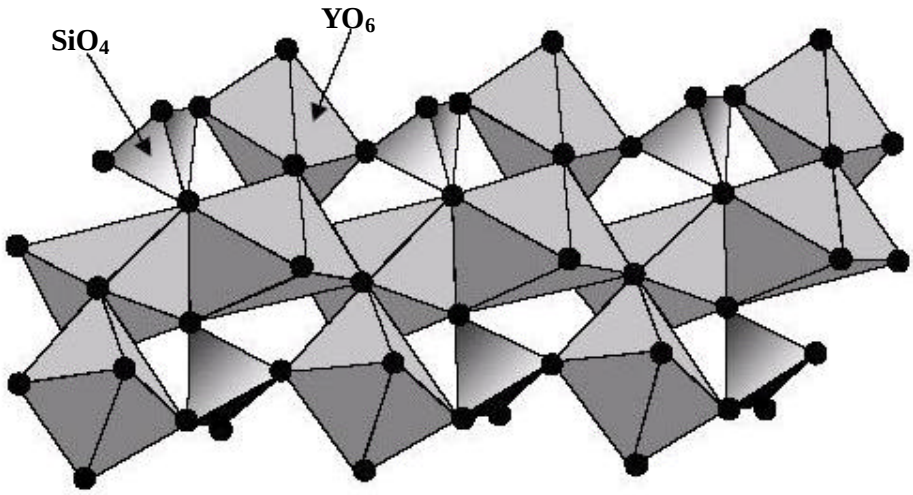

Figure 11: Schematic crystal structure of Y_2SiO_5 [22].

References

1. Shigeo Shionoya and William M. Yen, Phosphor Handbook, CRC Press LLC, Boca Raton, (1999) p. 4, 21, 49, 61, 85, 178, 186.
2. After glow decay [Online]. Available from http://www.duracorp.com/Articles/GlowAndBehold.htm [Accessed 9 March 2006].
3. A. M. Srivastava and C. R. Ronda, Phosphors, Electrochem. Soc. Inter, (2003) 48.
4. T. A. Trottier, H. C. Swart, S. L. Jones, J. S. Sebastian and P. H. Holloway, J. SID, **4/4** (1996) 351.
5. E. J. Bosze, G. A. Hirata, J. McKittrick and L. E. Shea, Mat. Res. Soc. Symp, **508** (1998) 269.
6. Visible light spectrum [online]. Available from http://www.bmb.leeds.ac.uk/pdt/science.htm [Accessed 10 January 2005].
7. J. Sebastian, S. Jones, T. Trottier, H. C. Swart and P. Holloway, J. SID, **3/4** (1995) 147.
8. The Cathode Ray Tube [online]. Available from http://electronics.howstuffworks.com/tv3.htm [Accessed 10 January 2006].
9. P. H. Holloway, T. A. Trottier, B. Abrams, C. Kondoleon, S. L. Jones, J. S. Sebastian, and W. J. Thomas, J. Vac. Sci. Technol. B , **17(2)** (1999) 758.
10. Field Emission Displays [online]. Available from http://216.122.210.132/tech/tech.htm [Accessed 10 January 2005].
11. P. H. Holloway, J. Sebastian, T. Trottier, H. C. Swart and R. O. Peteren, Solid State Technol, (1995) 47.
12. Luminescence, [online]. Available from http://www.uvminerals.org/luminese.htm [Accessed 10 January 2006].
13. Cathodoluminescence [online]. Available from http://www.cmeba.univ-rennes1.fr/niveau2/PagePrincipeMEB.htm [Accessed 12 January 2006].
14. B. Van Zeghbroeck, Principles of Semiconductor devices, (2004), Chapter 2 [online]. Available from http://ece-www.colorado.edu/~bart/book/book/content5.htm [Accessed 20 January 2006].

15. Extrinsic semiconductors, [online]. Available from http://www.doe.carleton.ca/~tjs/475_pdf_02/snew14.pdf [Accessed 15 January 2006].
16. Characteristic Luminescence [online]. Available from http://www.kushkush.me.uk/ [Accessed 15 January 2006].
17. H. C. Swart and K. T. Hillie, Surf. Interface Anal, **30** (2000) 383.
18. E. J. Bosze, G. A. Hirata and J. McKittrick, Proc. Mater. Res. Soc, **558** (1999) 15.
19. Crystal Field Splitting [online]. Available from http://scienceworld.wolfram.com/ [Accessed 13 February 2006].
20. 5d Orbitals [online]. Available from http://cwx.prenhall.com/bookbind/pubbooks/hillchem3/medialib/media_portfolio/07.html [Accessed 20 January 2006].
21. Orbital energy diagrams [online]. Available from http://colossus.chem.umass.edu/genchem/Whelan/110_Fall_2004_Daily.html [Accessed 20 January 2006].
22. Reactions for Yttrium Silicate High-k Dielectrics, James Joseph Chambers, Ph. D thesis, 2000 p. 33, 41.
23. Crystal Field Splitting [online]. Available from http://www.wwnorton.com/chemistry/overview/ch10.htm [Accessed 13 February 2006].
24. N. Karar and H. Chander, J. Phys. D: Appl. Phys, **38** (2005) 3580.

Chapter 3

Degradation

This chapter contains the theory on the ESSCR model on degradation of phosphors and the theory on defects and the effect that it may have in the crystal structure. It also contains theory on the phenomenon of total internal reflection and ends off with a summary of the results from literature studies.

Light efficiency of the FED display technology strongly depends on the phosphor material. These phosphor materials are usually wide band gap semiconductors that have been doped with impurities to modify the energy gap for the appropriate light frequency output. The distinction between an impurity and a dopant is as follows: Impurities are elements or compounds that are present from raw materials or processing. For example, silicon crystals grown in quartz crucibles contain oxygen as an impurity. Dopants are elements or compounds that are deliberately added, in known concentrations, at specific locations in the microstructure, with an intended beneficial effect on properties or processing [1].

3.1 Literature review on phosphor degradation

FEDs operation is based on cathodoluminescence (CL), similar to CRTs but with different architecture. The huge surface to volume ratio associated with the FEDs' system presents a new set of problems that affect the overall FED picture operation.

3.1.1 High pressures

The residual gases in FED vacuum devices are critical to its performance and lifetime. These gases are hydrogen, oxygen, water, methane carbon monoxide and carbon dioxide, thus resulting in the high pressure conditions for operation of FEDs. Some of the sources of these gasses in sealed FEDs are out gassing, vaporization, leaks and evolution of gasses from bulk solutions [2].

These gasses need to be removed and the vacuum maintained with a vacuum pump as in the case of CRTs where barium (Ba) is used on the glass tube as a getter pump. However, to add vacuum pumps or getter mechanisms is not always convenient and not always possible for the sealed vacuum in FEDs.

These gases thus not only contaminate the field emitter tips but also cause degradation of the phosphor materials via the electron stimulated surface chemical reaction (ESSCR) (see Chapter 1). Degradation of sulphide based phosphors, for example, resulted in the generation of volatile species such as SO_2 and H_2S. These volatile species get created due to the reaction between the phosphor and reactive gas species such as H_2O, CO_x, H_2, etc., via the electron stimulated reactions (ESSCR) [3].

Previous studies showed that the CL degradation rate is linearly dependant on oxygen pressures. High oxygen pressures will increase the degradation rate [2, 4, 5].

3.1.2 Low voltages

Due to the small cathode – anode spacing (< 0.2 – 2 mm), the FED typically operates at a voltage below that of a CRT. FEDs require higher efficiency at lower voltages (lower than 10 kV, in comparison with CRTs that require voltages between 20 and 30 kV). The lower voltages mean FEDs operate with low energy electrons which have a shallower penetration depth for cathodoluminescence (CL).

The penetration range of primary electrons only depends upon the beam energy. Therefore a decrease in the primary electron beam energy would lead to a decrease in the penetration depth. The penetration depth of injected primary electrons can be calculated by the following relationship:

$$R = bV^n \quad (1)$$

where R is the penetration distance limit, V is the voltage (kV) and b and n are empirical values for the phosphor. This means that at low voltages, luminance comes from the surface region of the phosphor material [6].

Increasing the beam energy would thus lead to an increase in the number of generated electron-hole pairs. Phosphor light intensity typically decreases faster than linearly with a decrease in the operating voltage [7].

3.1.3 Beam energies

To maintain brightness and constant power, the FEDs require higher current densities. Luminescence quenching may occur at high current densities. Quenching is defined as the reduction of phosphor efficiency with changes of operating parameters or time [3]. Brightness/intensity is directly proportional to the beam power, P = VI, where *I* is the electron beam current and *V* the potential difference between the tip and the metal gate.

Maintaining the power level means increasing the current when reducing the voltage. However, low energy (1 – 2 kV) electron beam irradiation has been found to increase degradation of CL intensity of phosphors used in FEDs which is consistent with an electron stimulated surface chemical reaction (ESSCR) model [2, 8, 9, 10].

The degradation rate depends on the energy of the electron beam, decreasing with increasing beam energy. However increasing the beam energy may also result in an increase in local temperature and may lead to saturation, which affect the degradation rate and the phosphor performance. It is known that the phosphor efficiency decreases with increasing temperature (thermal quenching) [3].

3.1.4 Saturation

Saturation occurs due to ground state depletion whereby most of the centres are already in the excited state, leaving an insufficient number of available centres in the ground state to accept energy from excited carriers [11], resulting in a decrease in CL intensity.

3.1.5 Thermal quenching

Thermal quenching occurs at high temperatures when the thermal vibrations of the atoms surrounding the luminescent centre transfer the energy away from the centre resulting in a non-radiative recombination, and the subsequent depletion of the excess energy as phonons in the lattice [6]

3.1.6 Killers

If an impurity reduces the intensity of the luminescence, it is known as a killer. Any impurity or a lattice defect can serve as a non-radiative recombination centre if it is capable of capturing a carrier of one type and subsequently capturing the opposite type of carrier [6].

3.1.6.1 Defects

The effect of defect formation on the phosphor surface can influence the CL intensity and thus lead to degradation. Defects can lead to a decrease in CL intensity for example whereby a non–luminescent trap is formed during electron bombardment (ESSCR) [10] or it can increase the CL intensity such as the intrinsic defects in SiO_2 [13].

Point defects are localized disruptions in perfect atomic or ionic arrangements in a crystal structure. The disruption affects a region involving several atoms or ions. These imperfections may be introduced by movement of the atoms or ions when they gain energy by heating, during processing of the material, by introduction of impurities, or doping.

A point defect typically involves one atom or ion, or a pair of atoms or ions, and thus is different from extended defects, such as dislocations, grain boundaries, etc. The next three sections describe the, i) vacancy, ii) interstitial and iii) substitutional point defects.

i) Vacancies

A vacancy is produced when an atom or an ion is missing from its normal site in the crystal structure. Vacancies are introduced into metals and alloys during solidification, at high temperatures, or as a consequence of radiation damage. Vacancies play an important role in determining the rate at which atoms or ions can move around, or diffuse in a solid material, especially in pure metals.

ii) Interstitial defects

An interstitial defect is formed when an extra atom or ion is inserted into the crystal structure at a normally unoccupied position. Interstitial atoms or ions, although much smaller than the atoms or ions located at the lattice points, are still larger than the interstitial sites that they occupy. Consequently, the surrounding crystal region is compressed and distorted.

iii) Substitutional defects

A substitutional defect is introduced when one atom or ion is replaced by a different type of atom or ion. The substitutional atoms or ions occupy the normal lattice site. These atoms or ions may either be larger than the normal atoms or ions in the crystal structure, in which case the surrounding interatomic spacings are reduced, or smaller causing the surrounding atoms to have larger interatomic spacings [1].

Another type of killer action, that does not necessarily require free carriers for its quenching mechanism, is the removal of energy from the nearby luminescent centre by resonance energy transfer [6]. Atoms and molecules adsorbed at the surface of the phosphor particles and defects in the crystal can often become killers and may produce a "dead voltage layer".

3.1.7 Extra layer

Degradation is dependant on energy loss [14]. Itoh et. al. [15] showed the formation of a sulphide on the surface of the ZnS:Zn phosphor under electron irradiation in a

H_2O vapour ambient. This extra sulfate layer was the result of the dissociation of H_2O on the phosphor surface. The ESSCR as mentioned before, (Chapter 1) is a degradation mechanism, postulated by Swart et. al. [5, 10] and Sebastian et. al. [9] whereby a chemical change occurs on the surface of the phosphor, resulting in the formation of an extra layer on the surface with a different chemical composition. The chemical change on the surface is a result of electron beam irradiation in the presence of an ambient gas pressure.

According to the ESSCR model, the electron beam used to irradiate the phosphor sample, dissociates the water vapour and oxygen gas into atomic species which then react with the phosphor surface, resulting in the chemical change and formation of different chemical compounds [5, 7, 9].

These new compounds on the surface can be non – luminescent and thus reducing the luminescence of the material, resulting in the "dead layer" on the phosphor surface. Oosthuizen et al. [16] proved that a ZnO layer was formed on the surface after electron bombardment with the release of SO_2 gas.

If there is adventitious carbon present on the phosphor surface, the atomic species would then also react with the carbon to form volatile compounds resulting in depletion of carbon on the surface [10, 11].

The carbon on the surface leads to another extra layer which the incoming primary electrons have to penetrate before they reach the phosphor bulk for CL excitation. Thus the thicker the surface before entering the bulk, the greater the probability of energy loss through collisions and scattering, see Figure 1, resulting in a lower CL intensity [1, 8 - 11].

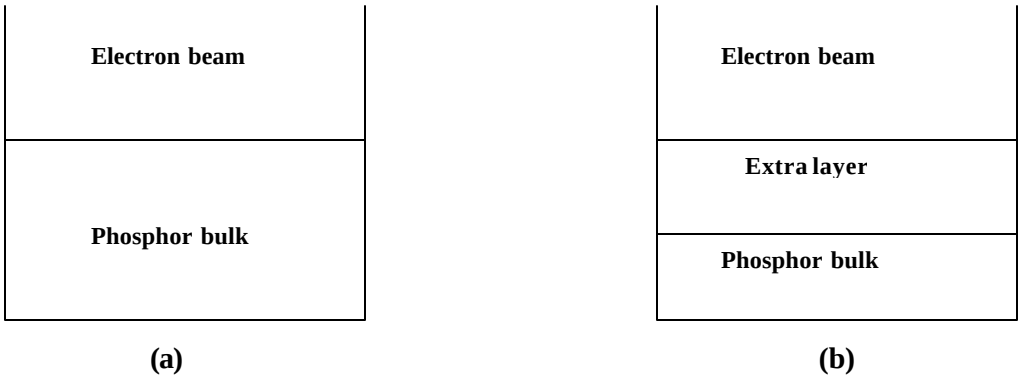

Figure 1: Schematic diagram proposing an extra layer on the phosphor surface due to ESSCR, a) before and b) after degradation.

3.1.8 Surface charging

When the primary electron beam is incident on a phosphor, secondary, back-scattered and Auger electrons are emitted from the surface at a rate different from the primary beam current, and this rate is dependant upon the beam energy and the phosphor properties. Therefore, positive or negative charges may accumulate on and below the surface to develop a space charge layer.

The accumulated charge alters the surface potential, which in turn alters the kinetic energy of the primary electrons and also increases the probability that the electron – hole pair will be swept apart before they can recombine radiatively. In some situations like in insulators such as La_2O_2S:Eu, an internal electric field may form, independent of whether there is zero, positive or negative charging effects relative to ground. The internal electric field may increase with an increase of electron beam current densities.

The fact that an internal field is induced during electron bombardment of phosphors and that transport of charge carriers is affected by electric fields suggest a possible mechanism for the CL quenching observed with time and increasing current density [3].

3.2 Some results from literature

There are many different ways of phosphor sample preparation such as laser ablation [8], sol-gel chemistry [17] and magnetron sputtering [18]. Pulsed laser deposition (PLD) has advantages over other deposition techniques with an important feature of maintaining the stoichiometry of the target material. Surface morphology and thickness can be controlled by varying some of the growth parameters, such as the ambient gas pressure and the number of pulses [19]. PLD was used for thin film preparation in this research study.

Trottier et al. [4] reported that the degradation rate of ZnS phosphors was about 3 times faster than that of Y_2O_2S:Eu, which led to more research being done on oxide based phosphors.

Research on Y_2SiO_5:Ce proved it to be a good candidate for ZnS:Ag blue emitting phosphor [13, 17, 20, 21, 22].

Holloway et al. [7] reported results on advantages of using thin film phosphors above phosphor powders. Powders have a much higher CL intensity but a significant advantage of thin films would be lower out gassing [8]. Therefore this research study includes an investigation of both thin films and phosphor powders.

Fitz-Gerald et al. [23] reported on coating the phosphor surface in order to prevent degradation. The results showed a much lower degradation rate with a CL brightness decreasing by only 12%. The coated layer should be transparent and not detrimental to the CL efficiency. Some of the thin films in this study were therefore coated with SnO_2 in order to investigate the effect of the coated layer on the CL intensity.

Hillie et al. [8] showed that the degradation rate was more severe in an O_2 ambient gas than in CO_2. He also showed that the degradation depends on the energy of the electron beam, which decreases with an increase in beam energy. [8, 14].

3.3 Total internal reflection

Total internal reflection is a phenomenon that occurs during light emission from thin films that leads to a decrease in the CL intensity, due to some of the light that gets reflected internally.

If light travels through a surface that separates two mediums, the light gets refracted. Unless an incident beam of light is perpendicular to the surface, the light's direction of travel gets changed by refraction at the surface. Figure 2 shows a light beam travelling from a glass medium to air.

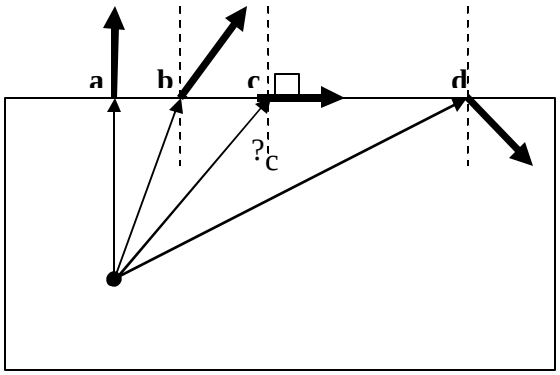

Figure 2: Schematic diagram illustrating the effect of total internal reflection for a light beam travelling from a glass medium to air.

Ray *a*, is perpendicular to the surface so part of the light gets reflected at the interface and the rest travels through it without a change in direction. As the angle of incidence increases, as for ray *b*, part of the light gets reflected and the rest gets refracted. The angle of refraction increases until it reaches 90° as for ray *c*. The incident angle is then said to be the critical angle, $?_C$. For angles of incidence larger than the critical angle, like ray *d*, there is no refracted ray and all the light is reflected. This effect is called total internal reflection.

The critical angle can be calculated by using Snell's Law:

$$n_2 \sin ?_2 = n_1 \sin ?_1 \qquad (2)$$

where n_2 and n_1 are dimensionless constants, called the index of refraction that is associated with a medium involved in the refraction. This index of refraction of a medium is equal to ***c/v***, where ***c*** is the speed of light in vacuum and ***v*** the speed in that medium. For vacuum, n is defined to be 1, and for air, n is very close to 1.0. By taking n_2 as the air medium and $?_2$ to be 90°, $?_1$ can be calculated as the critical angle [24].

References

1. D. R. Askeland and P. P. Phule, The Science and Engineering of Materials, Thompson Brooks/Cole, United States of America, (2003) p. 130.
2. P. H. Holloway, J. Sebastian, T. Trottier, S. Jones, H. C. Swart and R. O. Peterson, Mat. Res. Soc. Symp. Proc , **424** (1997) 425.
3. J. Bang, B. Abrams and P. H. Holloway, J of Appl. Phys, **94(11)** (2003) 7091.
4. T. A. Trottier, H. C. Swart, S. L. Jones, J. S. Sebastian and P. H. Holloway, J. SID, **4/4** (1996) 351.
5. H. C. Swart, L. Oosthuizen, P. H. Holloway and G. L. P. Berning, Surf. Inter. Anal, **26** (1998) 337.
6. Shigeo Shionoya and William M. Yen, Phosphor Handbook, CRC Press LLC, Boca Raton, (1999) p. 36, 566.
7. P. H. Holloway, T. A. Trottier, B. Abrams, C. Kondoleon, S. L. Jones, J. S. Sebastian and W. J. Thomas, J. Vac. Sci. Technol. B, **17(2)** (1999) 758.
8. K. T. Hillie and H. C. Swart, Appl. Surf. Sci, **183** (2001) 304.
9. J. Sebastian, S. Jones, T. Trottier, H. C. Swart and P. Holloway, J. SID, **3/4** (1995) 147.
10. H. C. Swart, J. S. Sebastian, T. A. Trottier, S. L. Jones and P. H. Holloway, J. Vac. Sci. Technol. A, **14(3)** (1996) 1697.
11. D. M. de Leeuw and G. W.'t Hooft, J. of Lumin, **28** (1983) 275.
12. H. C. Swart and K. T. Hillie, Surf. Interface Anal, **30** (2000) 383.
13. L. N. Skuja and W. Entzian, Phys. Stat. Sol. (a), **96** (1986) 191.
14. H. C. Swart, K. T. Hillie and A. P. Greeff, Surf. Interf. Anal, **32** (2001) 110.
15. S. Itoh, T. Kimizuka and T. Tonegawa, J. of Electrochrm. Soc, **136(6)** (1989) 1819.
16. L. Oosthuizen, H.C. Swart, PE Viljoen, PH Holloway, G. L. P. Berning, Appl. Surf. Sci, **120** (1997) 9.
17. P. J. Marsh, J. Silver, A. Vecht and A. Newport, J. Lumin, **97** (2002) 229.
18. K. T. Hillie, C. Curren and H. C. Swart, Appl. Surf. Sci, **177** (2001) 73.

19. Chen Li-Chyng, Particulates generated by pulsed laser ablation, in Pulsed Laser Deposition of Thin Films (eds. Chrisey D. B, Hulber, G. K), John Wiley & Sons, Inc, New York, (1994) p. 167.
20. R. Y. Lee, F. L. Zhang, J. Penczek, B. K. Wagner, P. N. Yocom and C. J. Summers, J. Vac. Sci. Technol. B, **16(2)** (1998) 855.
21. X. Ouyang, A. H. Kitai and R. Siegele, Thin Solid Films, **254** (1995) 268.
22. E. J. Bosze, G. A. Hirata, J. McKittrick and L. E. Shea, Mat. Res. Soc. Symp, **508** (1998) 269.
23. J. M. Fitz-Gerald, T. A. Trottier, R. K. Singh and P. H. Holloway, Appl. Phys. Lett, **72** (1998) 1838.
24. Halliday, Resnick and Walker, Fundamentals of Physics, John Wiley & Sons, Inc, United States of America, (2001) p. 823.

Chapter 4

Theory of research techniques and experimental procedure

The thin films investigated in this research were prepared by pulsed laser deposition (PLD). Theory on the PLD technique and characterization techniques of RBS, SEM, EDX, XRD, PL, CL, AES and XPS can be found in this chapter as well as the experimental procedure.

4.1 Pulsed laser deposition (PLD)

PLD is a technique where high-power laser pulses are used to evaporate matter from a target surface such that the stoichiometry of the material is preserved in the interaction. The evaporated particles form a plume that expands towards the substrate, adhering onto it, see Figure 1.

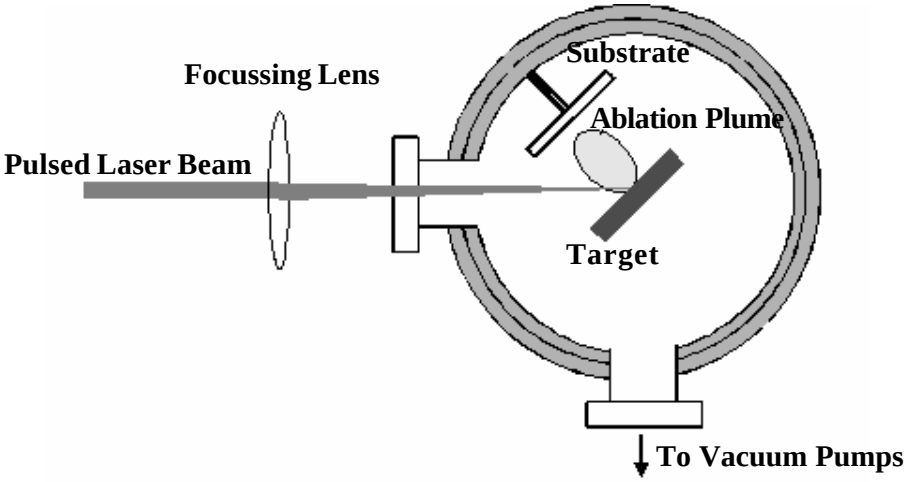

Figure 1: Schematic diagram of the PLD technique [1].

The ablation takes place in a vacuum chamber – either in vacuum or in the presence of some background gas. In the case of oxide films, oxygen (O_2) is the most common background gas. The target is mounted onto a carrousel that rotates and the substrate is mounted to a heatable sample stage. The output pulses of the laser is guided and focused onto the target by optical components – mirrors, lenses and windows. The

most important parameters to control are i) repetition rate of the laser, ii) the substrate temperature, iii) the target to substrate distance, iv) the laser energy and v) the pressure of the background gas [2].

4.1.1 Advantages of PLD

- It is conceptually simple: a laser beam vaporizes a target surface, producing a film with the same composition as the target.
- It is versatile: many materials can be ablated in a variety of gases.
- It is cost effective: one laser can serve many vacuum systems.
- It is a fast technique: high quality samples can be grown in 10 or 15 min [3].

The generation of particles by PLD is of great significance in the deposition of thin films. The particles can be classified into three categories. A specific type of particle is distinguished by whether the original matter, when just ejected from the target, is in the solid, liquid or vapour state. In general, the size of the particles formed from the vapour state tends to be in the nanometre range, while the other two counterparts are in the micron and submicron range.

The shape of the particles ejected formed from the liquid target tends to be spherical. While the particles formed from solid targets tend to be irregular in shape. The shape of the particles formed from vaporized species may be spherical or polyhedral. Surface morphology and thickness can thus be controlled by varying some of the growth parameters, such as the laser fluence, the laser wavelength, the ambient gas pressure and the target-to-substrate distance [10, 5].

4.1.2 Laser fluence

For a chosen material and a fixed laser wavelength, the laser fluence (amount of energy per pulse per unit area) has the most significant effect on the particle size and density. The laser fluence can be varied by varying the laser power or the laser spot size. At constant laser power, the particle number density is usually higher with tighter focus [5].

4.1.3 Laser wavelength

The laser wavelength, ?, comes into play mainly in the effectiveness of the absorption of the laser power by the target. The primary effect of the laser wavelength on particle generation is most likely due to the difference in the absorption coefficient when different laser wavelengths are used. Measurements that were done by Kautek et al. [5] on a 1 μm thick YBCO film, indicated the absorbance decreases with increasing wavelength. A decrease in absorbance result in a deeper penetration depth that would lead to more and larger particles generated by the laser [5].

4.1.4 Ambient gas pressure

The effect of inert ambient gas pressure on the nature of particles is most likely related to the increased collisions between the ejected species and the ambient gas as the ambient gas pressure increases. When a laser deposition experiment is done in vacuum, there are virtually no collisions between the ejected species before they reach the substrate. When the ambient gas pressure increases, the vapour species can undergo enough collisions that nucleation and growth of these vapour species to form particles can occur before their arrival at the substrate.

Since the growth mechanism is by diffusion, the residence time for the particles in the vapour controls the size of the particles. The longer the residence time, as is the case with increased ambient gas pressure, the larger the particle size [5].

4.1.5 Target-to-substrate distance

When a PLD experiment is done in a poor vacuum, with an ambient gas, or at a substantially large target-to-substrate distance in which coalescence of particles can take place, markedly different particle appearance may occur, depending on the position of the substrate. The specific effects of target-to-substrate distance and ambient gas pressure are interrelated.

Dyer et. al. [5] have shown that E/P_0 is the scaling parameter for plume range, where E is the laser-pulse energy and P_0 the background gas pressure. The length of the plume is L a $(E/P_0)^{1/3}$? with ? the ratio of specific heats of elements in the plume. When the target-to-substrate distance is much smaller than L there is no marked difference in particle size and density. As the target-to-substrate distance increases, the particle sizes increase. If the substrate is located far beyond L, the adhesion to the substrate of ejected matter is poor.

The particle size and density, thus strongly depend on the deposition parameters and by proper choice of parameters, particle generation can be minimized. Figure 2 shows the PLD system at Stellenbosch University that was used for the thin film ablation in this study.

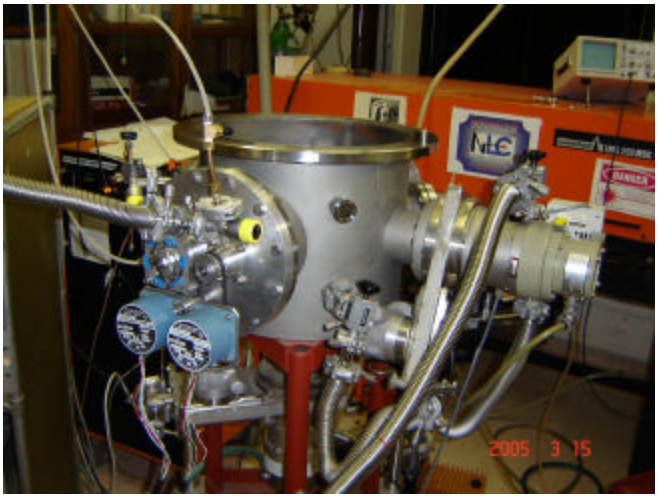

Figure 1: PLD System used for thin film ablation.

4.2 Rutherford backscattering spectrometry (RBS)

Film thicknesses in this study, were determined with RBS. It is a technique were energetic helium ions ($^4He^+$), typically having energies of several million electron volts, are directed at the sample of interest. Most of the ions implant into the sample, however some of these ions backscatter from the nuclei in the near surface (1 to 2 micron) of the sample, see figure 3.

The backscattered energy of these ions is related to the mass of the target material from which the ion backscatters. In the case of heavy target atoms such as tungsten, the backscattered energy is high (almost as high as the incident energy), but in the case of lighter target atoms such as oxygen, the backscattered energy is low.

This means that RBS is a very sensitive technique for detecting high atomic number materials like tungsten. The mass resolution or ability to distinguish between materials is very low for high atomic materials. However for light materials the resolution is very good. RBS is also used to measure the stoichiometry of thin films. This is the ratio of one material to another in the film [6].

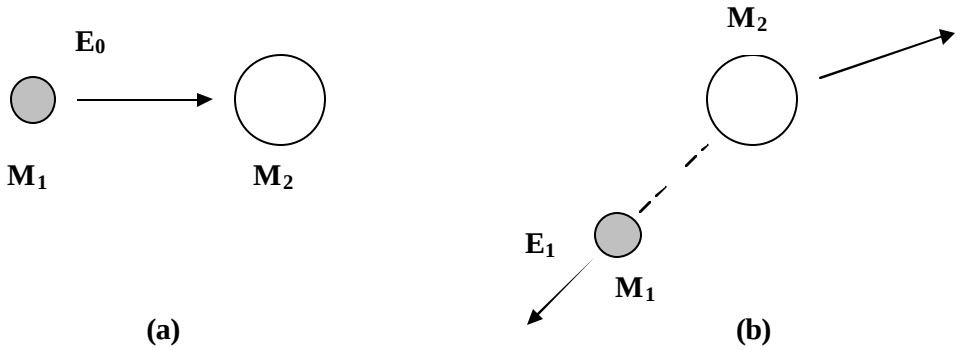

Figure 3: Schematic diagram of backscattering ion M_1 as illustration of RBS, a) before collision and b) after collision.

4.3 Scanning electron microscopy (SEM)

SEM is a type of electron microscopy capable of producing high resolution images of a sample surface. Electrons are mostly emitted via field emission, from a tungsten or lanthanum hexaboride (LaB_6) filament and accelerated towards an anode. The electron beam (typically having energies from a few keV to 50 keV) is focused by two condenser lenses into a beam with a very fine spot size.

The beam then passes through the objective lens, where pairs of scanning coils deflect the beam either linearly or in a raster fashion over a rectangular area of the sample surface, see figure 4. As the primary electrons strike the surface they are inelastically scattered by atoms in the sample. Through these scattering events, the primary beam

effectively spreads and fills a teardrop-shaped volume, known as the interaction volume, extending about 1 to 5 µm below the surface.

Interactions in this region lead to the subsequent emission of secondary electrons which are then detected, converted to a voltage and amplified to produce an image. X-rays, which are also produced by the interaction of electrons with the sample, may also be detected in a SEM equipped for Energy dispersive X-ray spectroscopy (EDX) [7].

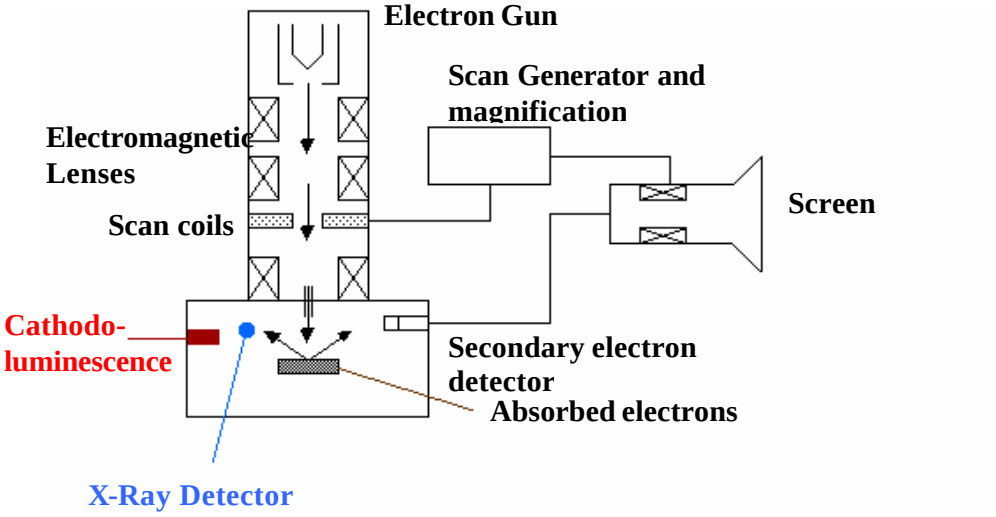

Figure 4: Schematic diagram of SEM [8].

There are two basic types of SEMs. The regular SEM, which requires a conductive sample and an environmental SEM used to examine a non-conductive sample without coating it with a conductive layer. Non-metallic samples, such as bugs, plants and ceramics should be coated so they are electrically conductive for SEM imaging. Figure 5 shows a photograph of the SEM system used in this research study.

Figure 5: SEM system used for measurements at the CSIR-NML Pretoria.

4.4 Energy dispersive spectrometry (EDS).

The surface chemical composition of the thin film grown in this study was determined by EDS spectroscopy in conjunction with SEM. Chemical analysis of a specimen can be obtained by measuring the energy and the intensity distribution of the X-ray signal generated by a focused electron beam impinging the sample. The electron gun of a scanning electron microscope is the source of the electron beam.

X-rays are the result from inelastic or energy-loss interactions between the incident electrons and the specimen atoms. The incident electrons interact with core electrons and by transferring sufficient energy to it, it can be removed from the target atom. A characteristic X-ray is occasionally emitted when the ionized atom 'relaxes' to a lower energy state by the transition of an outer-shell electron to the vacancy in the core shell. The X-ray is called characteristic because its energy equals the energy difference between the two levels involved in the transition and this difference is characteristic of the material, see figure 6.

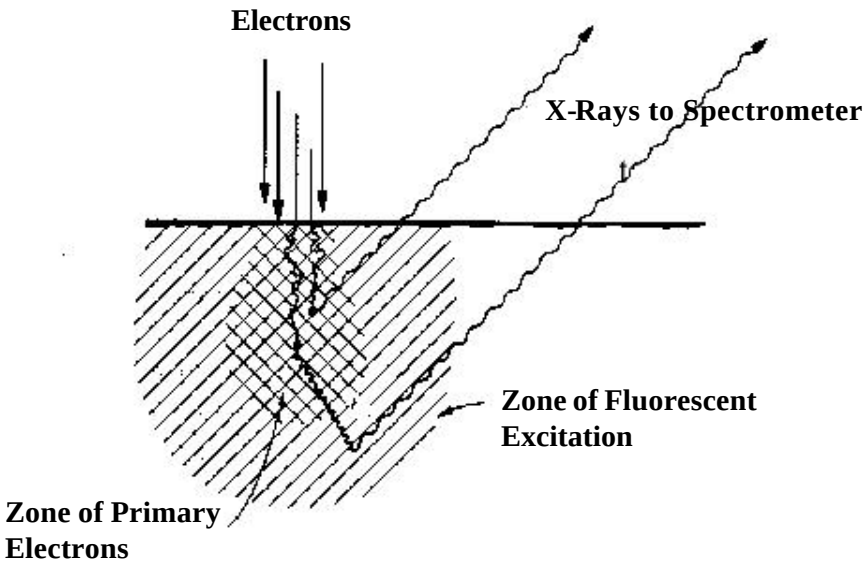

Figure 6: X-Rays emitted during EDS analysis [9].

The output of an EDS analysis is an EDS spectrum, see figure 7. The EDS spectrum is just a plot of how frequently an X-ray is received for each energy level. The EDS spectrum normally displays peaks corresponding to the energy levels for which the most X-rays have been received. Each of these peaks is unique to an atom, and therefore characteristic of a specific element. The higher a peak in a spectrum, the more concentrated the element in the specimen will be [9].

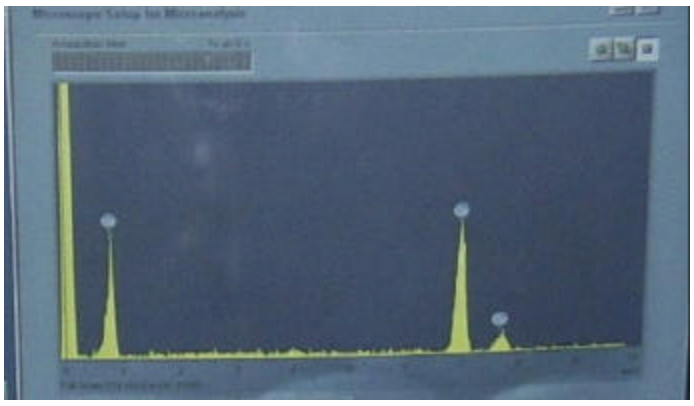

Figure 7: Example of an EDS spectrum of a Y_2SiO_5:Ce phosphor thin film.

EDS is used in hundreds of applications where knowledge of chemical information on the micro- scale is important. Major users include industry, university research institutes and government facilities. Typical applications are in materials research,

quality control, failure analysis, and forensic science. Industries that commonly use this technique include: semi-conductor and electronics, metals, ceramics, minerals, manufacturing, engineering, nuclear, paper, petroleum, bio-science, and the motor industry [9, 10].

4.5 Atomic force microscopy (AFM)

AFM stands for Atomic Force Microscopy or Atomic Force Microscope and is often called the "Eye of Nanotechnology". AFM, also referred to as SPM or Scanning Probe Microscopy, is a high-resolution imaging technique that can resolve features as small as an atomic lattice in the real space. It allows researchers to observe and manipulate molecular and atomic level features [11].

The atomic force microscope is one of about two dozen types of scanned-proximity probe microscopes, used to study surface topography and morphology. All of these microscopes work by measuring a local property - such as height, optical absorption, or magnetism - with a probe or "tip" placed very close to the sample. The small probe-sample separation (on the order of the instrument's resolution) makes it possible to take measurements over a small area [12].

AFM works by bringing a cantilever tip in contact with the surface to be imaged, as shown in figure 8. An ionic repulsive force from the surface applied to the tip bends the cantilever upwards. The amount of bending, measured by a laser spot reflected on to a split photo detector can be used to calculate the force. By keeping the force constant while scanning the tip across the surface, the vertical movement of the tip follows the surface profile and is recorded as the surface topography by the AFM.

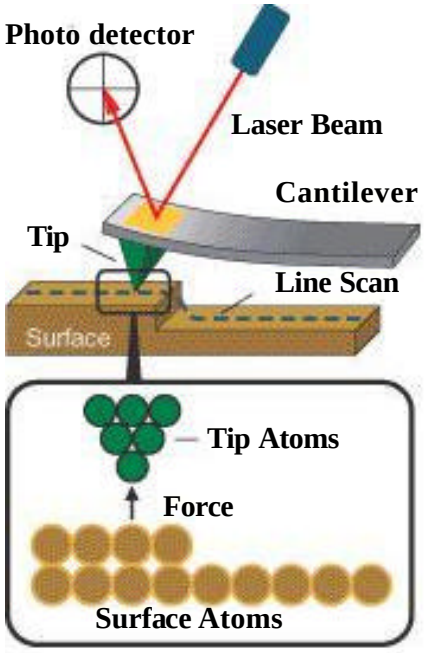

Figure 8: Schematic diagram of the AFM operated in repulsive contact mode [11].

AFM (figure 8) thus operates by measuring the attractive or repulsive forces between a tip and the sample. In its repulsive "contact" mode, the instrument lightly touches a tip at the end of a cantilever to the sample. As a raster-scan drags the tip over the sample, some sort of detection apparatus measures the vertical deflection of the cantilever, which indicates the local sample height. Thus, in contact mode the AFM measures hard-sphere repulsion forces between the tip and sample.

In no contact mode, the AFM derives topographic images from measurements of attractive forces; the tip does not touch the sample. AFMs can achieve a resolution of 10 pm, and unlike electron microscopes, it can image samples in air and under liquids. AFM incorporates a number of refinements that enable it to achieve atomic-scale resolution: [12]

- Sensitive detection
- Flexible cantilevers
- Sharp tips
- High-resolution tip-sample positioning
- Force feedback

4.6 X-ray diffraction (XRD)

The crystal structure of the phosphor sample used in this research study was determined by XRD. The planes were calculated using Bragg's Law by determining inter planar distances.

4.6.1 Crystal structure

To the naked eye, a solid appears as a continuous rigid body. Experiments have proved, however, that all solids are composed of discrete basic units called atoms. These atoms are arranged in a highly ordered manner relative to each other. Such a group of ordered atoms is referred to as a crystal. There are several types of crystalline structure, depending on the geometry of the atomic arrangement; knowledge of these is important in solid-state physics because these structures usually influence the physical properties of solids.

A solid is said to be a crystal if the atoms are arranged in such a way that their positions are exactly periodic. In some solids the atoms appear to be randomly arranged and this feature is called non-crystalline or amorphous solids, i.e. the crystalline structure is absent.

In crystallography, only the geometrical properties of the crystal are of interest. Replacing each atom by a geometrical point located at the equilibrium position of that atom result in a pattern of points having the same geometrical properties as the crystal. This geometrical pattern is the crystal lattice or simply the lattice. There are two classes of lattices: the Bravais and the non-Bravais.

In a Bravais lattice, all lattice points are equivalent, and hence by necessity all atoms in the crystal are of the same kind. On the other hand, in a non-Bravais lattice, some of the lattice points are non-equivalent. A non-Bravais lattice is sometimes referred to as a lattice with a basis [13]. Figure 9 shows a unit cell from a three dimensional lattice with the basis vectors **a,b** and **c** and the angles between the vectors.

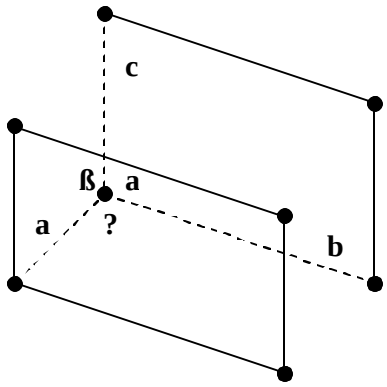

Figure 9: A unit cell from a three dimensional lattice illustrating the basis vectors a, b and c and the angles between the vectors.

Table 1: The 7 crystal systems divided into 14 Bravais lattices [13].

System	**Bravais lattice**	**Unit cell characteristics**
Triclinic	Simple	a ? b ? c a ? ß ? ? ? 90°
Monoclinic	Simple	a ? b ? c a = ß = 90° ? ?
	Base-centred	
Orthorhombic	Simple	a ? b ? c a = ß = ? = 90°
	Base-centred	
	Body-centred	
	Face-centred	
Tetragonal	Simple	a = b ? c a = ß = ? = 90°
	Body-centred	
Cubic	Simple	a = b = c a = ß = ? = 90°
	Body-centred	
	Face-centred	
Trigonal	Simple	a = b = c a = ß = ? ? 90°
Hexagonal	Simple	a = b ? c a = ß = 90°
		? = 120°

There are 14 Bravais Lattices which are divided into 7 crystal systems, see table 1. In table 1, 'simple' (SC) lattice refers to a lattice that only has points at the corners, a 'body-centred' (BCC) lattice has one additional point at the centre of the cell and a 'face-centred' (FCC) lattice has 6 additional points, one on each face.

In connection with X-ray diffraction from a crystal, it is important to know the inter planar distances between planes labelled by the same Miller indices, say (hkl). The distance is called $d_{hkl.}$ The orientation of a plane in a lattice is specified by giving its

Miller indices. To determine the Miller indices for a plane, the intercepts with the axis along the basis vectors **a,b** and **c** need to be found first. Say for example these intercepts are x,y and z, usually a fractional multiple of the basis vectors. Then form the fractional triplet

$$\left(\frac{x}{\mathbf{a}},\frac{y}{\mathbf{b}},\frac{z}{\mathbf{c}}\right),$$

invert it and then reduce it to a similar set having the smallest integers by multiplying by a common factor. This last set is then called the Miller indices of the plane [13].

4.6.2 Bragg's law

The Bragg law is the cornerstone of XRD analysis. It allows us to make accurate quantification of the results of experiments carried out to determine crystal structure. It was formulated in 1912 by W L Bragg, in order to explain the observed phenomenon that crystals only reflected X-rays at certain angles of incidence.

An X-ray incident upon a sample will either be transmitted, in which case it will continue along its original direction, or it will be scattered by the electrons of the atoms in the material, see figure 10. All the atoms in the path of the X-ray beam scatter X-rays. In general, the scattered waves destructively interfere with each other, with the exception of special orientations at which Bragg's law is satisfied.

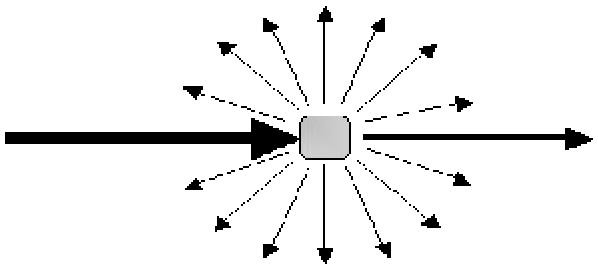

Figure 10: Schematic diagram of X-rays scattered by electrons of the atoms in the material [14].

Consider a simple crystal such as that illustrated in figure 11, with lattice planes separated by a distance d_{hkl}. As illustrated above, the scattered X-rays from this crystal will travel in random directions. A Bragg condition is such that the scattered rays from two parallel planes interact with each other in such a way as to create constructive interference. For this to happen the extra distance travelled by ray B, figure 12, must be an exact multiple of the wavelength of the radiation. This means that the peaks of each wave are aligned with each other.

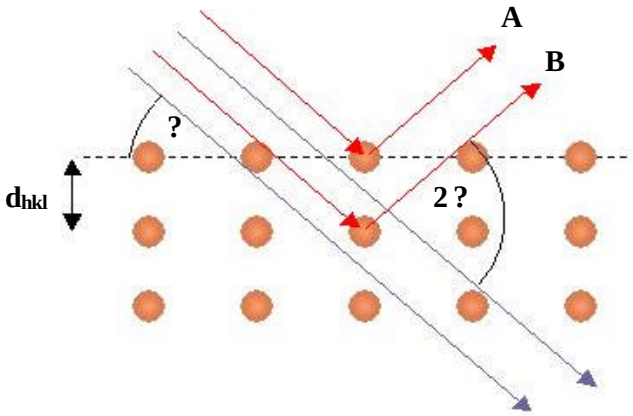

Figure 11: Schematic diagram of XRD illustrating Bragg's Law [14].

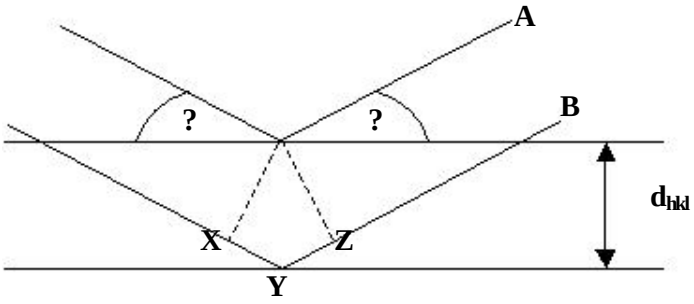

Figure 12: Schematic diagram as illustration to derive Bragg's Law [14].

The geometry of the Bragg condition is remarkably simple, and leads to the powerful result of the Bragg law:

The extra distance that ray B must travel is the distance X-Y-Z.

Thus X-Y-Z = n?

But X-Y = Y-Z = d sin ?

Hence, n? = 2 d sin ?

In order to consider the general case of hkl planes, the equation can be rewritten as:

$$n\lambda = 2 d_{hkl} \sin \theta_{hkl,}$$

since the d_{hkl} incorporates higher orders of diffraction i.e. *n* greater than 1.

The angle between the transmitted and Bragg diffracted beams is always equal to 2θ as a consequence of the geometry of the Bragg condition. This angle is readily obtainable in experimental situations and hence the results of X-ray diffraction are frequently given in terms of 2θ. However, it is very important to remember that the angle used in the Bragg equation must always be that corresponding to the angle between the incident radiation and the diffracting plane, i.e. θ.

The source of the X-rays incident on the sample, consists of an evacuated tube in which electrons are emitted from a heated tungsten filament, and accelerated by an electric potential (typically several tens of kilovolts) to impinge on a metal target. The interaction between the electrons and the target leads to the emission of X-rays: some having a wavelength characteristic of the target, and some having a continuous distribution of wavelengths between about 0.05 nm and 0.5 nm (the so-called "white radiation"). For most experiments, characteristic radiation is selected (using a filter or Bragg reflection from a suitable crystal) because of its intensity and accurately known wavelength [14].

4.7 Cathodoluminescence (CL)

Cathodoluminescence spectroscopy was used in this research to study the CL efficiency of the Y_2SiO_5:Ce phosphor thin films and powders.

Cathodoluminescence is an optical and electrical phenomenon where a beam of electrons generated by an electron gun (e.g. cathode ray tube) impacts on a phosphor causing it to emit visible light. In the case of a semiconductor specimen, the CL energy is equivalent to the energy gap between the conduction band and the valence band, see Chapter 2, section 2.3 and 2.4.

Conventionally, the cathodoluminescence method has been used widely for research of mineral specimens. Recently, it has received significant attention for developing optical devices such as the commercialization of blue LEDs and laser diodes. It is also used in various fields such as large capacity memory devices, devices for optical communication network and materials for various kinds of displays [15].

4.8 Photoluminescence (PL)

Photoluminescence spectroscopy is a contactless, nondestructive method of probing the electronic structure of materials and it was done on the Y_2SiO_5:Ce phosphor powders in this study. Light is directed onto a sample, where it is absorbed and imparts excess energy into the material. This process is called "photo-excitation." One way this excess energy can be dissipated by the sample is through the emission of light, or luminescence. In the case of photo-excitation, this luminescence is called "photoluminescence". The intensity and spectral content of this photoluminescence is a direct measure of various important material properties.

Specifically, photo-excitation causes electrons within the material to move into excited states. When these electrons return to their equilibrium states, the excess energy is released. The process may involve the emission of light (a radiative process) or it may not (a nonradiative process). The energy of the emitted light, or photoluminescence, is related to the difference in energy levels between the two electron states involved in the transition, that is, between the excited state and the ground state. The quantity of the emitted light is related to the relative contribution of the radiative process.

One application of PL spectroscopy is band gap determination. The most common radiative transition in semiconductors at or near room temperature is between states in the conduction and valence bands, with the energy difference being known as the band gap. Band gap determination is particularly useful when working with new compound semiconductors [16].

4.9 Auger electron spectroscopy (AES)

Auger Electron Spectroscopy (AES) is a surface analytical technique that determines the composition of the surface. The specimen is excited by an electron beam that can be focused into a fine probe.

4.9.1 The Auger effect

The Auger effect involves the de-excitation of an ionized atom by a non-radiative process. When an electron is ejected by an inner shell of an atom the resultant vacancy is soon filled by an electron from one of the outer shells, see Figure 13. This electron releases energy in the process of relaxation (see step 2).

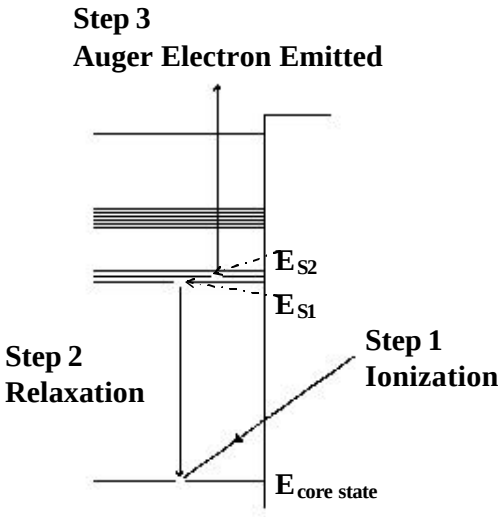

Figure 13: Schematic diagram of the Auger effect [17].

The energy released in Step 2 may appear either as an X-ray photon or be transferred to another electron which is ejected from the atom, which is then called the Auger electron. The Auger electrons move through the solid and loose some of their energy through inelastic collisions with bound electrons. However, if the Auger electron is released sufficiently close to the surface, it may escape from the surface with little or no energy loss and be detected by an electron spectrometer [18].

The primary, high energy, electrons (typically having a primary energy in the range 2 - 10 keV) have sufficient energy to ionize all levels of the lighter elements, and higher core levels of the heavier elements. Some of the electrons emitted from the surface have energies characteristic of the element from which they were emitted, and in some cases, the bonding state of those atoms.

The characteristic Kinetic Energy (KE) of the Auger electron is:

$$KE = E_{core\ state} - (E_{S1} + E_{S2}) \quad (1)$$

where S1 and S2 are the outer shell states. The KE of the Auger electron is independent of the mechanism of initial core hole formation. The orbital energies are determined by the element of the atom, thus the composition of a surface can be determined. The emission of a characteristic Auger electron is more probable for lighter elements than heavy elements (where electrons are more tightly bound to the nucleus), therefore it is more sensitive to the lighter elements [19].

For Auger spectroscopy to be conducted the specimen chamber and spectrometer must be maintained at Ultra High Vacuum (UHV) (typically at pressures of 10^{-9} and 10^{-10} Torr), as any gases present will both adsorb and scatter the very low energy Auger electrons as well as forming a thin 'gas layer' on the surface of the specimen degrading analytical performance [20].

4.9.2 Instrumentation

The basic components of an AES system are an electron gun (A), an electron spectrometer, analyzer (B), an electron detector (D) to record secondary electron images and an ion gun (C) for specimen cleaning and depth profiling, see Figure 14.

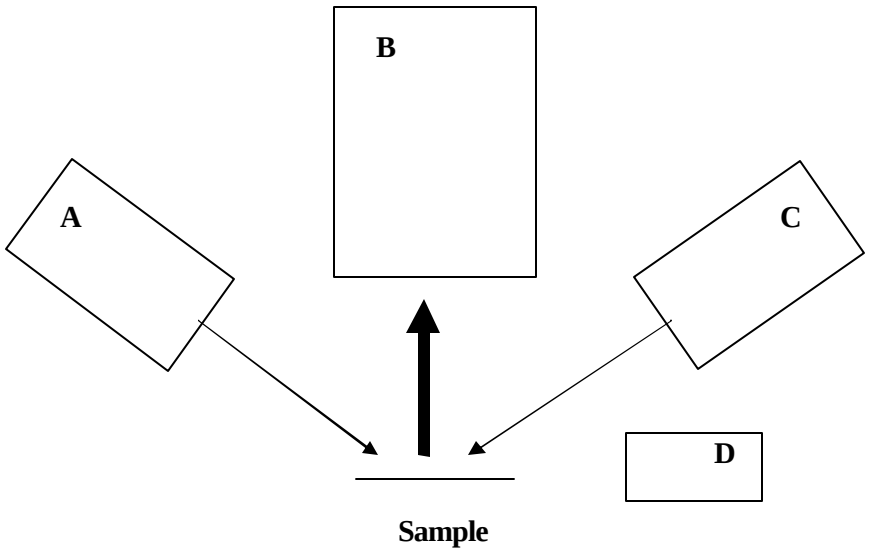

Figure 14: Schematic diagram of the basic components of an AES system.

The choice of the components will depend on the purpose of the system. The most commonly used analyzer for AES is the Cylindrical Mirror Analyzer (CMA). For practical reasons the electron gun may be incorporated into the inner cylinder of the CMA

4.9.3 Data recording

Auger spectroscopy is based upon the measurement of the kinetic energies of the emitted electrons. Each element in a sample being studied will give rise to a characteristic spectrum of peaks at various kinetic energies. Figure 15 shows an example of a direct Auger spectrum for palladium (Pd) metal - generated using a 2.5 keV electron beam to produce the initial core vacancies and hence to stimulate the Auger emission process. The main peaks for palladium occur between 220 and 340 eV. The peaks are situated on a high background which arises from the vast number of secondary electrons generated by a multitude of inelastic scattering processes [17].

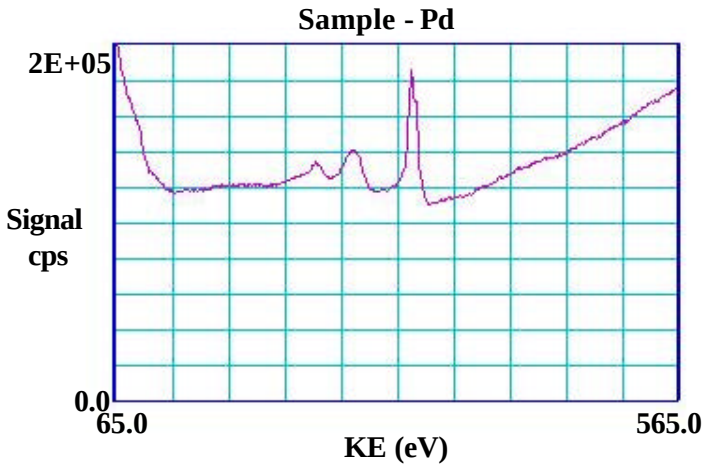

Figure 15: Auger spectrum of Pd metal - generated using a 2.5 keV electron beam [17].

The Auger electrons appear as peaks on a smooth background of back-scattered electrons. In the case of a clean surface the main peaks are readily seen and identified; however smaller peaks and those due to minor impurities on a contaminated surface are often difficult to pick out from the background.

As a result it has been usual to record Auger spectra in a differential form. The reason for this is because it is possible to actually measure spectra directly in this form and by doing so get a better sensitivity for detection. Figure 16 shows the differential spectrum of Figure 15. The differentiation removes much of the background and gives enhanced visibility to all the peaks [17].

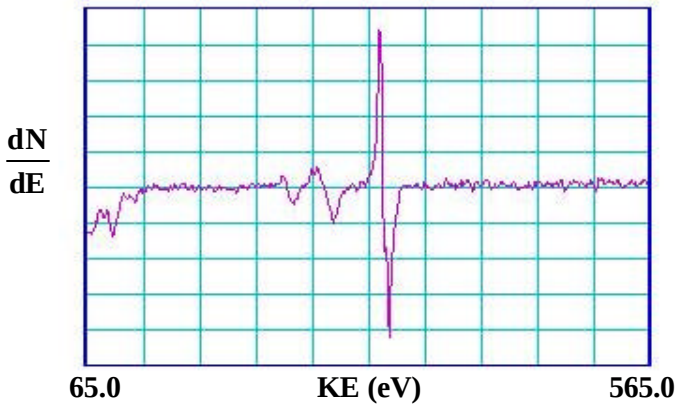

Figure 16: Differential spectrum of Pd metal - generated using a 2.5 keV electron beam [17].

4.9.4 Chemical effects

The primary use of AES peaks is to identify the elements present on the surface; particularly those involving valence electrons also carry information about the chemical state of the surface. Usually XPS is the preferred technique for investigating the chemistry of the surface as photoelectron peaks are sharper and chemical effects are more easily interpreted than is the case for the corresponding Auger peaks [21].

Useful chemical information can be deduced from Auger spectra. The chemical effect may appear as a simple peak shift, a change in peak shape or as both. A good example of peak shifts can be found in the book of Walls [21]. Both the KLL and LMM peaks showed shifts in position between pure silicon and the oxide or the nitride. These chemical effects severely complicate quantitative measurements.

4.9.5 Depth profiling

Depth profiling is one of the important applications of AES as it provides a convenient way of analyzing the composition of thin surface layers. The data is recorded as raw peak-to-peak heights plotted directly against sputtering time. The provision of composition-depth profiles by AES has had an enormous impact on the evaluation of thin films and surface coatings produced by a whole variety of methods for use in optical coatings, materials protection and for semiconductor metallization [21].

4.10 Residual gas mass analysis (RGA)

Residual Gas mass Analysis (RGA) was used in this research study to determine the different kind of gas species present in the environment during AES and CL spectroscopy. Residual gas analyzers operate by creating a beam of ions from samples of the gas being analyzed.

The molecules of the gas being analyzed are turned into ions by an ionizer through electron impact ionization, i.e., an electron beam is used to strike the gas atoms to

ionize them. This ionizing electron beam is generated by an emission filament and extracted by means of an electric field.

The resulting mixture of ions is then separated into individual species through their charge-to-mass ratios. To accomplish these, a typical RGA has three major parts, namely, an ionizer, a mass analyzer, and an ion detector. The output of an RGA is a spectrum that shows the relative intensities of the various species present in the gas. This output is known as a mass scan or mass spectrum.

The ions from the gas are distinguished from each other in terms of their masses by the mass analyzer of the RGA. There exist various techniques for mass separation, but mass analyzers used in RGA's usually employ the radio frequency (RF) quadrupole. The RF quadrupole has four cylindrical rods that are provided with combinations of AC and DC voltages of varying frequency. Only ions that possess the right mass-to-charge ratio can reach the ion collector for a given applied frequency.

In the semiconductor industry, RGA is used in identifying gases, vapours, or residues for the purpose of fixing leaks in vacuum systems and eliminating contaminants that cause process problems or product failures [22].

4.11 X-ray photo electron spectroscopy (XPS)

XPS is a surface analytical technique where primary excitation is accomplished by irradiating the specimen by a source of monochromatic X-rays. The X-rays cause photo-ionisation of atoms in the specimen and the response of the specimen is observed by measuring the energy spectrum of the emitted photo-electrons.

4.11.1 The photoelectric effect

Each atom present on the surface (except hydrogen) of the sample possesses core electrons not directly involved in the bonding. The 'binding energy' (E_b) of each core

electron is characteristic of the individual atom to which it is bound. Information on the binding energies of electrons within a sample allows qualitative elemental analysis.

In the basic XPS experiment, the sample surface is irradiated by a source of low-energy X-rays under ultra-high vacuum conditions. The incoming photons are absorbed by atoms in a molecule or solid, leading to ionization and the emission of a core (inner shell) electron. The photon having an energy of $E = h?$, which is the Einstein relation, with

h - Plank's constant (6.62×10^{-34} J.s)

? - frequency (Hz) of the radiation,

transfers its energy to the electron. If the energy is higher than E_b the electron may escape from the surface as a photoelectron and the process is called photo-ionisation.

The photo-electrons have a KE which is related to the X-ray energy, h? and binding energy E_b:

$$KE = h? - E_b \qquad (2)$$

If the photo-electrons have sufficient kinetic energy they are able to escape from the surface by overcoming the specimen work function, and photo-emission is said to occur. This entire process is referred to as the photo-electric effect [21, 23]. Figure 17 shows a schematic diagram of the photo-electric effect.

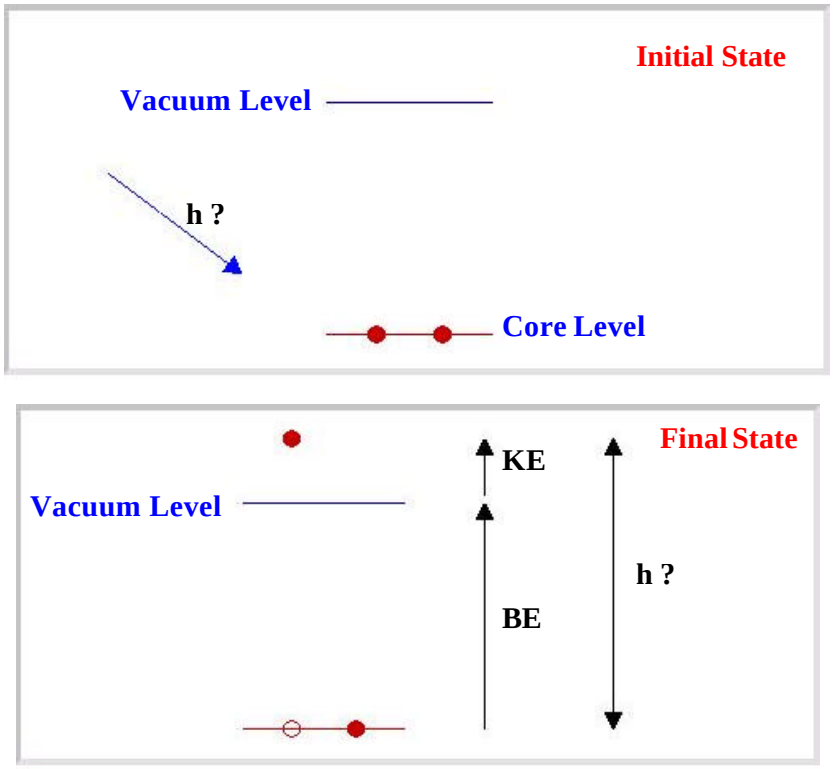

Figure 17: Schematic diagram illustrating the photoelectric effect [23].

By taking the specimen's work function into consideration the KE of the photo-electrons is then:

$$KE = h? - E_b - \Phi_s \qquad (3)$$

were Φ_s is the specimen's work function [21].

4.11.2 Chemical shifts

The fixed binding energies of the core-levels of atoms are sufficiently affected by their chemical environment to cause a detectable shift (ranging from 0.1 up to 10 eV or more in magnitude) in the measured photo-electron energy; an effect termed the "chemical shift" [21]. XPS is thus also termed as Electron Spectroscopy for Chemical Analysis (ESCA) due to the chemical shift effect.

4.11.3 Basic requirements

All XPS spectrometers must incorporate 1) a UHV environment, 2) a controlled source of X-rays, 3) a specimen manipulation system, 4) an electron energy analyzer and detection system and 5) a data recording, processing and output system.

1) UHV environment

A UHV environment is an essential requirement for almost every surface analysis technique available today. X-ray, electron and ion sources, electron analyzers and detectors will operate only under high vacuum or ultra-high vacuum conditions. UHV conditions are achieved through the use of stainless steel and glass construction materials, combined with suitable UHV pumping facilities.

2) X-ray source

One of the necessary characteristics of an X-ray source suitable for XPS is that the X-ray energy should be sufficiently high to excite core-level electrons of all elements. The two elements mostly used as X-ray sources for XPS are magnesium (Mg) and aluminium (Al). Most commercial XPS instruments are fitted with twin X-ray sources incorporating both Al and Mg anodes.

The advantage of having both AlK_a and MgK_a radiation available lies in the fact that photo-ionisation produces not only photo-electrons, but also, via Auger decay of the electron - hole formed, Auger electrons. The kinetic energy of the Auger electron is independent of the X-ray energy used to create the hole, whereas the kinetic energy of the photoelectron is related to the X-ray energy via the Einstein relation, see section 4.11. 1.

The binding energy of Auger peaks during XPS analysis appears to change by 233 eV on going from AlK_a to MgK_a radiation (or visa versa) whereas the photoelectron peaks do no shift in binding energy. This feature of XPS may be used not only to differentiate between photo-electron and Auger peaks in the spectrum, but also to

resolve photo-electron and Auger peaks which may otherwise overlap with each other [21].

3) The specimen

In principle, all types of samples including gases and liquids, may be studied by XPS, but limitations on instrument design usually restrict the range to low vapour pressure ($< 10^{-6}$ Torr), solid samples. Restrictions may also be imposed on sample size. Early instruments were designed to hold only one sample at a time but modern spectrometers are able to handle a number of powders, fibre or bulk solid samples independently and simultaneously. Methods of sample mounting are numerous and are often dictated by the nature of the sample itself.

4) The electron energy analyzer

The electron energy analyzer is the heart of every XPS spectrometer. Its function is to disperse photo-electrons emitted from the specimen, according to their energies, across a detector or detector array. The analyzer used is the spherical sector (or concentric hemispherical) electrostatic analyzer (SSA).

5) Data recording, processing and output

Following energy dispersion in the SSA, the photo-electrons are made to enter an electron multiplier detector or detector array. Here each incident photo-electron causes a secondary electron cascade resulting in an output pulse of up to 10^8 electrons with less than 0.1 μs duration. Since the detector output is in the form of discrete pulses, XPS is ideally suited to conventional digital spectrum acquisition and processing techniques [21].

4.11.4 Depth profiling

It is also possible to use XPS to investigate the variation of composition with depth into the sample in several ways, thereby producing a composition-depth profile of the surface of interest [21].

4.12 Experimental procedure

4.12.1 Y_2SiO_5:Ce thin films growth

Silicon (Si) (100) substrates were cleaned in acetone for 5 min, in an ultrasonic water bath and then for 5 min in methanol. The substrates were blown dry with nitrogen (N_2) gas. Commercially available Y_2SiO_5:Ce standard phosphor powders were pressed into a pellet and annealed at 600°C for about 16 hr.

The Lambda Physic EMG 203 MSC excimer XeCl laser with wavelength (?) = 308 nm was used to grow the thin films. The laser energy was 81.81 mJ, vacuum base pressure was 3 x 10^{-5} Torr before the system was backfilled with oxygen ambient gas to a pressure of 7.5 x 10^{-4} Torr, the substrate temperature was 400°C, repetition rate was 10 Hz, target to substrate distance was 3.7 cm, 6600 laser pulses were used to ablate the phosphor layer and 1200 pulses were used to ablate the SnO_2 layer on some of the thin films.

4.12.2 Characterization of the Y_2SiO_5:Ce thin films

RBS was used to measure the thickness of the thin films by using a 3.100 MeV $^4He^+$ beam. SEM images were taken with the Gemini LEO 1525 Model at the CSIR – NML (Council for Scientific and Industrial Research – National Metrology Laboratory), Pretoria and at the centre for Confocal and Electron Microscopy, UFS with the Jeol 6400 Winsem model, to determine surface morphology of the thin films.

AFM, that was done with the Digital Instruments Multi Mode with Nano Scope IV Controller and JV Scanner model, and EDS, done with the Oxford 1525 model, analysis were used to monitor surface morphology and topography of the thin films. The crystal structure of the thin films was determined with XRD, using a Siemens Diffractrometer D5000 equipped with a Cu source.

4.12.3 Characterization of the Y_2SiO_5:Ce phosphor powders

SEM images were taken with the Gemini LEO 1525 Model at the CSIR – NML (Council for Scientific and Industrial Research – National Metrology Laboratory), Pretoria, to determine surface morphology of the commercially available Y_2SiO_5:Ce phosphor powders, obtained from Phosphor Technology. The crystal structure of the powders was determined with XRD, using a Siemens Diffractrometer D5000 equipped with a Cu source.

4.12.4 AES, CL spectroscopy and RGA for both the thin films and phosphor powders

AES and CL spectroscopy, both excited by the same electron beam, using 2 keV electrons with beam current densities between 26.3 $mA.cm^{-2}$ and 52.63 $mA.cm^{-2}$ were used to monitor changes in the surface chemical composition and luminous efficiency.

The Auger and CL measurements were made in an ultrahigh vacuum (UHV) chamber with a PHI Model 549 system, in oxygen pressures between 1×10^{-8} Torr and 1×10^{-6} Torr. CL data for the peak intensity at ? = 440 nm, were collected for 24 hrs with a Ocean Optics S2000 spectrometer. RGA was performed to determine the volatile gas species during electron bombardment, by using the Anavac-2 mass analyzer.

4.12.5 PL spectrometry for the phosphor powders

PL, excited by a HeCd laser, ? = 325 nm, power of 8.8 mW, was also performed on the phosphor powders at the Nelson Mandela Metropolitan University (NMMU).

4.12.6 XPS for both the thin films and the phosphor powders

XPS was done to determine the chemical composition of the phosphor surface before and after 24 hr electron beam bombardment. XPS data were collected with a Quantum 2000 system, using monochromatic Al K_a X-rays and Multipak, version 6, computer software.

References

1. Pulsed Laser Deposition [online]. Available from http://www.chm.bris.ac.uk/ [Accessed 5 March 2005].
2. Laser Ablation Technique, [online]. Available from http://www.hut.fi/Units/AES/projects/prlaser/ablation.htm [Accessed 5 March 2005].
3. Pulsed Laser Deposition, [online]. Available from http://www.esrf.fr/UsersAndScience/Experiments/CRG/BM25/inhouseresearch/supportlaboratory/PLD [Accessed 14 February].
4. K.T. Hillie and H.C. Swart, Appl. Surf. Sci, **183** (2001) 304.
5. Chen Li-Chyng, Particulates generated by pulsed laser ablation, in Pulsed Laser Deposition of Thin Films (eds. Chrisey D. B, Hulber, G. K), John Wiley & Sons, Inc, New York, (1994) p. 167.
6. Thin Film Analysis, Inc, San Jose, CA 95135, (408) [online]. Available from http://www.tfainc.com [Accessed 25 November 2005].
7. Scanning electron microscopy – Wikipedia, the free encyclopedia, [online]. Available from http://en.wikipedia.org/wiki/Electron_microscope [Accessed 25 November 2006].
8. Scanning Electron Microscopy [online]. Available from http://www.uccs.edu/ [Accessed 5 April 2005].
9. Energy Dispersive Spectroscopy [online]. Available from http://ion.eas.asu.edu/descript_eds.htm [Accessed 17 February 2006].
10. J. I. Goldstein, D. E. Newbury, P. Echlin, D. C. Joy, C. Fiori and E. Lifshin, Scanning Electron Microscopy and X-ray Microanalysis, Plenum Press, Springer, (1981) p. 6.
11. Atomic Force Microscopy, [online]. Available from www.molec.com/what_is_afm.html [Accessed 22 February 2006].
12. The tip-sample interaction in atomic force microscopy and its implications for biological applications ", Ph.D. thesis by David Baselt, California Institute of Technology.
13. M. Ali Omar, Elementary Solid State Physics: Principles and Applications, Addison – Wesley Publishing Company, United States of America, (1975) p. 4, 6.

14. X-Ray Diffraction, [online]. Available from http://www.doitpoms.ac.uk/tlplib/index.php [Accessed 10 December 2005].
15. Cathodoluminescence, [online]. Available from http://www.jeol.com/jeolnews/jeol_news601/News%20home/35/index.html [Accessed on 14 March 2006].
16. NREL Measurements and Characterization - Photoluminescence Spectroscopy, [online]. Available from http://www.nrel.gov/measurements/photo.html [Accessed 15 December 2005].
17. Auger, [online]. Available from http://www.phi.com/genf.asp_Q_ID_E_281 [Accessed 17 February 2006].
18. Auger Electron Spectroscopy, [online]. Available from http://www.chem.qmul.ac.uk/surfaces/scc/scat5_2.htm [Accessed 15 December 2005].
19. The Auger Process, [online]. Available from http://www.phi.com/genf.asp_Q_ID_E_281 [Accessed 16 December 2005].
20. Auger Electron Spectroscopy, [online]. Available from http://en.wikipedia.org/wiki/Auger_electron_spectroscopy [Accessed 17 December 2005].
21. J. M. Walls, Methods of surface analysis, Cambridge University Press, Great Brattain, (1989), p. 110, 111, 117, 132, 135, 140, 143, 152.
22. Residual Gas Analysis, [online]. Available from http://www.semiconfareast.com/rga.htm [Accesses 18 December 2005].
23. Photoelectron Spectroscopy, [online]. Available from http://www.chem.qmul.ac.uk/surfaces/scc/scat5_3.htm [Accessed 20 December 2005].

Chapter 5

Characterization and degradation of powders - Results and Discussion

Chapter 5 contains the results obtained and the discussions of the characterization of the phosphor powders, the emission mechanism in Ce^{3+} and the formation of SiO_2 on the surface during degradation.

5.1 SEM

SEM images of the commercially available Y_2SiO_5:Ce phosphor powders were obtained to determine the surface morphology. Figure1a) shows the SEM image of the powders taken with 2 keV electrons with a magnification of 600x, and b) shows the same area but with a magnification of 1000x. Figure 1 shows that the Y_2SiO_5:Ce phosphor powders was agglomerated.

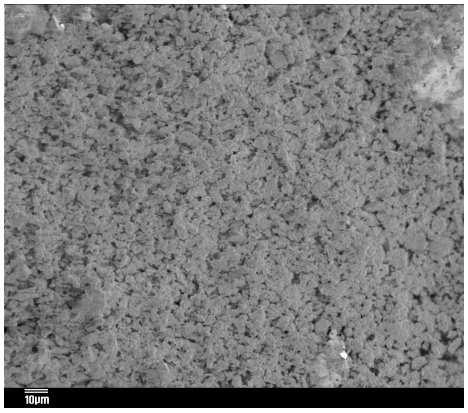

(a)

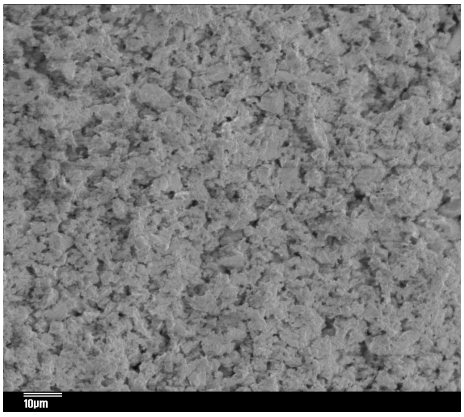

(b)

Figure 1: a) SEM image of the powders taken with 2 keV electrons with a magnification of 600x, and b) the same surface area with a magnification of 1000x.

5.2 XRD

XRD results (figure 2) showed the peaks of the monoclinic crystal structure of Y_2SiO_5:Ce phosphor powders used in this research. As mentioned, it is very difficult to study the crystal structure of Y_2SiO_5:Ce.

The crystal planes were calculated by using Bragg's law. A crystal system is described by three vectors. In the monoclinic system, the crystal is described by vectors of unequal length, as in the orthorhombic system. Two of the vectors are perpendicular, while the third makes an angle other than 90° with the plane formed by the first two.

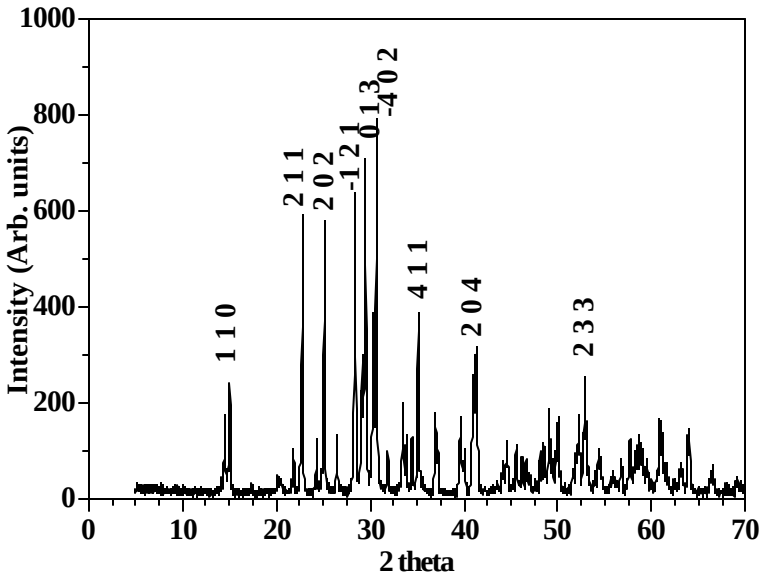

Figure 2: XRD results for the Y_2SiO_5:Ce phosphor powders.

5.3 Degradation

5.3.1 Electron beam size

The electron beam, used for AES and CL spectroscopy, was measured to be about 220 μm in diameter. The electron beam current was measured with an electrometer while moving the electron beam horizontally from the inside of the hole of the Faraday cup (beam current at maximum) to the outside, in the Auger vacuum chamber, a method used by Oosthuizen et al. [1]. Figure 3 shows the electron beam current plotted against moving distance. Figure 4 shows the differentiated spectrum of figure 3, with the electron beam diameter measured at full width half maximum (FWHM). A diameter of 220 μm results in an electron beam surface spot size area of 3.8×10^{-8} m^2.

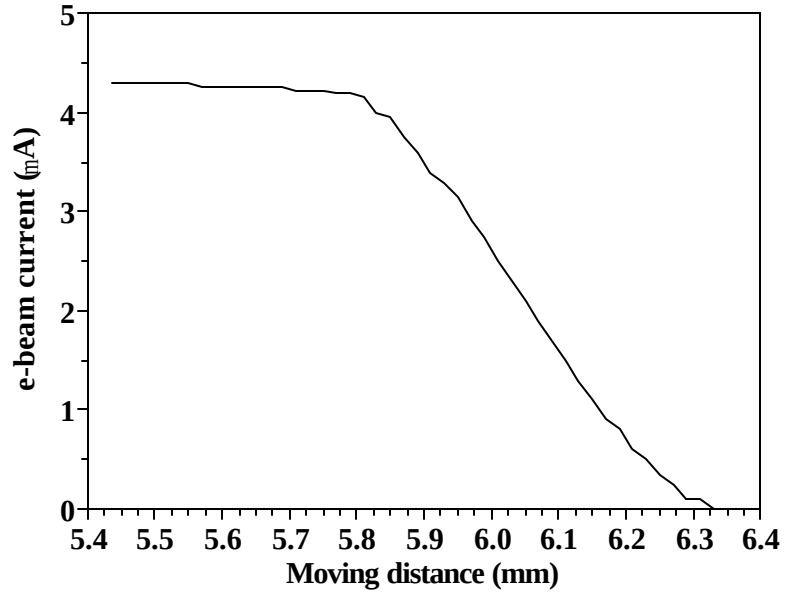

Figure 3: The electron beam current plotted against moving distance.

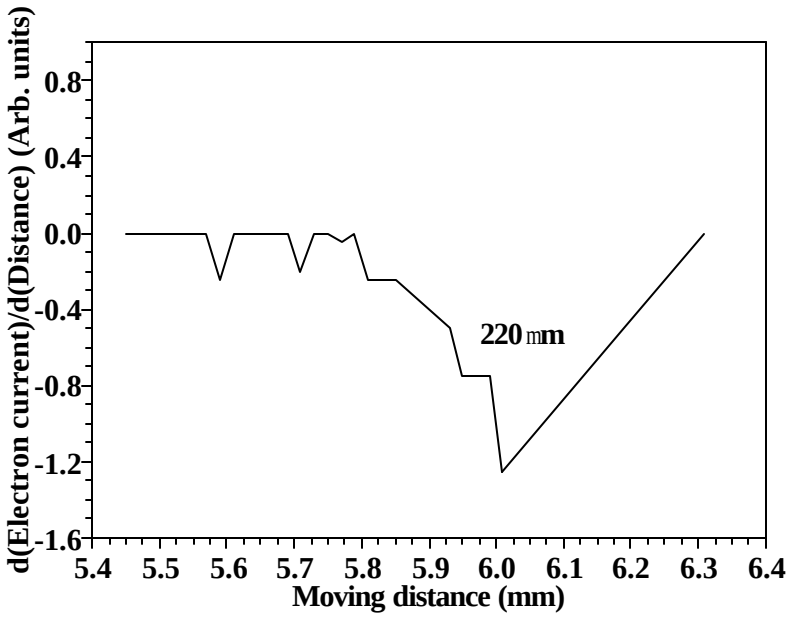

Figure 4: Differentiated spectrum of the electron beam current with the beam diameter measured at FWHM.

5.3.2 AES and CL spectroscopy

Figure 5b) shows the Auger peak to peak heights (APPHs) for Carbon (C 272 eV), Silicon (Si 65 – 92 eV), Yttrium (Y 110 – 135 eV) and Oxygen (O 503 eV) with the CL (440 nm) plotted against electron dose ($C.cm^{-2}$) in an oxygen pressure of 1×10^{-6} Torr with the electron current density at 26 $mA.cm^{-2}$. Due to the low concentration of

Ce it was not detected by AES. As expected, the chemical bonding state of Y and Si in Y_2SiO_5:Ce have a major effect on the energy position of the low energy peaks in the AES spectra of the Y_2SiO_5:Ce phosphor powders, figure 5a). The electron current density was calculated to be 26.3 $mA.cm^{-2}$ by using an electron beam current of 10 µA. Time and beam current were converted to coulomb load (C) and the beam area was used to convert it to electron dose ($C.cm^{-2}$).

The presence of Si in its pure form should be manifested by a peak at 92 eV and Y with peaks at 100, 110 and 127 eV [2]. Si in SiO_2 was previously measured at 80 eV [3]. In the present case the main peaks were measured at 83.5 eV and 124.5 eV for Si and Y, respectively. Yttrium has a very low sensitivity factor for AES electrons. No major changes in the APPHs were measured during the degradation process as shown in Figure 5b). The CL intensity, however, decreased until about 300 $C.cm^{-2}$ and then slowly increased. The increase in the CL intensity against the wavelength for the light emitted from the powders before and after 24 hr degradation is shown in Figure 6a). Figure 6b) shows the area under the curves plotted against time in hr. Lee and Kim [4] measured the CL degradation of coated and uncoated Y_2SiO_5:Ce phosphors. The measurements were done for coulomb doses of up to 150 C cm^{-2}. A decrease of about 12% of the original intensity was measured for the uncoated phosphor. The degradation was however not measured for higher electron doses as in the present case.

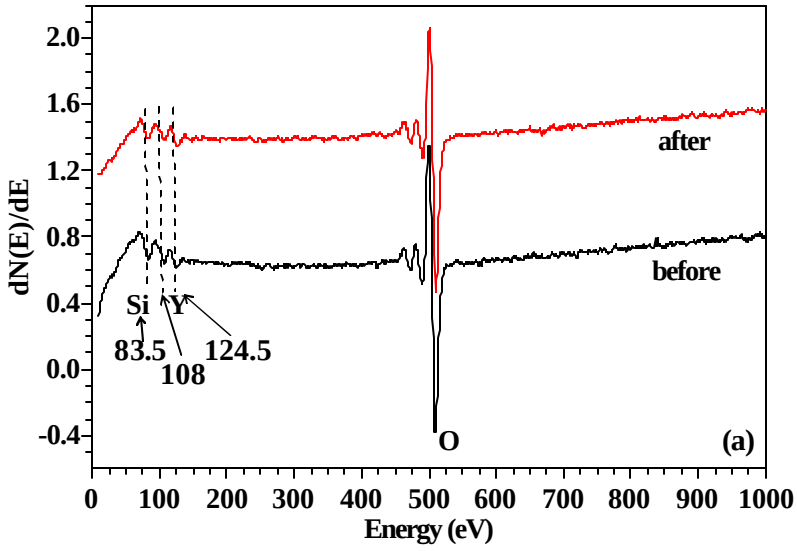

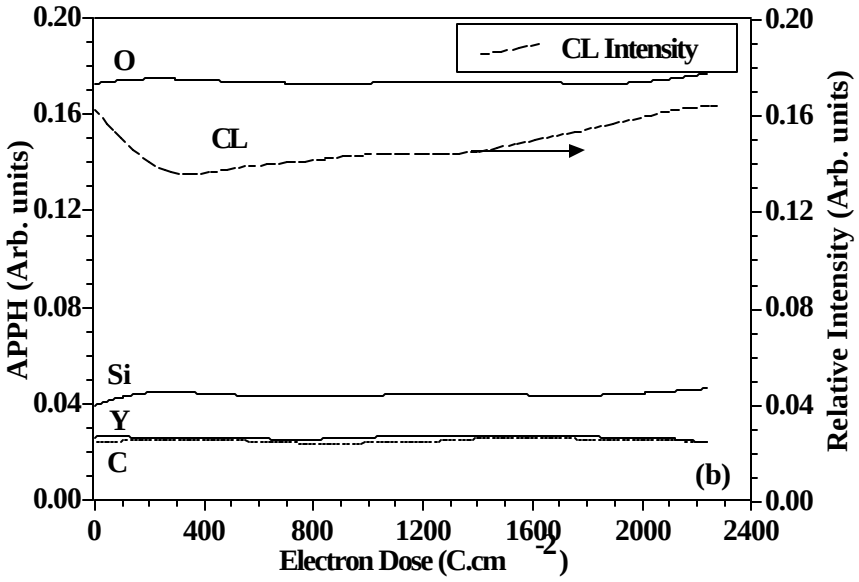

Figure 5: a) AES spectra in the powders before and after degradation and b) the APPHs and CL against Electron Dose (C.cm^{-2}).

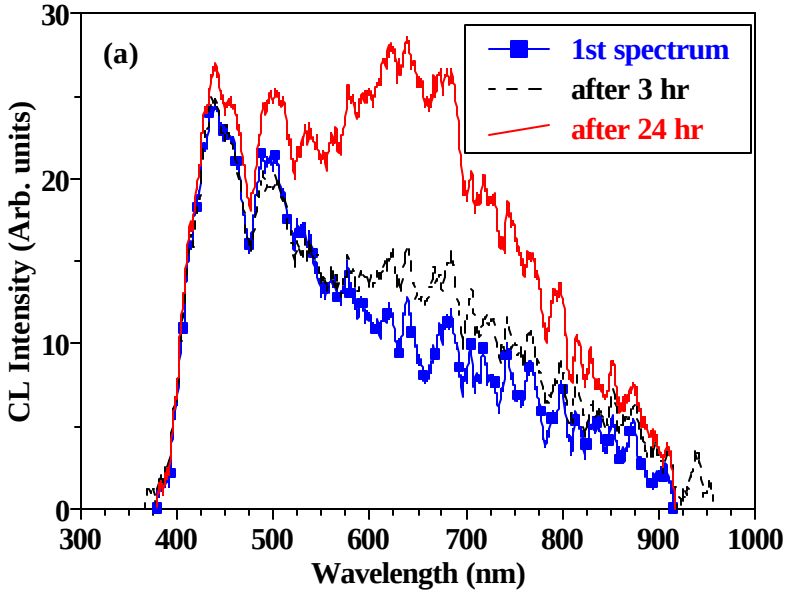

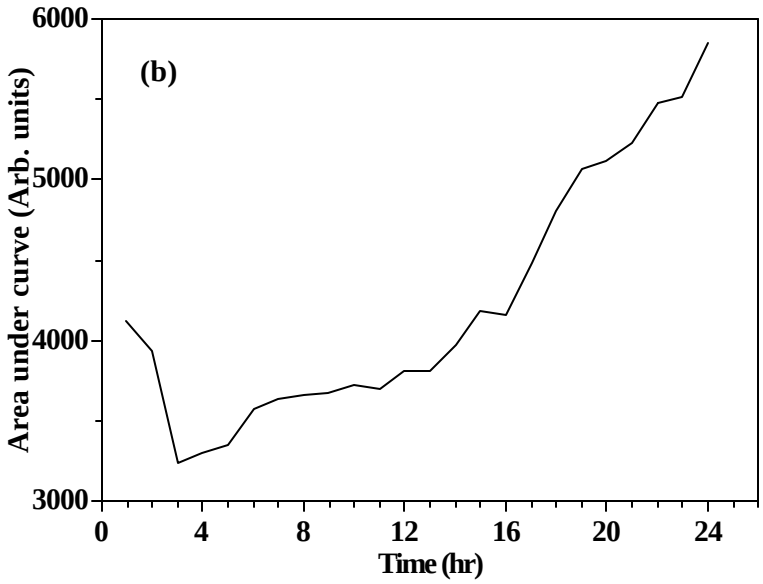

Figure 6: (a) CL intensity against the wavelength for the light emitted from the powders before and after 3 hr and 24 hr electron bombardment and (b) the area under the curves in a) versus time in hr.

The first spectrum in figure 6a) shows the emission of the bright blue colour visibly detectable with the human eye with two main peaks at the wavelengths of 440 and 500 nm. This spectrum is characteristic of the doublet character of blue light emission from Ce^{3+}, due to the 4f ground state splitting [5, 6, 7]. In Ce^{3+} the 5d and 6s electrons shield the inner 4f electron. This results in the 5d ? 4f transition to be very sensitive to the host lattice and crystal field [8]. The 4f level is affected by the crystal field and it is different in host materials with different crystal structures. Different crystal fields leads to different splitting effects of the 4f energy level. [9] see section 2.6.

It is postulated [5, 7] that in Y_2SiO_5:Ce the transition is more likely to be from the lowest 5d level to the $^2F_{5/2}$ level, emission at 440 nm (higher energy) see figure 7. Bosze et al. [10], reported similar results. Due to the difficult crystal structure of Y_2SiO_5:Ce the Ce^{3+} ion can be positioned at different sites in the host lattice, resulting in the broad band emission at 440 and 500 nm.

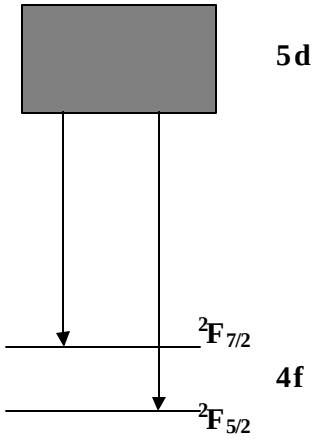

Figure 7: Schematic proposed diagram of the transition from the 5d energy levels to the 4f levels in Ce^{3+}.

The CL increase in Figure 5b) after an electron dose of 300 $C.cm^{-2}$, is the result of the increased intensity of a peak arising between 600 and 700 nm (maximum intensity at 650 nm), contributing with emission that extends into the blue region between 600 and 400 nm, as can be seen in figure 6a). The variation in CL intensity from 700 to 1000 nm can be attributed to noise. The colour of the blue light thus changed to whitish, which is due to a chemical composition change on the phosphor surface. The decrease at first and then the increase in CL intensity are also indicated by figure 6b), which shows the decrease in the integrated luminescence within the first 3 hrs and then the increase until 24 hr.

5.4 RGA

RGA was done during AES and CL spectroscopy and the results indicated a lower intensity of some of the gasses with the electron beam off, figure 8, than with the electron beam on. The higher intensity of the volatile species with the electron beam on in an oxygen gas pressure of 1×10^{-6} Torr is due to ESSCR with adventitious carbon, hydrogen and oxygen in the environment.

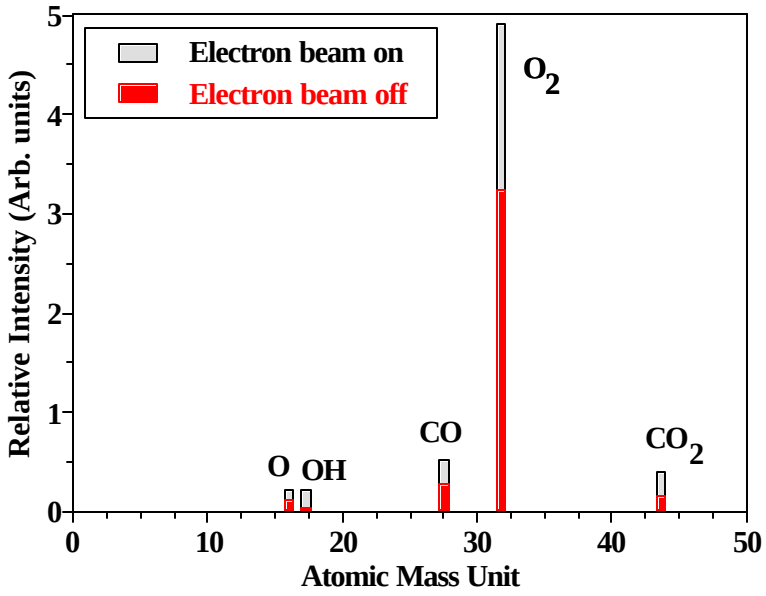

Figure 8: RGA results for the electron beam on and off.

5.5 PL spectroscopy

Figure 9 shows the blue PL emission spectrum which is in agreement with results reported thus far for PL spectroscopy of Y_2SiO_5:Ce [5, 7]. The emission of blue light as shown in figure 6, between 400 and 500 nm, is a result of transitions from the 5d energy level in Ce^{3+} to the $^2F_{5/2}$ and $^2F_{7/2}$ energy level.

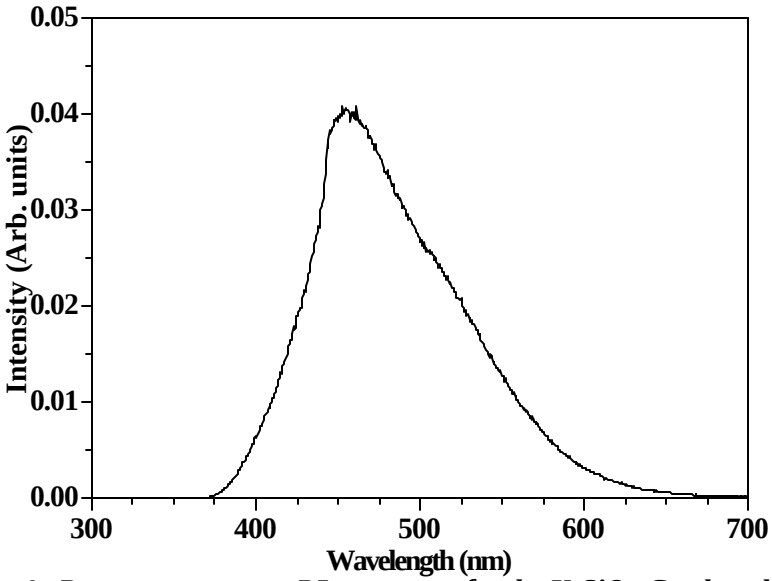

Figure 9: Room temperature PL spectrum for the Y_2SiO_5:Ce phosphor powders.

5.6 XPS

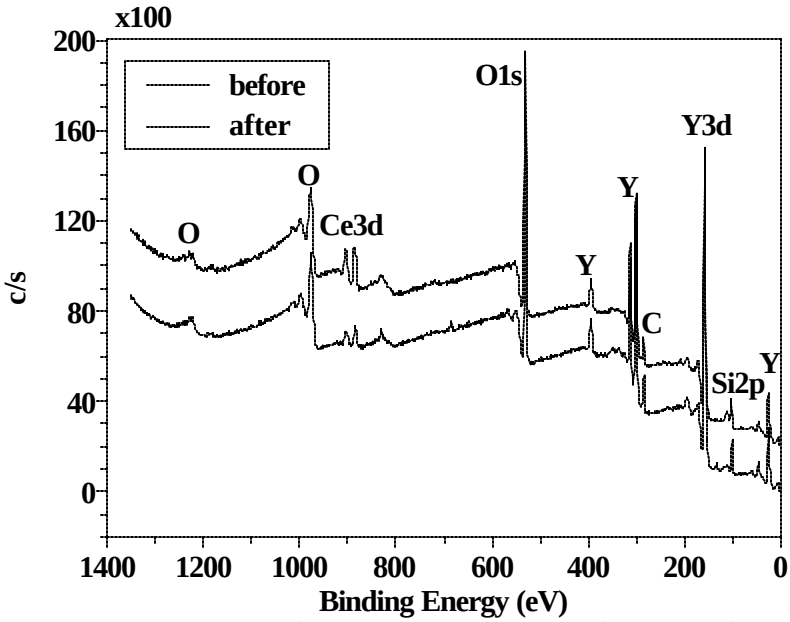

Figure 10: An XPS survey of the surface elements before and after degradation for 24 hr.

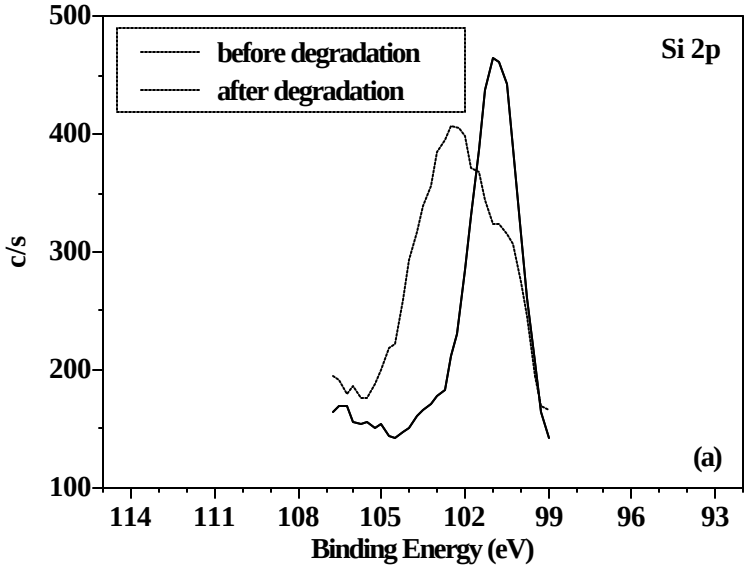

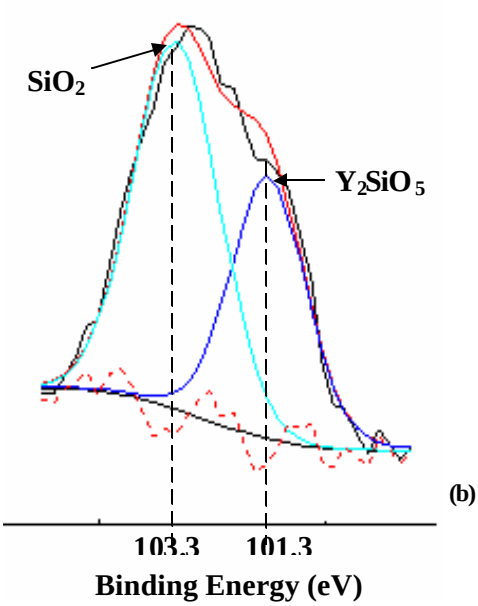

Figure 11: (a) Measured XPS results for the Si 2p peak before and after 24 hr degradation, (b) fitted results for Si 2p in the Y_2SiO_5 and in the SiO_2 chemical state.

Figure 10 shows the XPS survey spectrum of the Y_2SiO_5:Ce before and after 24 h degradation. Although the Ce could not be detected with AES the concentration was still high enough to be detected with XPS (Note: The relative probabilities of relaxation X-ray emission and electron emission changes with atomic number [11].) A clear increase in the Ce peak intensity was measured after degradation. An extra shoulder is detected at the high binding energy side of the Si 2p peak. The O1s peak is much broader on the spectrum measured after degradation. It is therefore clear that a chemical reaction occurred during the degradation process.

Figure 11a) shows the high resolution Si 2p XPS peak, before and after degradation. Figure 11b) shows the fitted results from an XPS spectrum of the Si 2p peak after degradation. The peak shape changed due to an extra peak that developed at higher binding energies. The Si peak position for the yttrium silicate (Y_2SiO_5) chemical state was measured at 101.3 eV before degradation. The extra Si peak measured at 103.3 eV was attributed to the silica (SiO_2) [12] chemical state after degradation. The Si 2p peak measured at 101.3 eV in figure 11 before degradation is consistent with a Si 2p photoelectron peak position for a thin film containing bonds of Y-O-Si, measured at 101.0 eV by Chambers et al. [13, 14].

This shows that the Si 2p peak in SiO_2 shifted to higher binding energy than that for Si in the Y_2SiO_5:Ce bonding state, indicating the silicon in Y_2SiO_5:Ce is in a lower oxidation state than the silicon in SiO_2. The O1s XPS peak of Y_2SiO_5:Ce was measured at 530.4 eV before degradation (Figure 12a)). The peak broadened on both the high and low binding energy side. Figure 12b) shows the fitted results from an XPS spectrum of the O1s peak after degradation. The fitted peaks at 529, 530.4, 532.1 and 533.6 eV correlate well with CeO_2 [15], the Y_2SiO_5:Ce O1s peak measured in this study before degradation and the last two peaks with SiO_2 [16, 17], respectively.

The Ce 3d peak before and after 24 hr degradation is shown in Figure 13a). The peak fit after degradation is shown in Figure 13b). The peaks were at 881.7 and 885.4 eV before degradation and 882.7 and 886.5 eV after degradation, which is in agreement with Ce in the CeO_2 oxidation stage [18] and CeH_3 [19]. The Y 3d 157.6 and 159.2 eV peak intensities before degradation (figure 14) decreased due to the coverage of the Y_2SiO_5 with SiO_2, CeO_2 and CeH_3 without a distinct shift in binding energy position. It must be pointed out that there was a slight shift in the Y 3d peak to 157.1 eV which might be an indication of the formation of Y_2O_3 [20].

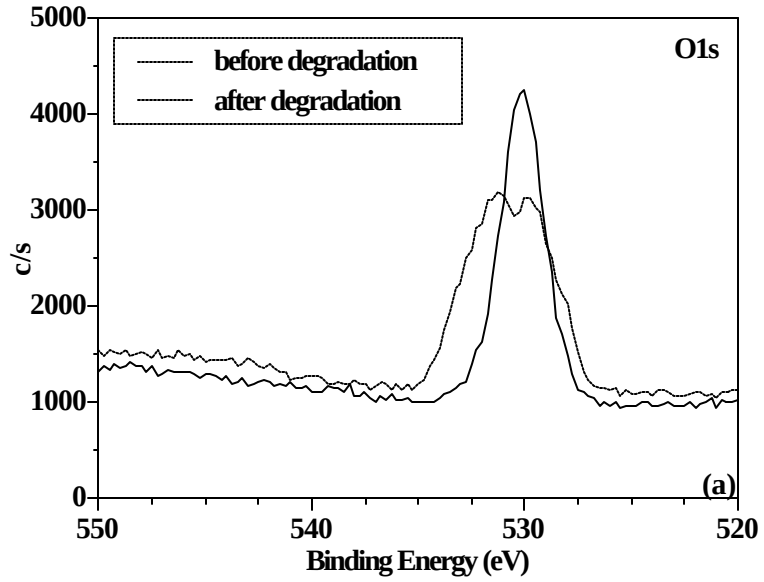

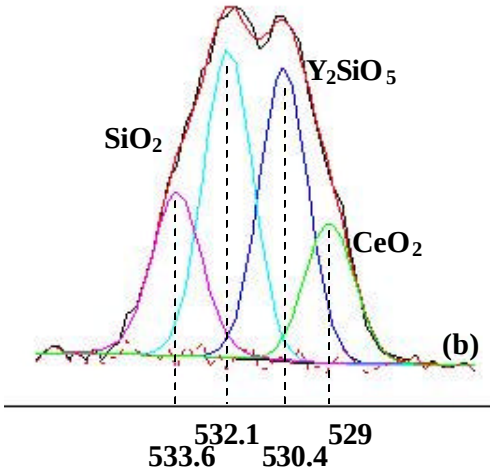

Figure 12: (a) Measured XPS results for the O 1s peak before and after 24 hr degradation, (b) fitted results for O 1s after degradation in the SiO_2, Y_2SiO_5 and CeO_2 chemical state.

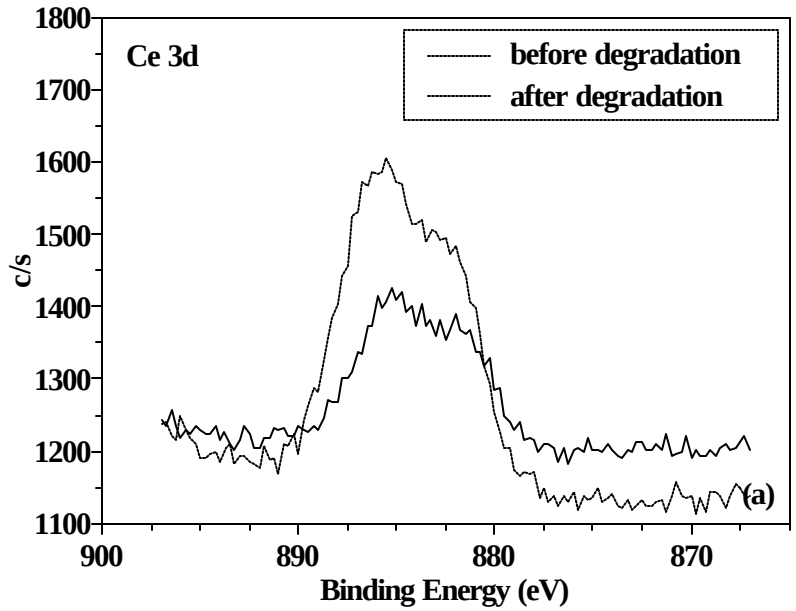

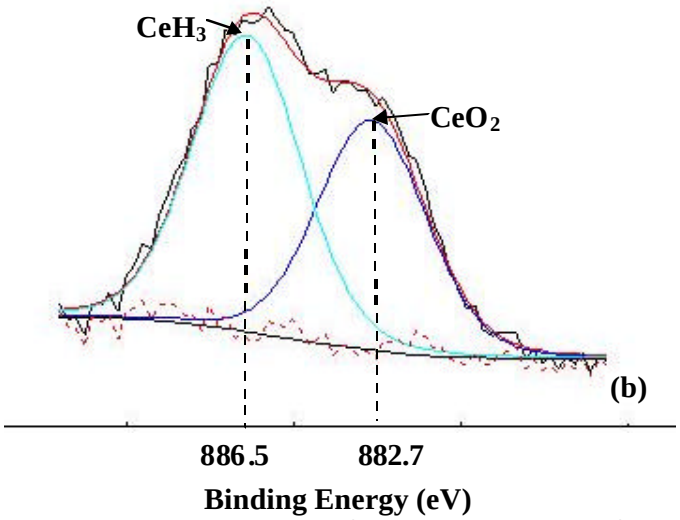

Figure 13: (a) Measured XPS results for the Ce 3d peak before and after 24 hr degradation, (b) fitted results for Ce 3d after degradation.

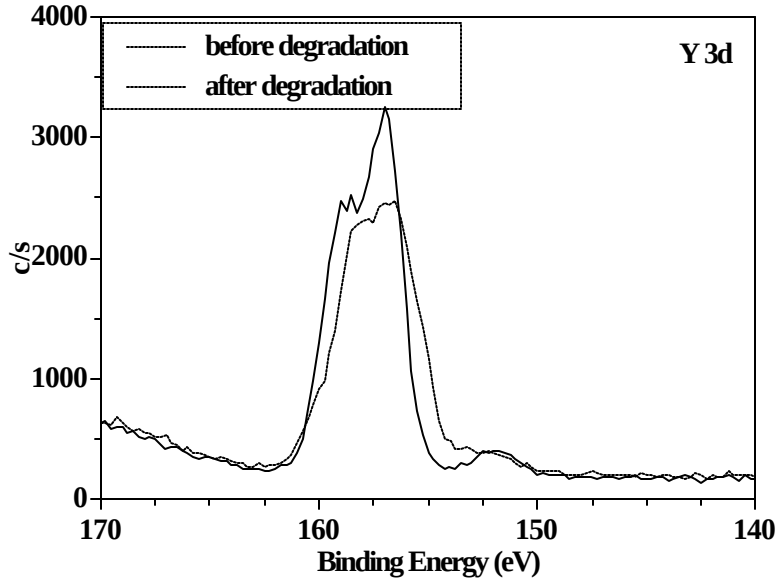

Figure 14: XPS results for the Y 3d peaks before and after 24 hr degradation.

The surface reaction on Y_2SiO_5:Ce is consistent with the well known ESSCR model [6, 21]. The ESSCR mechanism explains the formation of SiO_2 plus CeO_2 and CeH_3, whereby the electron beam dissociates the oxygen gas, as well as water vapour from the background gases into atomic species, which then react with the surface atoms to form a different chemical layer. In a situation where adventitious carbon is present on the surface, the carbon would be depleted as volatile species, such as CO_2.

The increase in CL intensities indicates that the newly formed layer is luminescent and thus contributing to the emission peak between 600 and 700 nm. SiO_2 has a band gap and the electron beam irradiation can break the Si-O bonds and cause intrinsic defects [15, 22]. Skuja et. al. [23, 24] reported two peaks for SiO_2 at 1.9 eV (650 nm) and 2.7 eV (459 nm) with a theory that the two peaks are related to intrinsic defects involving broken Si-O bonds. A definite contribution from the SiO_2 1.9 eV defect leads to the increase in the CL intensity between 600 and 700 nm, thus also resulting in the change in colour. There could be a very low intensity contribution from the 2.7 eV defect to the peak emission between 400 and 500 nm, which results in the increase in the intensity in that region. Violet/blue light emission (379.5 nm) was previously observed at room temperature from thin CeO_2 films deposited on Si (111) [25]. No evidence of emission in the 600 to 700 nm range for CeO_2 was found.

The formation of the luminescent SiO_2 layer on the surface of the Y_2SiO_5:Ce therefore lead to the degradation of the blue emitting Y_2SiO_5:Ce phosphor powders to a whitish light emitting phosphor. Although the formation of SiO_2 was measured, (Figure 11), by XPS, it must be pointed out that reported results on the PL [7] and CL [8] of $Y_2Si_2O_7$:Ce indicated an emission peak in the deep red region at around 642 nm, which is much stronger in intensity than another peak at around 420 nm (deep blue). $Y_2Si_2O_7$ has a different crystal field than Y_2SiO_5 and doping it with Ce^{3+} leads to a difference in the splitting effects of the 4f energy level. Possible reactions that might have occurred during electron bombardment:

$$2Y_2SiO_5 \rightarrow 4Y + 2SiO_2 + 3O_2$$
$$Si + O_2 \rightarrow SiO_2$$

5.7 $Y_2Si_2O_7$:Ce and SiO_2:Ce

Since $Y_2Si_2O_7$:Ce is polymorphous, it is very difficult to study its crystal structure [8]. The different crystal structures are a result of different contributing factors such as sample preparation [5, 26] and annealing affects [7]. Each crystal structure would thus lead to a different transition resulting in a double shoulder peak between 400 and 700 nm. XPS results on $Y_2Si_2O_7$:Ce could not be found in the literature to give

complete clarification on the matter. The formation of small amounts of $Y_2Si_2O_7$:Ce on the surface is therefore not completely excluded. A shift of less than 2 eV in the 2p Si peak (as measured for SiO_2) is however expected.

Another possibility for the increase in the CL intensity between 400 and 500 nm could be due to SiO_2:Ce. Ntwaeaborwa et. al. [27] reported on the photoluminescence of SiO_2:Ce, which resulted in a broad band emission spectrum between 400 and 500 nm (blue light) for 1 mol % concentration Ce. This broad band is due to the transitions in Ce^{3+} and therefore could also possibly contribute to the increased CL intensity in figure 5c), but not to the increase in the peak intensity between 600 and 700 nm.

Conclusion

The degradation of the Y_2SiO_5:Ce phosphor powders investigated with AES and CL spectroscopy first resulted in a decrease in CL intensity measured at 450 nm and then an increase after about 300 $C.cm^{-2}$ due to the chemical change in the phosphor surface. XPS and CL indicated that the change in peak shape is due to the formation of a luminescent SiO_2 layer on the surface which is formed according to the ESSCR mechanism. The emission of light from the SiO_2 defect levels contributed to the CL intensity in the 600 to 700 nm wavelength range. The colour changed from blue to orange-reddish during the degradation process. CeO_2 and CeH_3 were also formed on the phosphor surface during the degradation process.

References

1. H.C. Swart, L. Oosthuizen, P. H. Holloway and G. L. P. Berning, Surf. Inter. Anal, **26** (1998) 337.
2. K. R. Brown and D. A. Bonnell, J. Am. Ceram. Soc, **82(9)** (1999) 2423.
3. B. Carriere and J.P. Deville, Surface Sci., **80** (1979) 278.
4. R. Y. Lee and S. W. Kim, J. of Lumin., **93** (2001) 93.
5. Q. Y. Zhang, K. Pita, S. Buddhudu and C. H. Kam, J. Phys. D: Appl. Phys, **35** (2002) 3085.
6. J. Sebastian, S. Jones, T. Trottier, H. C. Swart and P. H. Holloway, J. SID, **3/4** (1995) 147.
7. N. Karar and H. Chander, J. Phys. D: Appl. Phys, **38** (2005) 3580.
8. X. Ouyang, A. H. Kitai and R. Siegele, Thin Solid Films, **254** (1995) 268.
9. H. C. Swart and K. T. Hillie, Surf. Interface Anal, **30** (2000) 383.
10. E. J. Bosze, G. A. Hirata and J. McKittrick, Mat. Proc. Symp. Mat. Res. Soc. Proc, **558** (1999) 15.
11. J. T. Grant in *Practical Surface Analysis*, Second edition, Ed by D. Briggs and M.P. Seah, John Wiley, New York, p61 (2003).
12. M. Laczka, W. Beier and L. Stoch, Glastechn. Berichte, **62** (1989) 320.
13. J. J. Chambers, B. W. Busch, W. H. Schulte, T. Gustafsson, E. Garfunkel, S. Wang, D. M. Maher, T. M. Klein and G. N. Parsons, Appl. Surf. Sci, **181(1-2)** (2001) 78.
14. J.J. Chambers and G.N. Parsons, J. Appl. Phys, **90(2)** (2001) 918.
15. E.Paparazzo, Surface Sci. **234** (1990) L253.
16. D. Sprenger, H. Bach, W. Meisel and P. Gulich, J. Non-cryst. Solids, **126** (1990) 111.
17. T.A. Clarke and E.N. Rizkalla, Chem. Phys. Lett., **37** (1976) 523.
18. D.D. Sarma and C.N.R, J. Electron Spectrosc. Relat. Phenom. **20** (1980) 25.
19. L. Schlapbach, J. Osterwalder and H.C. Siegmann, J. Less-Common Metals, **88** (1982) 291.
20. Y. Uwamino, Y. Ishizuka, H. Yamatera, J. Electron Spectrosc. Relat. Phenom, **34** (1984) 69.
21. P.H. Holloway, J. Sebastian, T. Trottier, S. Jones, H.C. Swart and R.O. Peterson, Mat. Res. Soc. Symp. Proc, **424** (1997) 425.

22. X. Liu, J. C. H. Phang, D. S. H. Chan and W. K. Chim, J. Phys. D, Appl. Phys, **32** (1999) 1563.
23. L.N. Skuja and W. Entzian, Phys. Stat. Sol. a, **96** (1986) 191.
24. L. N. Skuja, A. N. Streletsky and A. B. Pakovich, Solid State Comm, **50** (1984) 1069.
25. F. Gao, G. Li, J. Zhang, F. Qin, Z. Yao, Z. Liu, Z. Wang,. and L. Lin,Chin. Phys. Lett., **18** (2001) 443.
26. P.J. Marsh, J. Silver, A. Vecht and A. Newport, J. Lumin, **97** (2002) 229.
27. O.M. Ntwaeaborwa, H.C. Swart, R.E. Kroon, P.H. Holloway and J.R. Botha , Surf. Interface Anal, **38** (2006) 458.

Chapter 6

Thin film characterization - Results and Discussion

Thin films of Y_2SiO_5:Ce coated and uncoated with SnO_2 were grown with PLD. RBS was used to determine the thicknesses of both the Y_2SiO_5:Ce phosphor layer and the SnO_2 coated layer. Chapter 6 contains the results and discussion of the characterization of the thin films.

6.1 RBS

RBS results indicated that the Y_2SiO_5:Ce thin films grown with 6600 were non-uniform. The coated thin layer of SnO_2 was 58 nm thick. SEM, AFM and EDX also indicated that the Y_2SiO_5:Ce layer was non-uniform. The Y_2SiO_5:Ce phosphor layer consisted of spherical shaped particles not uniformly distributed on the surface.

6.2 SEM

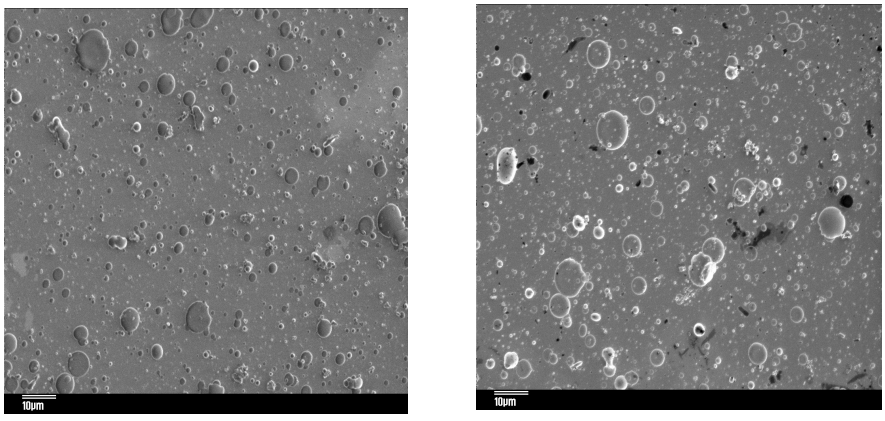

(a) **(b)**

Figure 1: SEM images of the uncoated a) and coated b) phosphor thin films with a magnification of 1000x (10 kV electrons). Scale – 10 µm .

Figure 1, shows the SEM images of both the uncoated a) and coated b) thin film surfaces. The surface displayed spherically shaped particles not uniformly distributed with different sizes. Figure 2 shows a SEM image of a coated phosphor particle with a diameter of about 12.3 µm.

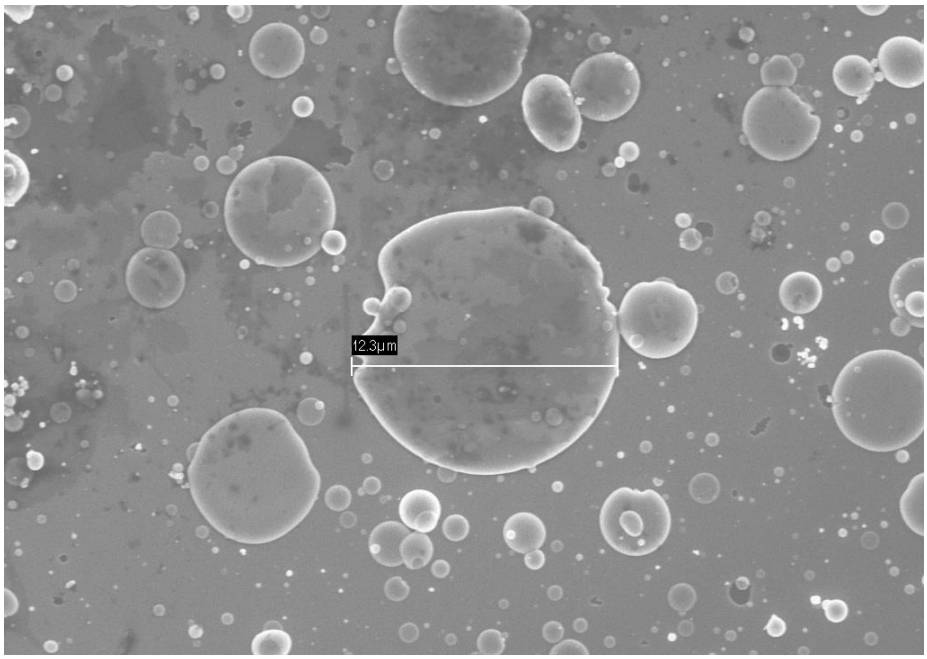

Figure 2: Coated phosphor particle with a diameter of 12.3 µm, magnification of 22400x.

6.3 AFM

AFM results as shown in figure 3 and 4 indicated that the particle size distribution varied between 10 nm to micron sized particles.

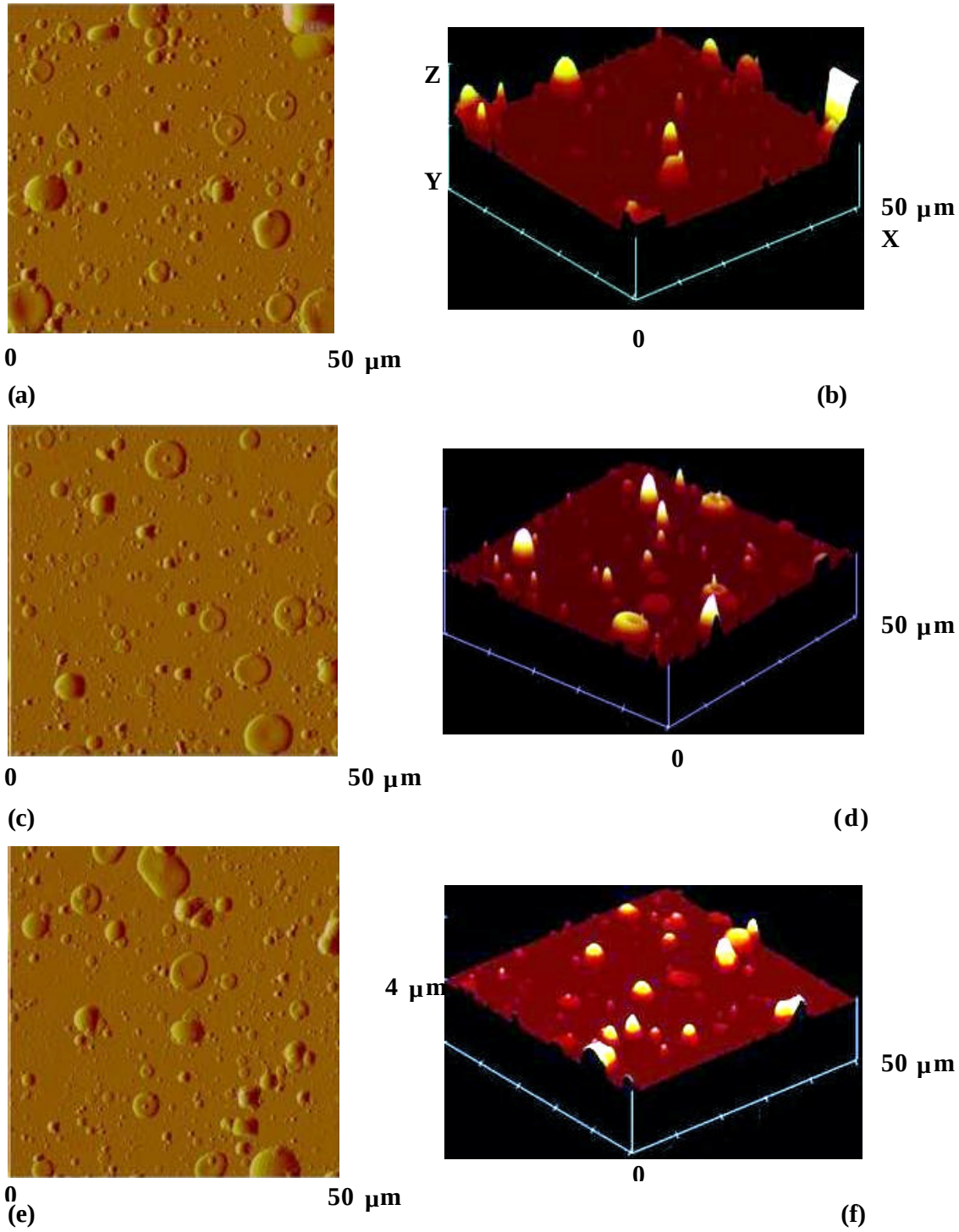

Figure 3: AFM results indicating the topographic a), c) and e) images for 3 different locations on the uncoated thin film as well as the 3D images b), d) and f).

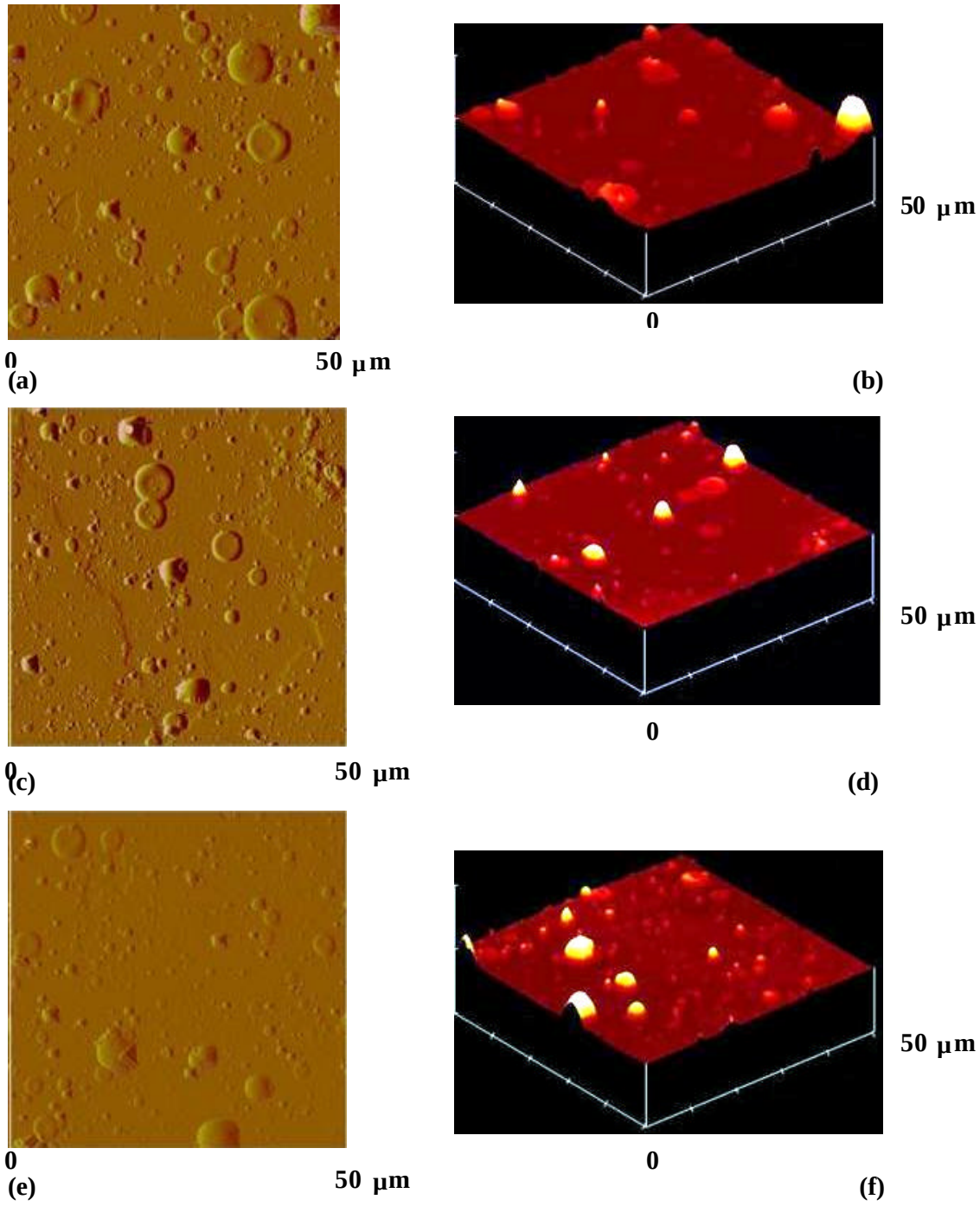

Figure 4: AFM results indicating the topographic a), c) and e) images for 3 different locations on the coated thin film as well as the 3D images b), d) and f).

The AFM images were obtained in contact mode. Contact mode is the most common method of operation of the AFM. As the name suggests, the tip and sample remain in close contact as the scanning proceeds. Figure 3 and 4 indicates that the surface is not smooth, but covered with spherical particles. The height image data obtained by the

AFM is three-dimensional. The usual method for displaying the data is to use a colour mapping for height, for example black for low features and white for high features [1].

6.4 EDS analysis

Results from EDS also indicated nano- and micron meter size, tin oxide agglomerated particles randomly distributed on the surface of the coated thin film (see figure 5b). Areas marked with **X** and **L** in figure 5a) and **T, Y, L, X** in b) are the areas analyzed by EDS. The electron beam used (10 kV energy electrons, resolution of 5 nm), resulted in X-rays to be analysed that escaped from a depth of 1 to 2 µm [2].

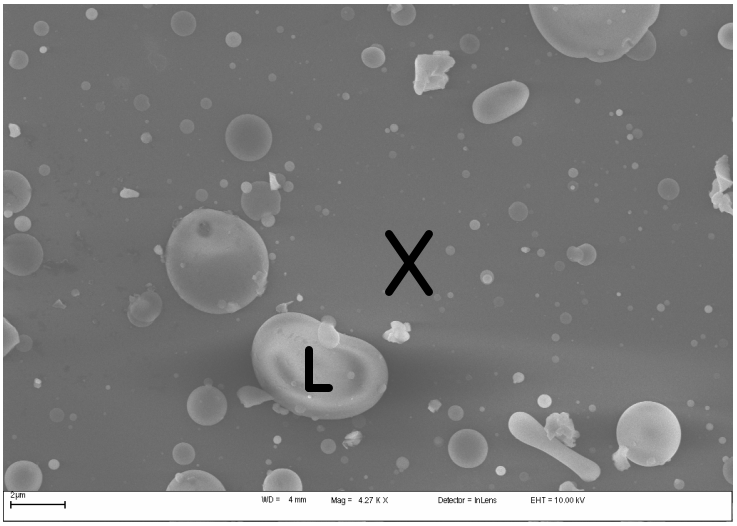

(a)

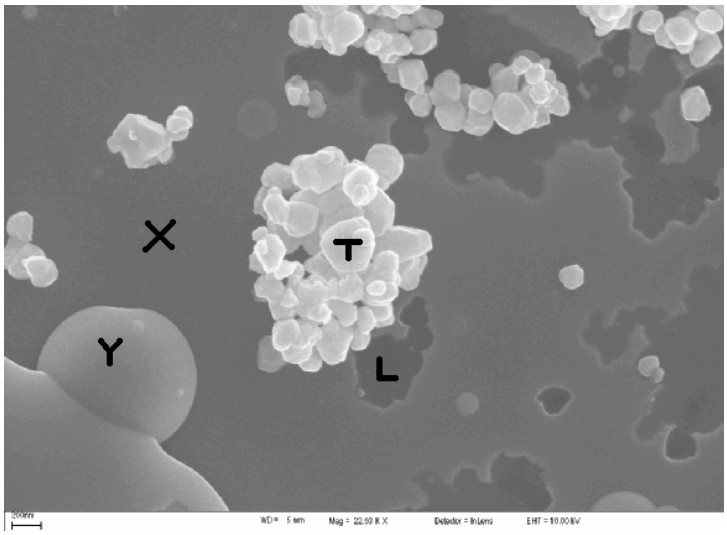

(b)

Figure 5: SEM images (10 kV electrons) of surface areas analyzed with EDS for the uncoated a) magnification of 4270x, scale – 2 μm and coated b) magnification of 22500x,scale – 200 nm, thin films.

Figure 6 shows the resulting EDS spectra for the uncoated thin films and figure 7 for the coated thin films.

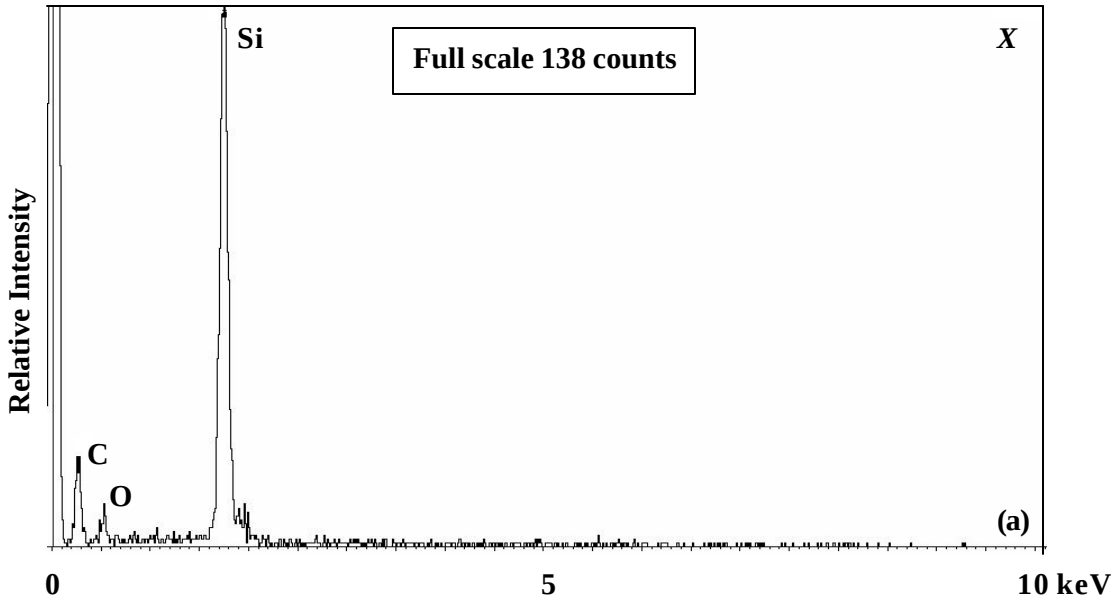

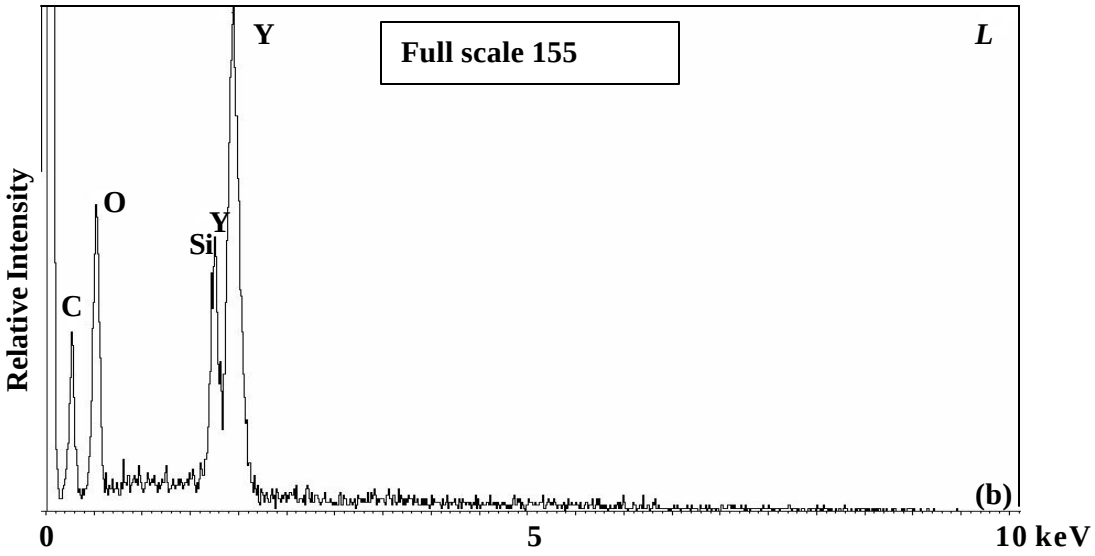

Figure 6: EDS spectra for the uncoated thin film on the marked areas a) X and b) L.

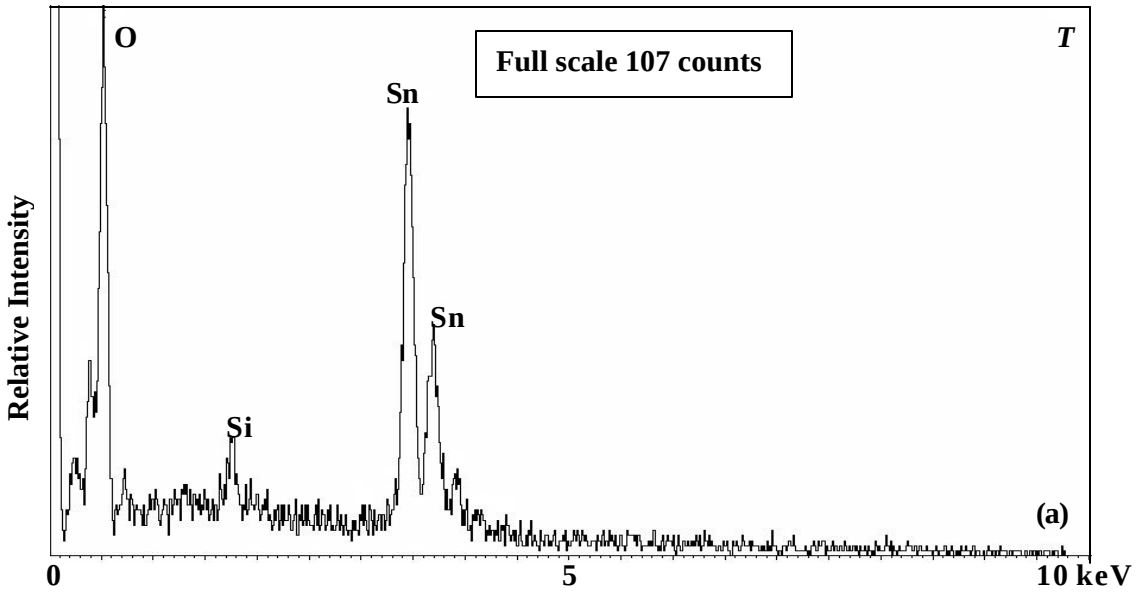

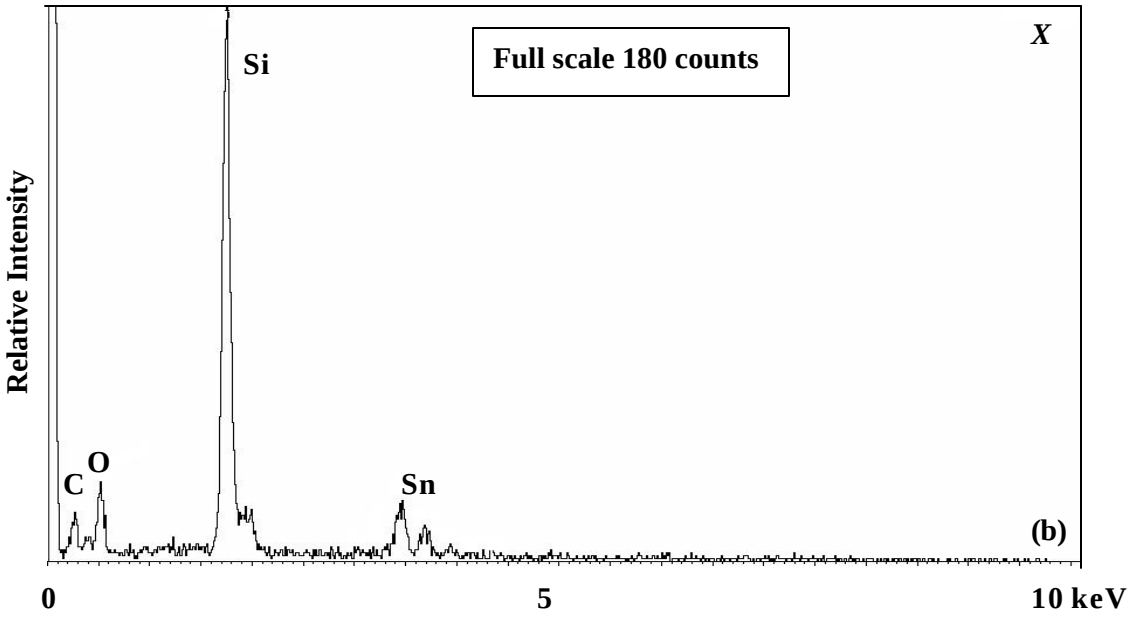
Full scale 180 counts
X
Si
C
O
Sn
(b)
Relative Intensity
0
5
10 keV

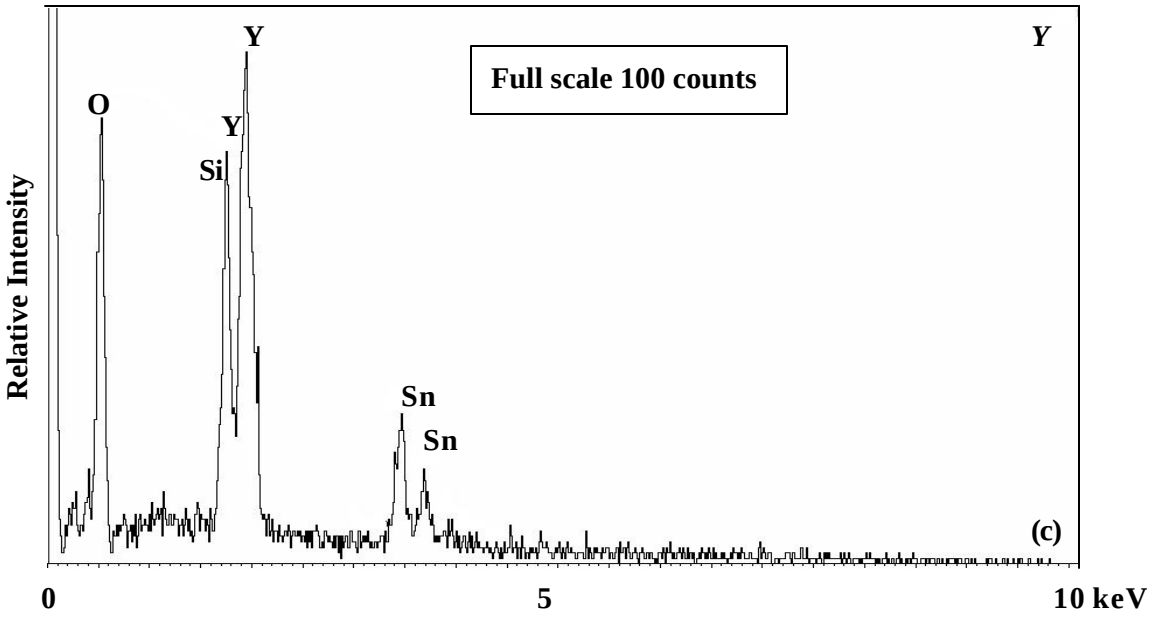
Full scale 100 counts
Y
O
Y
Si
Sn
Sn
(c)
Relative Intensity
0
5
10 keV

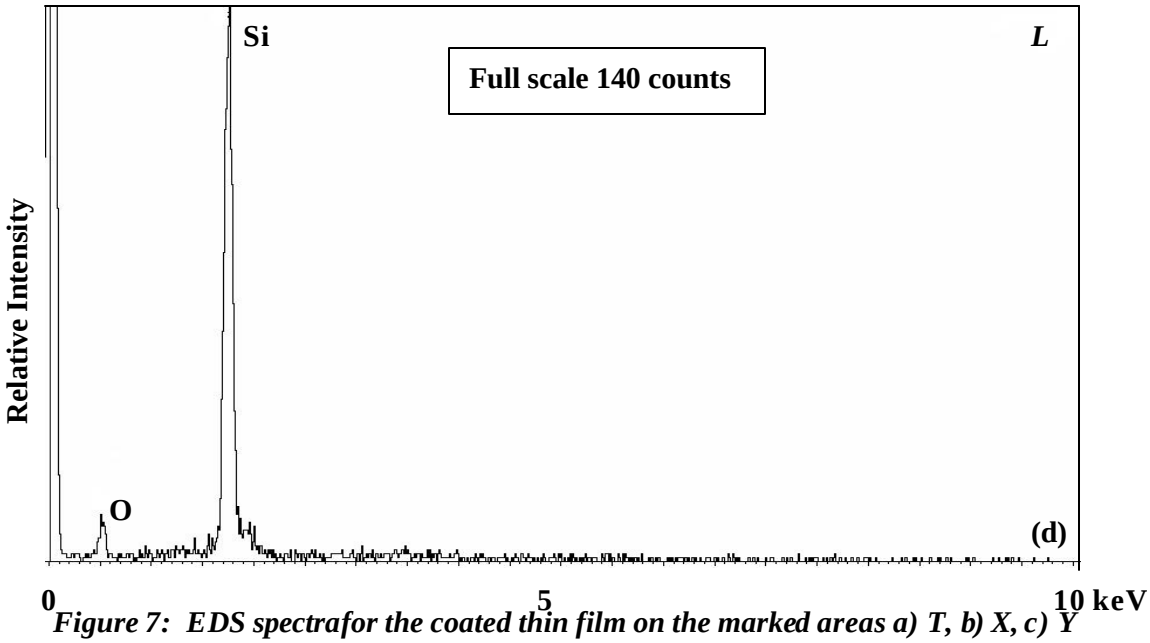

Figure 7: EDS spectrafor the coated thin film on the marked areas a) T, b) X, c) Y and d) L.

EDS results are listed in Table 1.

Table 1: Listed EDS results for the uncoated and coated thin films.

	Weight %				
	C	**O**	**Si**	**Y**	**Sn**
(a) Uncoated					
X	41		59		
L	21	22	8	49	
(b) Coated					
T		31	2		67
X	10	14	41		35
Y		28	9	37	26
L		12	88		

For the uncoated thin film, the area marked **X** (figure 6a)), correspond to a composition of 59 % Si and 41 % adventitious C. **L**, figure 6b), was measured on the spherical particle and the results indicated it to be the Y_2SiO_5:Ce phosphor particle. The Ce concentration was too low to be measured. Figure 6b) and 7c) show an overlapping of the Si and Y peaks at about 1.75 keV. Figure 6b) also shows a high concentration of Y from the particle having a diameter of about $4\,\mu m$.

The area marked with **T** in figure 7a) is agglomerated SnO_2 particles. The area marked with **X**, figure 7b), is the thin film surface consisting of 41 % Si contribution due to the substrate, 10 % adventitious C, 14 % O and 35 % Sn coated layer. **Y,** figure 7c), was measured on the spherical shaped particle and the results showed Si, Y and Sn, thus indicating the particles to be the Y_2SiO_5:Ce phosphor particles coated with SnO_2. The area marked with **L**, figure 7d) resulted in a high concentration of Si, 88 % and 12 % O, which is the Si substrate. This is an area on the surface were some of the particles came loose due to handling.

6.5 XRD

XRD was done on both the coated and uncoated thin films to determine the crystal structure. Figure 8a) shows the XRD results for the uncoated and b) for the coated thin films.

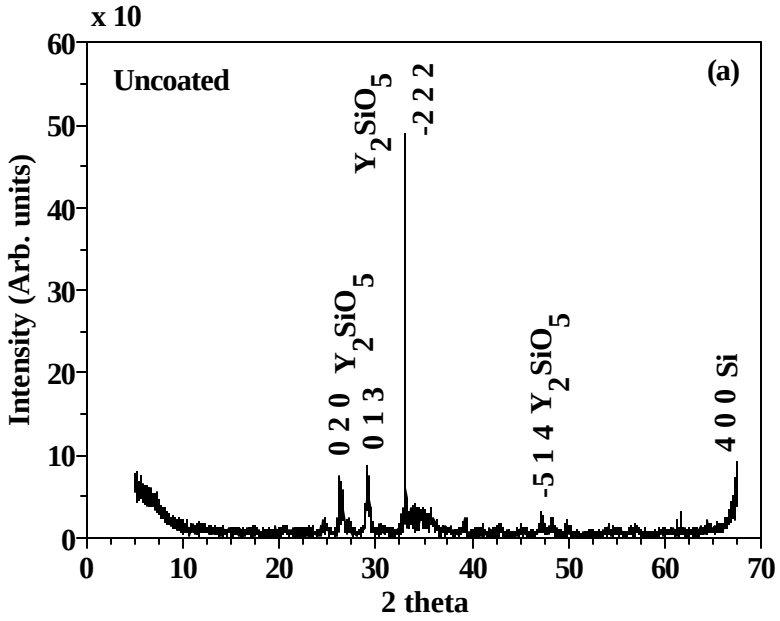

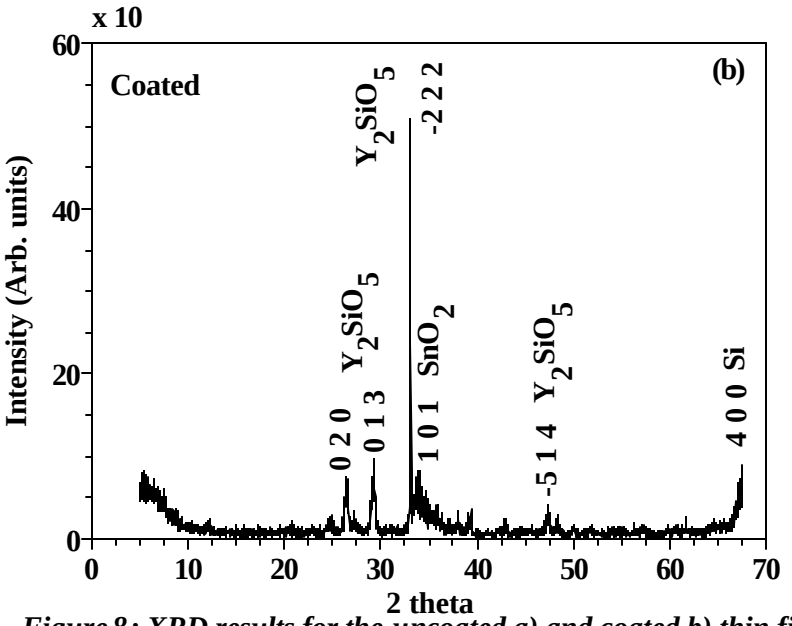

Figure 8: XRD results for the uncoated a) and coated b) thin films.

Figures 8a) and b) shows the [020], [013], [-222] and [-514] planes of the monoclinic Y_2SiO_5 and the [400] plane for the Si substrate. The increase in the peak at 33.8 degrees in figure 8b), with respect to the broad peak in that region in figure 8a), may be due to the [101] plane for tetragonal SnO_2. Two different monoclinic structures have been found in literature [3], a low temperature phase X1 and a high temperature phase X2. The X1 phase has the space group $P21/c$, whereas the space group $B2/c$ is assigned to the X2 phase. Both X1 and X2 phases have two different Y^{3+} sites, the coordination numbers of which are 7 and 9 for the X1 phase and 6 and 7 for the X2 phase. The Y_2SiO_5 peaks as measured in the XRD spectrum are in agreement with the X1 phase. No evidence of the X2 phase was found in this study. These XRD results are different than the XRD results obtained for the powders, because the growth of the Y_2SiO_5:Ce crystals onto the Si [100] substrate is different in orientation than for the powders.

6.6 More PLD pulses

Some of the thin films were also ablated with 18 000 pulses in an effort to grow a more uniform phosphor layer onto the Si (100) substrate.

6.6.1 PLD

The same deposition parameters were used except for the laser energy which was 172.73 mJ and the number of pulses which was 18 000. The system was backfilled to oxygen pressures of 7.5×10^{-4} Torr and 7.5×10^{-3} Torr.

6.6.2 EDS

Figure 9a) shows the SEM image of the areas that was analysed with EDS on the thin film that was ablated in an increased oxygen pressure of 7.5×10^{-3} Torr and b) shows the thin film ablated in 7.5×10^{-4} Torr with 18 000 pulses.

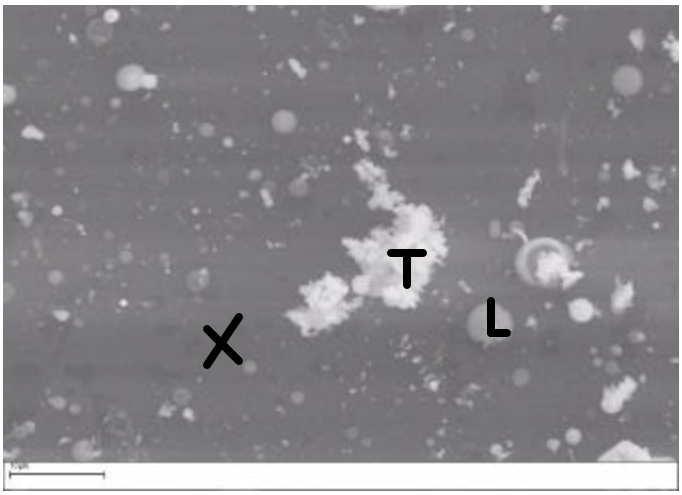

(a)

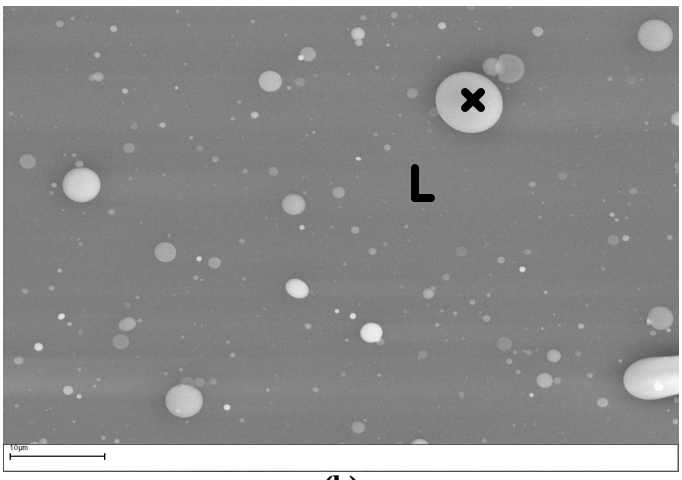

(b)

Figure 9: SEM images (20 keV electrons) of the areas analysed with EDS, for a) the thin film ablated in an oxygen pressure of 7.5 × 10^{-3} Torr and for b) the thin film ablated in 7.5 × 10^{-4} Torr. Magnification - 1600x; scale - 10 μm.

Figure 9a) shows more spherically shaped particles on the surface as well as an agglomeration of particles (area **T**). Figure 9b) also just shows more particles on the surface. EDS analysis of areas **T** and **L** in figure 9a), indicated the particles are Y_2SiO_5:Ce while region **X** corresponded to the Si substrate as can be seen from figure 10.

Area **L** in figure 9b) also correspond to Si substrate, which means that the increased number of pulses did not have the desired result of a more uniform phosphor layer on the substrate surface.

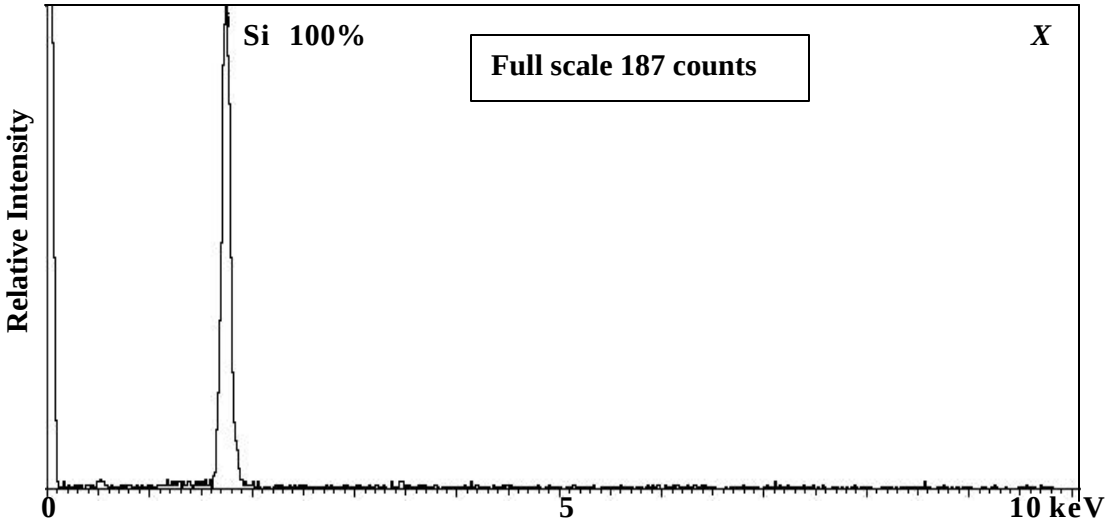

Figure 10: EDS spectrum of the thin film surface (area X in figure 9a)), with the Y_2SiO_5:Ce phosphor ablated onto the substrate using 18 000 pulses in an increased oxygen pressure of 7.5 × 10^{-3} Torr.

Spherical particles of different sizes are typically found in laser ablation experiments [3, 5]. Hirata et. al. [5] reported on rounded particles of different sizes that are formed from local melting and ejected from the target onto the substrate on the smooth surface of $Y_3Al_5O_{12}$:Tb thin films grown by PLD.

Conclusion

Characterization (RBS, SEM, AFM, EDS, XRD) were successfully done on the phosphor thin films. AFM and EDS showed that the Y_2SiO_5:Ce phosphor was ablated onto the Si (100) substrate as spherical shaped particles. RBS, XRD and EDS showed that the SnO_2 was successfully grown as a uniform coated layer onto some of the phosphor thin films. PLD with more pulses in this case however did not have the effect of a more uniform phosphor layer onto the surface. The system setup for PLD was however changed, having the effect of increased laser energy.

References

1. Atomic Force Microscopy, [online]. Available from www.molec.com/what_is_afm.html [Accessed 22 February 2006].
2. EDS, [online]. Available from http://www.cascade.co.uk/xps.pdf [Accessed 24 March 2006].
3. J. Wang, S. Tian, G. Li, F. Liao and X. Jing, J. of the Electrochem. Soc, **148 (6)** (2001) H61.
4. Chen Li-Chyng, Particulates generated by pulsed laser ablation, in Pulsed Laser Deposition of Thin Films (eds. Chrisey D. B, Hulber, G. K), John Wiley & Sons, Inc, New York, (1994) p. 167.
5. G. A. Hirata, O. A. Lopez, L. E. Shea, L. Y. Yi, T. Cheeks, J. McKittrick, J. Siqueiros, M. Avalos-Borja, A. Esparza and C. Falcony, J. Vac. Sci. Technol. A, **14(3)** (1996) 1694.

Chapter 7

Thin film CL, AES and XPS - Results and Discussions

This chapter contains the results and discussions for the CL spectroscopy and AES experiments were done in different O_2 gas ambient and beam currents, as well as the light emission process from the thin film surface.

7.1 CL spectroscopy and AES

CL spectroscopy and AES were done in vacuum and different oxygen pressures with two different beam current densities to monitor chemical changes on the surface of the thin films that were grown by PLD. The coated thin film was bombarded with a beam current of 20 µA, on the same spot, by electrons, starting at UHV. The pressure in the system was then increased (after 24 hrs), by leaking oxygen gas into the system to a pressure of 1×10^{-8} Torr. After 16 hours the pressure was increased to 1×10^{-7} Torr. After 24 hrs the beam current was then decreased to 10 µA while the pressure was kept constant. Finally the pressure was then increased to 1×10^{-6} Torr, after another 24 hours. This was done to test the role of oxygen and also to deplete the adventitious C on the surface. A new spot was also degraded starting with an oxygen pressure of 1×10^{-6} Torr from the onset. The CL intensity data was collected at 440 nm. The uncoated thin film was then bombarded by electrons in 1×10^{-6} Torr oxygen pressure for 24 hr. The results are presented and discussed in this chapter.

Uncoated thin film

7.1.1 AES and CL spectroscopy for the uncoated thin film - oxygen pressure - 1×10^{-6} Torr - beam current 10 µA

AES and CL spectroscopy was done for the uncoated thin film in an oxygen pressure of 1×10^{-6} Torr with the electron beam current at 10 µA. AES results for the uncoated thin film showed that the carbon depleted from the surface while measuring

the AES spectrum, with a change in peak shape for silicon (see figure 1). The low sensitivity factor of the Auger electrons for Y resulted in the detection of only the low energy peaks for Y as indicated in figure 1, see section 5.3.2.

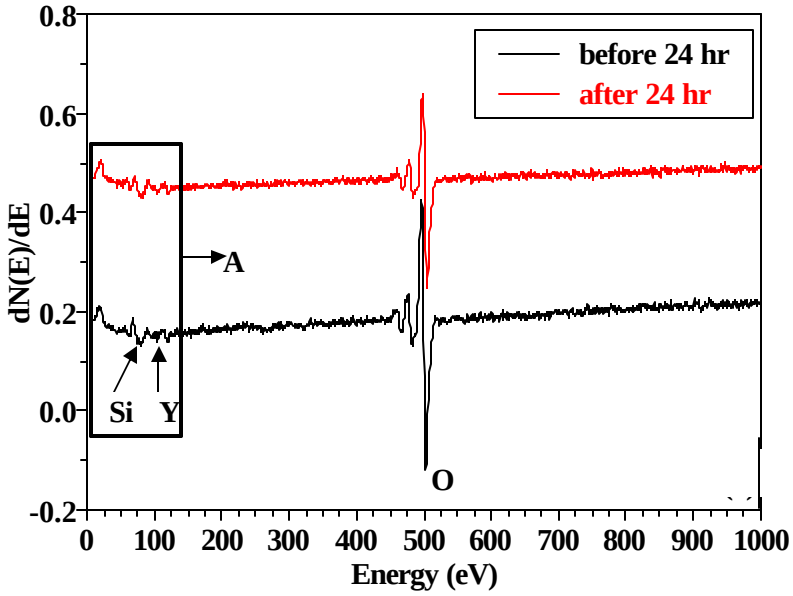

Figure 1: AES spectra for Si and Y in the uncoated thin film at 1×10^{-6} Torr oxygen pressure with a current density of 26.32 mA.cm^{-2} before and after 24 hr electron bombardment.

Figure 1 shows the low energy AES spectrums for Si and Y before and after 24 hr electron bombardment, represented by the area marked with **A** in figure 1. The CL stayed constant, then after 18 hr there was a definite decrease in the CL intensity.

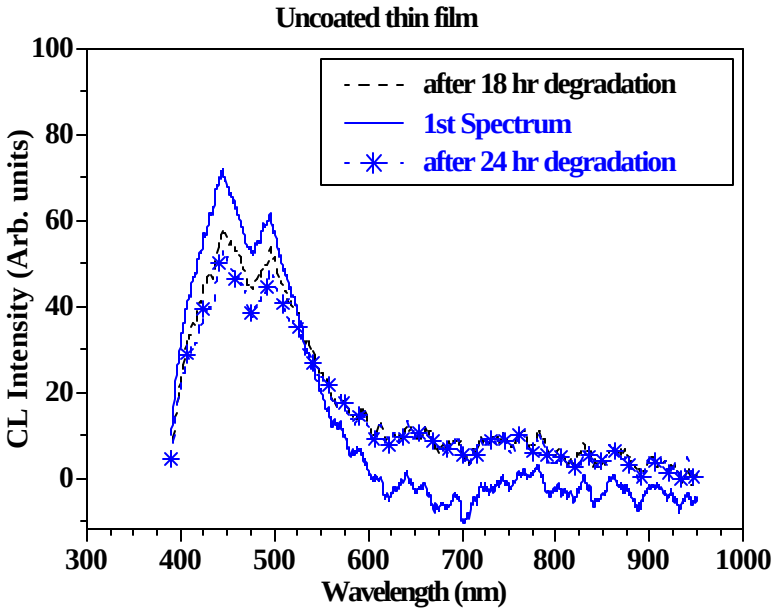

Figure 2: CL intensity against wavelength for the uncoated thin film before and after 18 hr and 24 hr degradation.

Figure 2 shows a decrease in the main emission peak at 450 nm and a small increase in a peak between 600 and 700 nm. After 24 hr the main peak showed a further decrease but emission between 600 and 700 nm stayed almost constant. One possible reason for the small increase in the peak at 650 nm in figure 2) could thus be from a contribution from the 1.9 eV defect from SiO_2 (see chapter 5) [1, 2, 3]. The low energy AES spectrum for Si before and after 24 hr electron bombardment for the uncoated thin film, showed a very small change in peak shape, figure 1. The change in the Si peak shape could thus be due to the formation of a very low concentration of a SiO_2 layer on the surface of the phosphor particles.

Coated thin film

7.1.2 Vacuum - beam current 20 µA

AES in vacuum (2.4×10^{-9} Torr) before 24 hr electron bombardment (with a beam current of 20 µA resulting in a current density of 52.65 $mA.cm^{-2}$), showed a large amount of adventitious carbon on the surface of the thin film (figure 3). The C shows an increase until 300 $C.cm^{-2}$ during which the Sn, O and Si APPHs decrease. The C then shows a very slow decrease until about 1600 $C.cm^{-2}$.

The Sn/C and O/C ratios show an almost linear decrease in the relative APPH at first, which means that the APPH of C increased with respect to the Sn and O APPHs. The carbon is thus creating an extra layer on the surface that increases the energy loss of the primary electrons, see section 3.1.7. The CL intensity (measured at 450 nm) decreased within the first 700 $C.cm^{-2}$, then stayed almost constant due to the protective C layer, see figure 3. The CL decrease is a result from the increased C on the surface. The peak emission between 400 and 500 nm is the characteristic double shoulder peak for CL emission of Y_2SiO_5:Ce, [4, 5, 6] (see section 5.3.2).

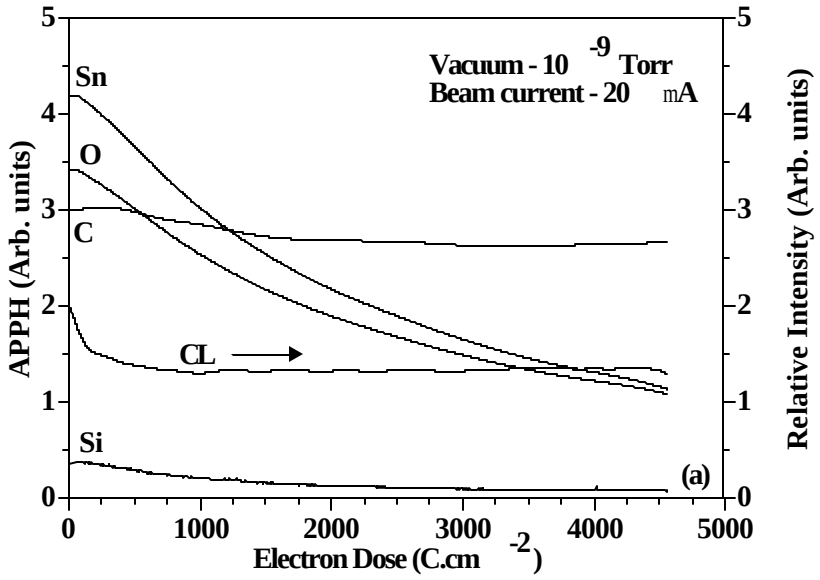

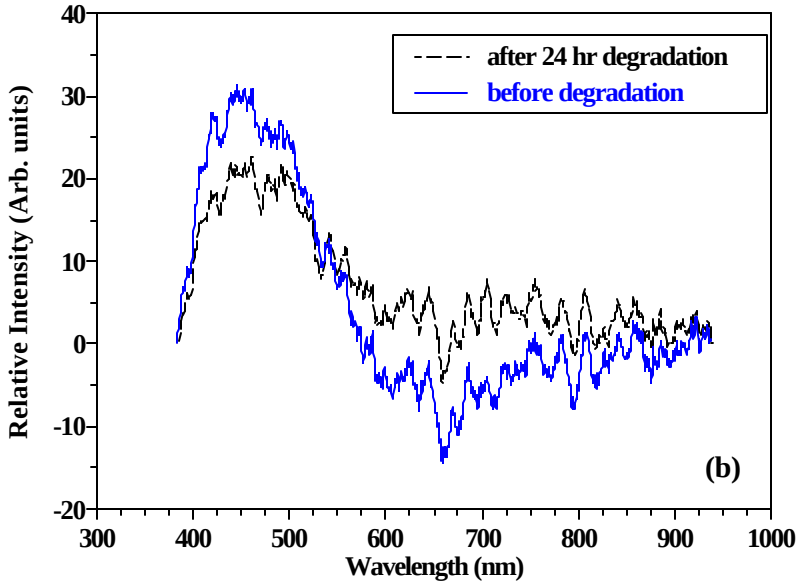

Figure 3: a) Auger peak to peak heights and CL intensity against electron dose ($C.cm^{-2}$) during degradation in vacuum, b) CL intensity against wavelength for the coated thin film in vacuum with a current density of 52.65 $mA.cm^{-2}$ before degradation and after 24 hr degradation.

The oxygen pressure in the system was therefore increased to deplete the carbon from the surface due to electron stimulated reactions, see section 3.1.7.

7.1.3 Oxygen pressure - 1 × 10^{-8} Torr - beam current 20 µA

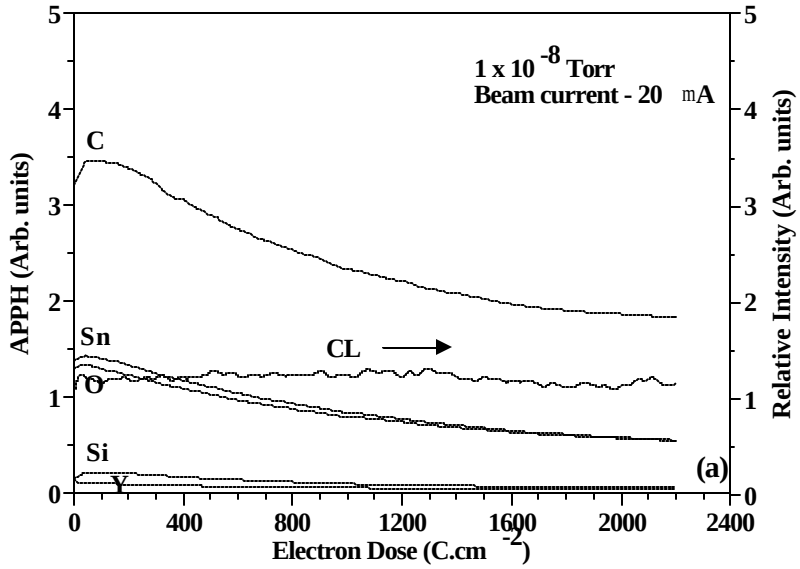

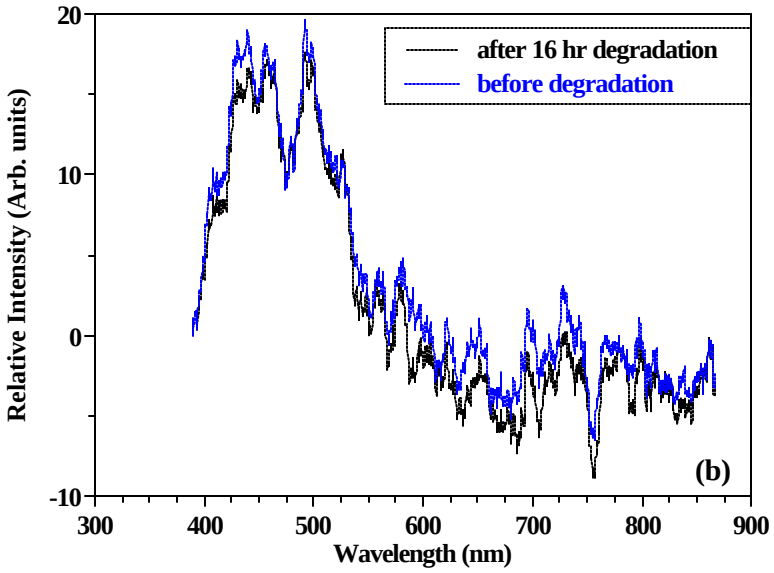

Figure 4: a) Auger peak to peak heights and CL intensity against electron dose ($C.cm^{-2}$) at 1×10^{-8} Torr oxygen pressure, b) CL intensity against wavelength for the coated thin film in 1×10^{-8} Torr oxygen pressure with a current density of 52.65 $mA.cm^{-2}$ before and after degradation for 16 hr.

The increase in the oxygen pressure showed little change in the CL intensity after about 16 hr, figure 4. The carbon was still not depleted from the surface although it showed a decrease; the concentration was still very high compared to the Sn and O concentration on the surface. The Sn/C and O/C ratios again showed a decrease but not as linear as for figure 3a). This is an indication that the C is depleting from the surface and that the Sn and O APPHs are increasing. It seems that the C adsorption from background gases and the removal of C due to ESSCR is traded against each other at these experimental conditions. The expectation would thus be that a further increase in the oxygen pressure would result in an increased CL intensity due to C removal. The oxygen pressure was therefore further increased to 1×10^{-7} Torr.

7.1.4 Oxygen pressure - 1×10^{-7} Torr - beam current 20 µA

Figure 5a) shows the Auger peak to peak heights with the increasing CL intensity against electron dose ($C.cm^{-2}$), for 24 hrs as expected in 7.1.2.

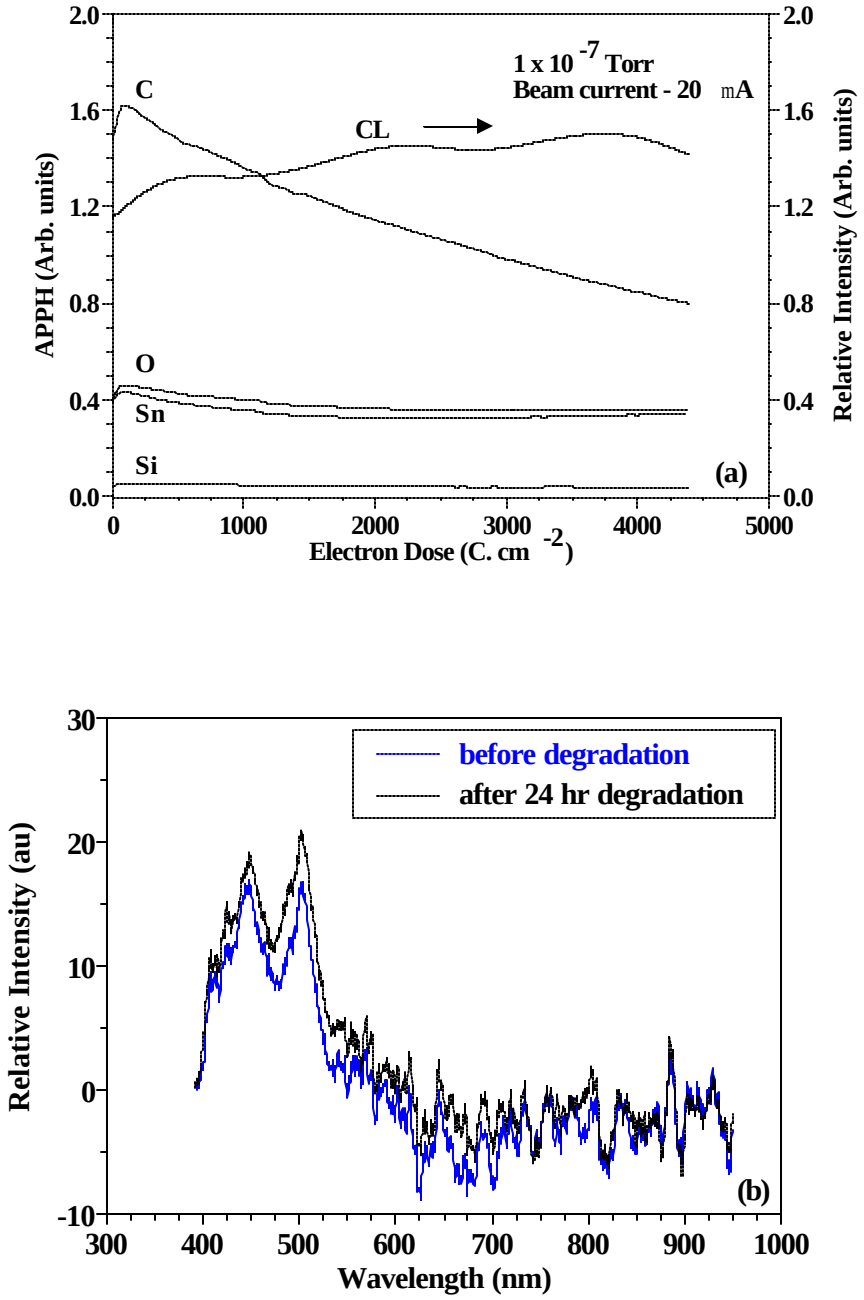

Figure 5: a) Auger peak to peak heights as a function of electron dose at 1 × 10^{-7} Torr oxygen pressure and b) CL intensity against wavelength for the coated thin film at 1 × 10^{-7} Torr oxygen pressure with a current density of 52.65 mA.cm^{-2} before and after degradation for 24 hr.

The carbon gets depleted from the surface according to the well known ESSCR model [5, 7] as volatile species such as CO_2 but the concentration is still much higher than the Sn and the O. The Sn/C and O/C APPHs ratios again showed an increase within the first 1000 C.cm^{-2} which means that the Sn and O APPHs are increasing as the C is

decreasing. Figure 5b) shows the increased CL against wavelength between 400 and 600 nm, after 24 hr. The increase in emission between 400 and 600 nm in figure 5b) is thus due to the depletion of C and therefore an increased area of exposure of the Y_2SiO_5:Ce phosphor particles to the electron beam. The beam current was then decreased to 10 μA with the expectation that the CL would show a further increase as a result of more depletion of the C on the surface.

7.1.5 Oxygen pressure - 1×10^{-7} Torr - beam current 10 μA

A lower beam current of 10 μA gives in a current density of 26.32 $mA.cm^{-2}$ with a lower temperature of contact with the electron beam on the thin film surface, which leads to a longer mean stay time of the oxygen species on the surface for electron stimulated reactions to occur and deplete the carbon from the surface [8, 9]. Figure 6 shows a definite decrease in the C APPHs and an increase in both the Sn and O APPHs. This means that the lower beam current thus resulted in the longer mean stay time of the reactive O species on the surface, which then reacted with the C to form volatile species (see section 7.1.4). As the C layer is decreasing, more of the phosphor particle's surface is getting exposed to the electron beam for CL, thus the increase in the CL intensity.

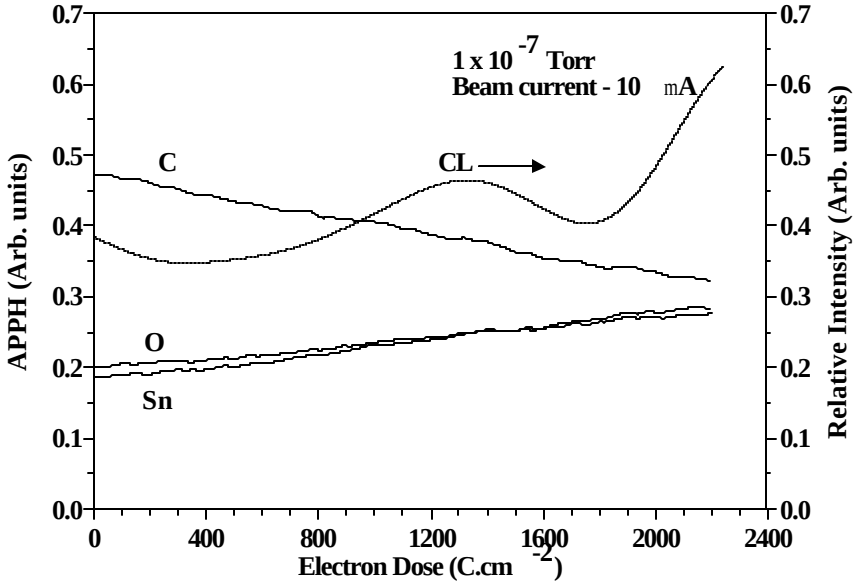

Figure 6: Auger peak to peak heights for the coated thin film at 1 × 10^{-7} Torr oxygen pressure with a current density of 26.32 mA.cm^{-2} as a function of electron dose for 24 hrs of electron bombardment.

7.1.6 Oxygen pressure - 1 × 10^{-6} Torr - beam current 10 µA

Figure 6 shows that the C was still not completely depleted from the surface, thus the O pressure was further increased to 1 x 10^{-6} Torr with a current density kept constant at 26.32 mA.cm^{-2}. Figure 7 shows the depletion of carbon as well as SnO_2 on the surface with an increase in the CL intensity during electron bombardment.

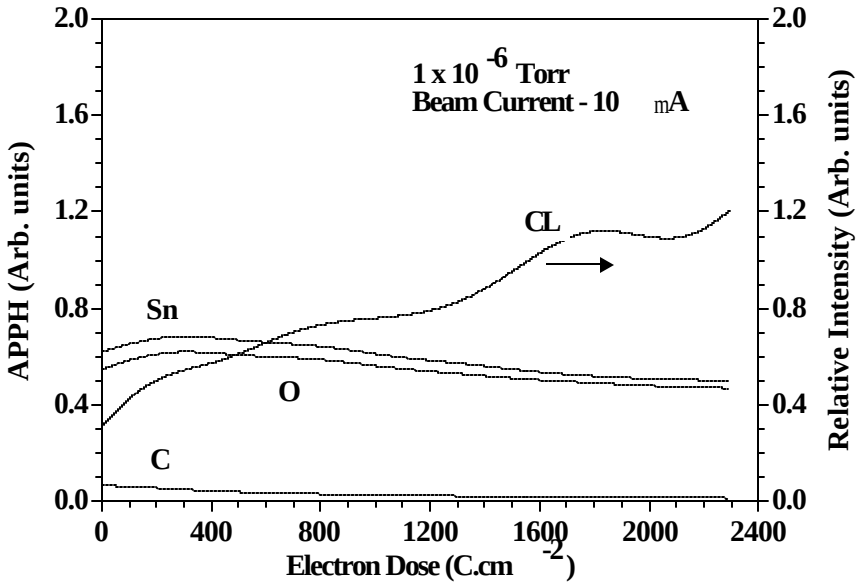

Figure 7: Auger peak to peak heights for the coated thin film at 1×10^{-6} Torr oxygen pressure with a current density of 26.32 mA.cm^{-2} as function of electron dose for 24 hrs electron bombardment.

The APPH of C decreases within the first 400 C.cm^{-2} during which the APPHs of both Sn and O increase and then show a decrease. The ratio of Sn/O is almost constant initially with a slight decrease after 24 hr exposure, which means that the Sn decreases relative to the O. The CL shows a definite increase as the C gets depleted. After the depletion of the C the CL continues to increase while the SnO_2 was also depleted from the surface due to ESSCR. The CL increased while the SnO_2 covering layer on the surface was slowly removed during electron bombardment.

The electron beam was then focussed on a different surface area in order to investigate if the CL would definitely reach a constant level if the C is depleted from the surface, which would be an indication that the SnO_2 layer acts as a successful coating layer.

7.1.7 Oxygen pressure - 1×10^{-6} Torr - beam current 10 µA - different area on the coated thin film surface

Figure 8 shows the AES results before and after 24 hr electron bombardment on a different area on the coated thin film in an oxygen pressure of 1×10^{-6} Torr with the current density at 26.32 $mA.cm^{-2}$.

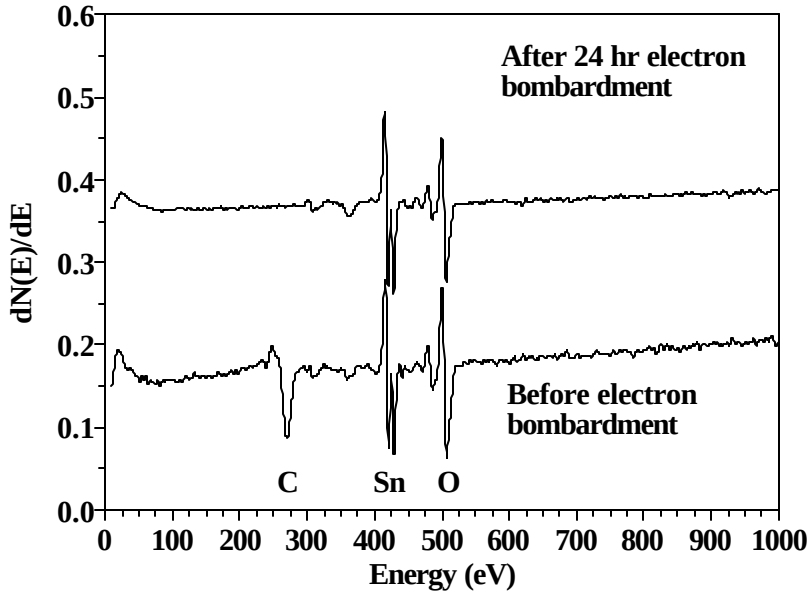

Figure 8: AES results before and after 24 hr electron bombard ment on a different area on the coated thin film at 1×10^{-6} Torr oxygen pressure with the current density of 26.32 $mA.cm^{-2}$.

As the C decreases the Sn and O APPHs increased and then almost stayed constant. The C gets depleted from the surface within the first 300 $C.cm^{-2}$ (about 3 hr), see figure 9a), due to electron stimulated reactions (ESSCR) [7] in the oxygen environment, resulting in the increase of the CL.

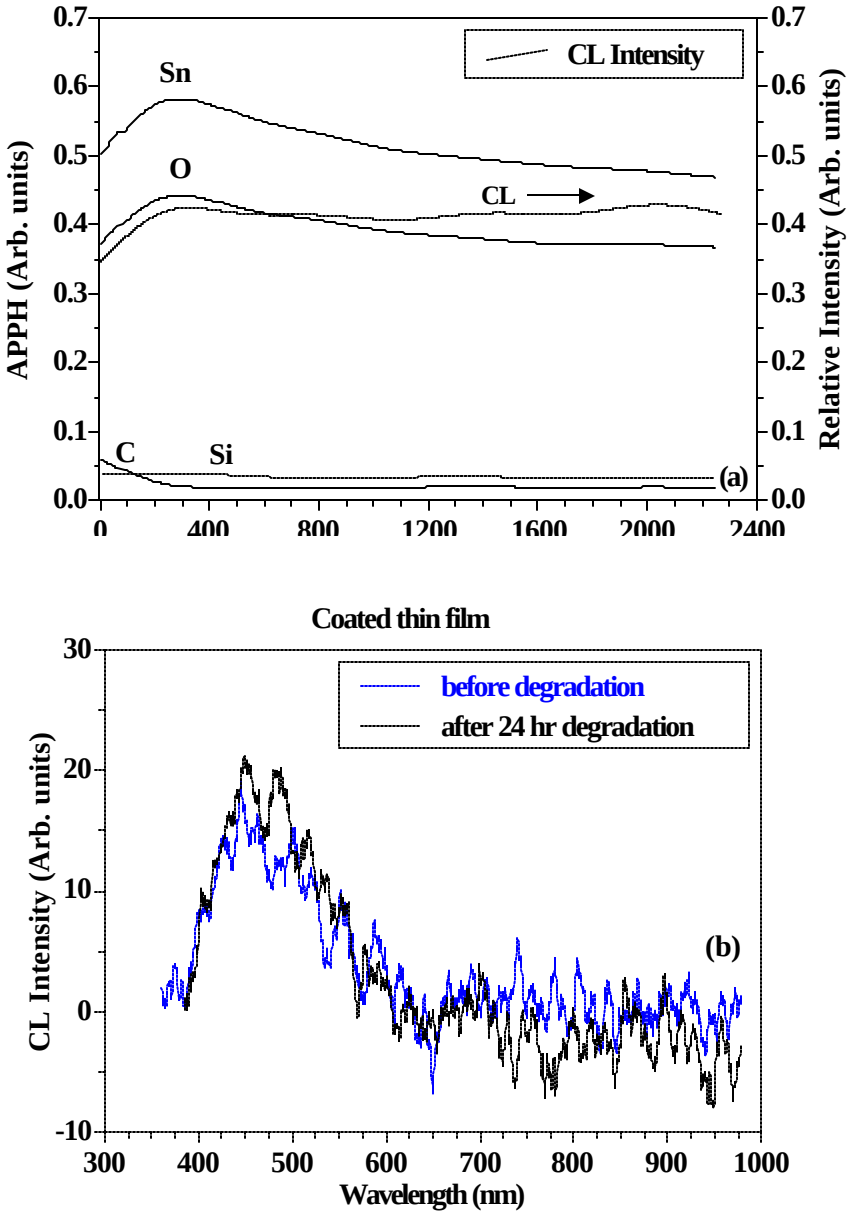

Figure 9: a) Auger peak to peak heights as function of electron dose at an oxygen pressure of 1 × 10^{-6} Torr and b) CL intensity against wavelength for a different surface area on the coated thin film at 1 × 10^{-6} Torr oxygen pressure with a current density of 26.32 mA.cm^{-2} before and after degradation for 24 hr.

As mentioned before, the adventitious C forms an extra layer on the surface of the thin films that increases the energy loss of the primary electrons penetrating it on their way to excite the electron-hole pairs in the phosphor bulk. A decrease in the C layer increases the CL intensity, which then stayed almost constant. Figure 9b) shows the increase in the main emission peak between 400 and 500 nm. This proves that the

SnO_2 layer acts as a protective coating layer that resulted in a constant CL intensity after 24 hr electron bombardment, but the layer unfortunately will also be removed with continued electron bombardment as seen in figure 7. The constant CL intensity means that no chemical changes occurred on the surface of the phosphor thin films which could either result in an increased (extra luminescent layer, see chapter 5) or decreased (extra non – luminescent layer) CL.

Light emission from both thin films in a 1×10^{-6} Torr oxygen environment, was blue before and after 24 hrs electron bombardment. The CL intensity of the uncoated thin film was about 60 % higher than for the coated thin film (see figure 10). The SnO_2 layer at first prevented the phosphor surface to degrade as there was no change in the chemical composition of the surface, proved by XPS results (not shown here). The lower CL intensity of the coated thin film is thus due to the energy loss of primary electrons penetrating the SnO_2 layer on the phosphor surface, as well as scattering effects of the photons exiting the phosphor surface and the SnO_2 layer. A uniform layer covering the surface of the spherical particles results in a small critical angle for transmission and a large fraction of the light being totally internally reflected [5]. See also section 7.1.1 for the decrease in the CL of the uncoated thin film.

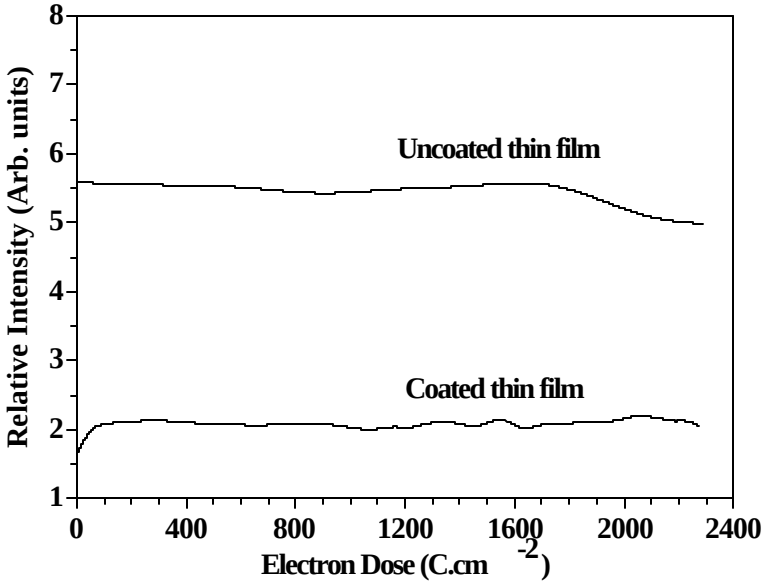

Figure 10: CL intensity as function of electron dose ($C.cm^{-2}$) for the coated and uncoated thin films in 1×10^{-6} Torr oxygen pressure with a beam current density of $26.32\ mA.cm^{-2}$

7.2 RGA

RGA was performed for both the uncoated and coated thin films to monitor the volatile species in the environment during electron bombardment for AES and CL spectroscopy. Figure 11a) shows the RGA results for the uncoated and b) for the coated thin film, in an oxygen pressure of 1 $\times 10^{-6}$ Torr and the beam current density of 26.32 mA.cm^{-2}.

The intensity of the OH, CO and CO_2 gas species increased with the electron beam on, due to electron stimulated reactions that depletes the carbon from the thin film surface into volatile species [7]. There is clearly a difference between the percentage changes for the various species, especially for the CO and CO_2 which might be attributed to the volatile species coming from the C on the coated thin film.

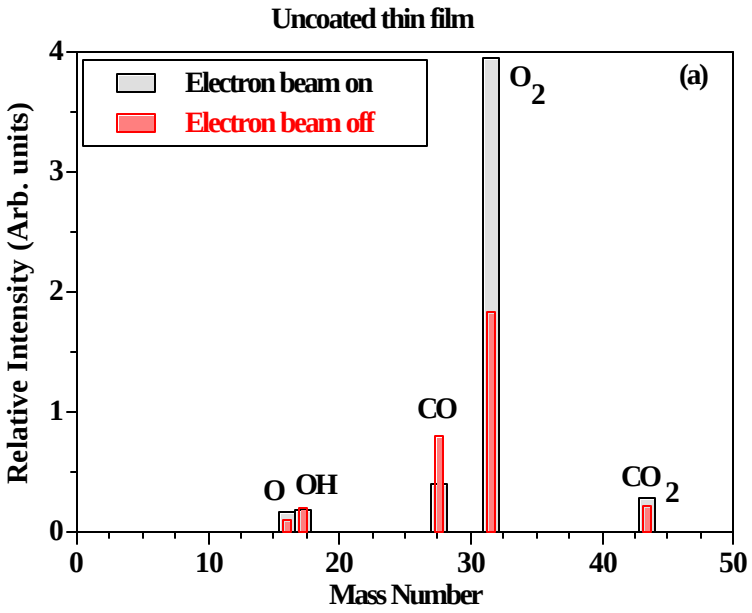

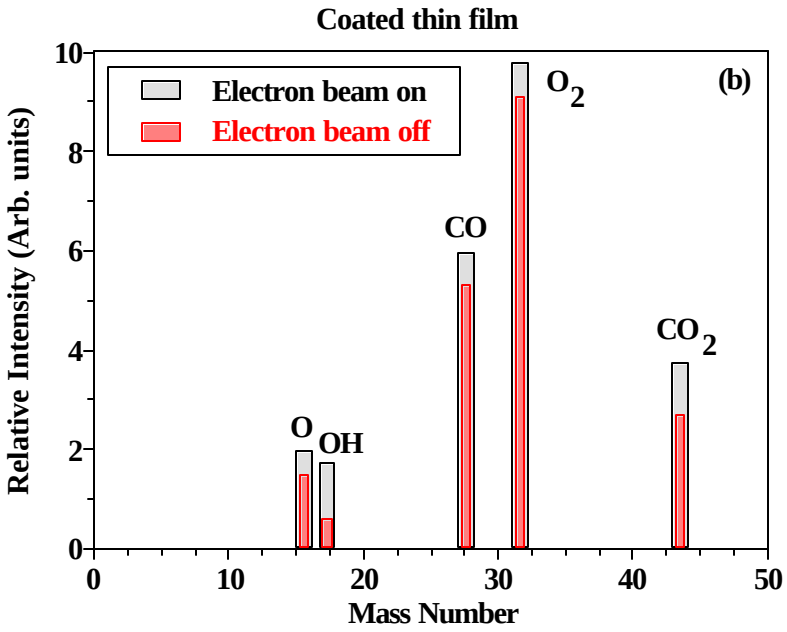

Figure 11: a) RGA for the coated and b) the uncoated thin film, with the electron beam on and off.

7.3 Light emission

Chen [10] wrote a chapter on the generation of particles by pulsed laser deposition. The nature of the particles, the energy, the size, the chemistry and microstructure all depend upon the type of material used as the target and the effects of the deposition parameters, eg the ambient gas pressure. The effect of inert ambient gas pressure on the nature of particles is most likely related to the increased collisions between the ejected species and the ambient gas as the ambient gas pressure increases. When a laser deposition experiment is done in vacuum, there are virtually no collisions between the ejected species before they reach the substrate.

When the ambient gas pressure increases, the vapour species can undergo enough collisions that nucleation and growth of these vapour species can occur to form particles before their arrival at the substrate. Since the growth mechanism is by diffusion, the residence time for the particles in the vapour controls the size of the particles. The longer the residence time, as is the case with increased ambient gas pressure, the larger the particle size.

Light emission from the spherical shaped phosphor particles on the thin film surface is affected much less by total internal reflection. Figure 12 shows a schematic diagram of photons with energy hν exiting a spherical shaped particle compared to a uniform layer.

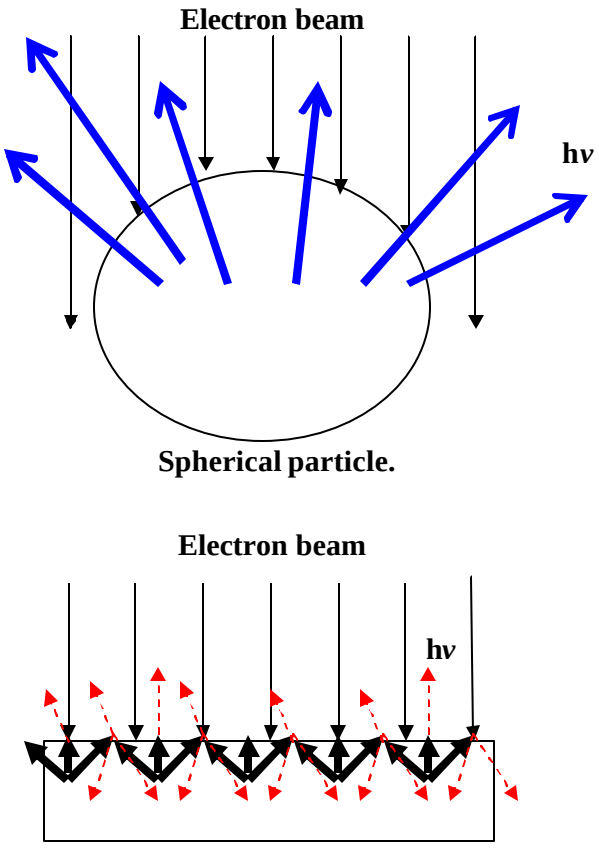

Figure 12: Schematic diagram of photons exciting a spherical particle compared to the total internal reflection effects in a uniform layer.

The spherical surface of the particles results in more photons exiting the surface and contributing to the high CL intensity of the thin films. Figure 13 illustrates the light emission from such thin films.

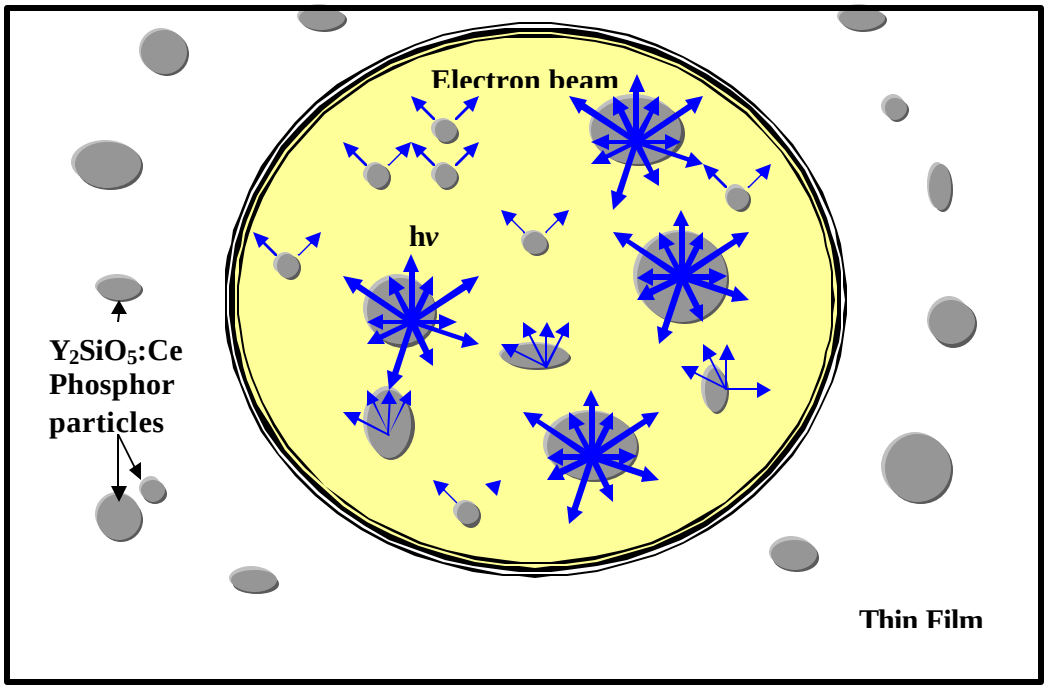

Figure 13: Schematic illustrating light emission from a phosphor thin film with spherical particles on the surface, resulting from a 220 μm diameter electron beam.

Electrons impinge on the thin film surface in an electron beam with a diameter of 220 μm, which results in photon excitation from an area on the surface containing a number of spherical particles that vary in size from a few nano-metres to micron sized particles. The photons are scattered from the particles in all directions, thus creating the bright blue light emission visible with the human eye.

Conclusion

The depletion of the adventitious C on the surface of the SnO_2 coated phosphor thin films occurred during 24 hr electron bombardment in an oxygen pressure of 1×10^{-6} Torr with an electron beam current of 10 μA. An increased oxygen pressure resulted in more reactive oxygen species which reacted with the C to create volatile species such as CO_2. The decrease in the beam current resulted in a lower temperature of contact between the electron beam and the thin film surface which resulted in a longer mean stay time of the oxygen species on the surface for depletion of the C via the

ESSCR model. The coated thin film resulted in a lower but constant CL intensity than for the uncoated thin films. SnO_2 was therefore successfully ablated onto some of the phosphor thin films as a coating layer which resulted in no degradation at first, but the coating was also depleted after continued electron bombardment. The small decrease in the CL intensity in the uncoated thin film could be due to a possible formation of SiO_2. Light emission from the spherical shaped phosphor particles from both the thin films showed the characteristic double shoulder peak for Y_2SiO_5:Ce between 400 and 500 nm. The high CL intensity from the thin films is due to the spherical shaped particles which have a larger critical angle for total internal reflection.

References

1. L. N. Skuja and W. Entzian, Phys. Stat. Sol. (a), **96** (1986)191.
2. E. J. Bosze, G. A. Hirata and J.McKittrick, Mat. Proc. Symp. Mat. Res. Soc. Proc, **558** (1999) 15.
3. E. J. Bosze, G. A. Hirata, J. McKittrick and L. E. Shea, Mat. Res. Soc. Symp, **508** (1998) 269.
4. Q. Y. Zhang, K. Pita, S. Buddhudu and C. H. Kam, J. Phys. D: Appl. Phys, **35** (2002) 3085.
5. H. C. Swart and K. T. Hillie, Surf. Interface Anal, **30** (2000) 383.
6. N. Karar and H. Chander, J. Phys. D: Appl. Phys, **38** (2005) 3580.
7. Sebastian, S. Jones, T. Trottier, H. Swart and P. Holloway, J. SID, **3/4** (1995) 147.
8. K. T. Hillie and H. C. Swart, Appl. Surf. Sci, **183** (2001) 304.
9. H. C. Swart, K. T. Hillie and A. P. Greeff, Surf. Interf. Anal, **32** (2001) 110.
10. Chen Li-Chyng, Particulates generated by pulsed laser ablation, in Pulsed Laser Deposition of Thin Films (eds. Chrisey D. B, Hulber, G. K), John Wiley & Sons, Inc, New York, (1994) p. 167.

Chapter 8

Conclusion and future work

This chapter contains the overall conclusion of the results obtained for the Y_2SiO_5:Ce phosphor powders and thin films as well as future work regarding this research study.

8.1 Powders

Y_2SiO_5:Ce is an organic phosphor that was investigated as an alternative for sulphide based phosphors for application in FEDs. Surface morphology of the phosphor powders was studied with SEM and it showed an agglomeration of the particles. XRD that was done to determine the crystal structure showed the monoclinic crystal structure of Y_2SiO_5:Ce. The degradation of the Y_2SiO_5:Ce phosphor powders was found to take place by the electron beam stimulated surface reactions that were manifested by the formation of a luminescent SiO_2 layer on the phosphor surface, proved by XPS. XPS and CL indicated that the change in the Si 2p peak shape is due to the formation of the luminescent SiO_2 on the surface. Light emission in Y_2SiO_5:Ce is a result of characteristic luminescence with transition in Ce^{3+} from the 5d to the 4f energy levels thus resulting in a double shoulder peak at 440 and 500 nm.

Light emission in SiO_2 is due to the 1.9 eV (peak between 600 and 700 nm) and 2.7 eV (peak between 400 and 500 nm) intrinsic defects as a result of oxygen vacancies. This resulted in a peak arising between 600 and 700 nm and an increase in the CL intensity measured at 440 nm. The surface reactions correlated with the increased CL intensity. CeO_2 and CeH_3 were also formed on the phosphor surface during the degradation process.

Degradation of this Y_2SiO_5:Ce phosphor powders in a high ambient gas pressure with low excitation energy electrons would thus not be a very effective replacement for the traditional blue ZnS phosphor powders, unless methods can be found to prevent it from degrading to a whitish emitting phosphor powder.

8.2 Thin films

Application in FEDs would however be in thin film form, therefore Y_2SiO_5:Ce phosphor thin films were grown in order to investigate whether the degradation would proceed in the same way as for the powders.

The pulsed laser deposition technique that was used for growing the phosphor thin films (using 6600 pulses) resulted in a non – uniform layer grown onto the Si (100) substrate. AFM, SEM and EDS indicated that the non – uniform phosphor layer consists of spherical shaped Y_2SiO_5:Ce particles randomly distributed on the surface. These particles differ in size from a few nano-meters to micron sized particles. XRD also showed the monoclinic crystal structure of Y_2SiO_5:Ce.

AES, CL spectroscopy and XPS results showed no severe chemical changes on the thin film surface as for the powders. Adventitious C that was present on the thin film surface before electron bombardment got depleted from the surface due to the ESSCR model, in an O pressure of 1×10^{-6} Torr with an electron beam current density of 26.32 $mA.cm^{-2}$. RGA indicated an increase in the CO and CO_2 gas species during electron bombardment. Some of the phosphor thin films were also coated with a uniform SnO_2 layer. The thin films that were coated with SnO_2 resulted in a lower but more constant CL intensity than the uncoated thin films at first; however; the SnO_2 layer also gets depleted from the surface due to electron interactions.

Thin films were also grown using 18 000 pulses in a higher ambient oxygen pressure of 7.5×10^{-3} Torr in order to create a more uniform layer on the surface. The SEM and EDS results indicated that the phosphor layer was again non – uniform with the spherical particles randomly distributed.

Light emission from the thin films is affected to a lesser extent by total internal reflection compared with a uniform thin layer. The photons get scattered from the particles in all directions, resulting in a relative high CL intensity.

The Y_2SiO_5:Ce phosphor thin films could thus be a good alternative for the traditional blue ZnS phosphor in thin film form if the thin films could be grown onto the

substrate as a uniform layer. SnO_2 proved to be a sufficient coating layer that resulted in a more constant CL intensity, which was, however, lower than the uncoated thin film CL intensity. The very thin SnO_2 layer also started to degenerate from the thin film surface due to the electron interactions.

8.3 Future work

1. In future, research needs to be done on how to prevent the Y_2SiO_5:Ce phosphor powders from degradation for application in FEDs. A possible method could be to investigate the effect of applying a transparent conductive surface layer to the phosphor powders.

2. Research could also be done on growing a uniform Y_2SiO_5:Ce thin film layer and investigating the effect on the CL intensity and degradation for application in FEDs. Pulsed reaction crossed beam laser deposition (PRCBLD) is an example of a different PLD growth technique that could be investigated for growing a uniform layer. This growth technique controls the oxygen inlet with a computerised valve, linked to the laser beam frequency.

3. Applying a thicker SnO_2 coating layer on the thin film surface could result in a much lower CL intensity which would make this Y_2SiO_5:Ce thin film phosphor not applicable in FED. It would however prevent it from degrading. Future work could include investigating a different coating layer that would not degenerate from the surface and finding a way of preventing the SnO_2 to deplete.

4. Further future work could also include investigating the effect of temperature and a different ambient gas pressure (for example CO_2) on the CL intensity of both the powders and thin films, as it will contribute to the environmental effects for operation in the FEDs.

5. Some other experimental aspects of this Y_2SiO_5:Ce phosphor in future could also involve characterization using glow discharge optical electron spectroscopy (GDOES) and time of flight – secondary ion mass spectroscopy (TOF-SIMS)

Appendix A

Publications

[1] E. Coetsee, H. C. Swart and J. J. Terblans, Degradation of Y_2SiO_5:Ce phosphor powders, J. Lumin, accepted May 2006.

[2] E. Coetsee, H. C. Swart, J. J. Terblans, O. M. Ntwaeaborwa, K. T. Hillie, W. A. Jordaan and U. Buttner, Characterization of Y_2SiO_5:Ce thin films, Opt. Mat, accepted June 2006.

[3] E. Coetsee, H. C. Swart and J. J. Terblans, Cathodoluminescence of Y_2SiO_5:Ce thin films.
In preparation.

Conference

[1] E. Coetsee, J. J. Terblans, O. M. Ntwaeaborwa, U. Buttner and H. C. Swart, Characterization of Pulsed Laser Ablated Cerium doped Yttrium Silicate (Y_2SiO_5:Ce) thin films on Si (100), SAIP Pretoria (2005).

[2] E. Coetsee, H. C. Swart, J. J. Terblans, O. M. Ntwaeaborwa, K. T. Hillie, W. A. Jordaan and U. Buttner, Cathodoluminescence of Y_2SiO_5:Ce thin films, SAIP at UWC July 2006.

[3] E. Coetsee, H. C. Swart and J. J. Terblans, Degradation of Y_2SiO_5:Ce phosphor powders, SAIP at UWC July 2006.

[4] E. Coetsee, H. C. Swart, J. J. Terblans O. M. Ntwaeaborwa, K. T. Hillie and U. Buttner, Energy Dispersive Spectroscopy (EDS), Scanning Electron (SEM) and Atomic Force Microscopy (AFM) of Y_2SiO_5:Ce thin films.
To be presented at SAIP MSSA at NMMU December 2006.

[5] H. C. Swart, J. J Terblans, E Coetsee, O. M. Ntwaeaborwa, M. S. Dhlamini and P. H. Holloway, A short review on the ESSCR mechanism for phosphor degradation.
To be presented at the AVS 53rd International Symposium & Exhibition, San Francisco, CA, USA, to be presented 12- 17 November 2006.

[6] E Coetsee, JJ Terblans and HC Swart, Cathodoluminescence Degradation of Y_2SiO_5:Ce Thin Films, AVS 53rd International Symposium & Exhibition, San Francisco, CA, USA, to be presented 12- 17 November 2006.